NASA TECHNICAL NOTE

NASA TN D-8218 c.1

LOAN COPY: RE
AFWL TECHNICAL
KIRTLAND AFB

0133777

TECH LIBRARY KAFB, NM

NASA TN D-8218

PERFORMANCE OF AN ISOLATED TWO-DIMENSIONAL WEDGE NOZZLE WITH FIXED COWL AND VARIABLE WEDGE CENTERBODY AT MACH NUMBERS UP TO 2.01

Donald L. Maiden

Langley Research Center
Hampton, Va. 23665

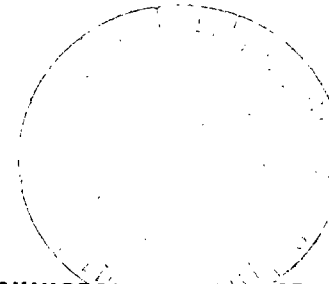

NATIONAL AERONAUTICS AND SPACE ADMINISTRATION • WASHINGTON, D. C. • SEPTEMBER 1976

TECH LIBRARY KAFB, NM

0133777

1. Report No.	2. Government Accession No.	3. Recipient's Catalog No.
NASA TN D-8218		

4. Title and Subtitle
PERFORMANCE OF AN ISOLATED TWO-DIMENSIONAL WEDGE NOZZLE WITH FIXED COWL AND VARIABLE WEDGE CENTERBODY AT MACH NUMBERS UP TO 2.01

5. Report Date
September 1976

6. Performing Organization Code

7. Author(s)
Donald L. Maiden

8. Performing Organization Report No.
L-10611

9. Performing Organization Name and Address
NASA Langley Research Center
Hampton, VA 23665

10. Work Unit No.
505-11-41-11

11. Contract or Grant No.

12. Sponsoring Agency Name and Address
National Aeronautics and Space Administration
Washington, DC 20546

13. Type of Report and Period Covered
Technical Note

14. Sponsoring Agency Code

15. Supplementary Notes

16. Abstract

A wind-tunnel investigation has been conducted to determine the aeropropulsion performance (thrust minus drag) of an isolated, two-dimensional wedge nozzle with a simulated variable-wedge mechanism and a fixed cowl. The investigation was conducted statically and at Mach numbers from 0.60 to 1.20 in the Langley 16-foot transonic tunnel and at a Mach number of 2.01 in the Langley 4-foot supersonic pressure tunnel. The ratio of exhaust jet total pressure to free-stream static pressure was varied up to 27 depending on free-stream Mach number. The results indicate that the aeropropulsion performance of the two-dimensional fixed-cowl variable-wedge nozzle is slightly lower (0.7 to 1.4 percent of ideal thrust) than that achieved for a two-dimensional wedge nozzle with a translating shroud, although part of the difference in performance is attributed to internal-performance differences. The effects of cowl boattail angle, internal expansion area ratio, and wedge half-angle on the performance of the two-dimensional wedge nozzle are discussed.

17. Key Words (Suggested by Author(s))	18. Distribution Statement
Nonaxisymmetric nozzle Two-dimensional wedge nozzle	Unclassified – Unlimited Subject Category 02

19. Security Classif. (of this report)	20. Security Classif. (of this page)	21. No. of Pages	22. Price*
Unclassified	Unclassified	124	$5.25

*For sale by the National Technical Information Service, Springfield, Virginia 22161

PERFORMANCE OF AN ISOLATED TWO-DIMENSIONAL WEDGE NOZZLE WITH FIXED COWL AND VARIABLE WEDGE CENTERBODY AT MACH NUMBERS UP TO 2.01

Donald L. Maiden
Langley Research Center

SUMMARY

A wind-tunnel investigation has been conducted to determine the aeropropulsion performance (thrust minus drag) of an isolated, two-dimensional wedge nozzle with a simulated variable-wedge mechanism and a fixed cowl. The investigation was conducted statically and at Mach numbers from 0.60 to 1.20 in the Langley 16-foot transonic tunnel and at a Mach number of 2.01 in the Langley 4-foot supersonic pressure tunnel. The ratio of exhaust jet total pressure to free-stream static pressure was varied up to 27 depending on free-stream Mach number.

The results of this investigation indicate that the aeropropulsion performance of the two-dimensional fixed-cowl variable-wedge nozzle is slightly lower (0.7 to 1.4 percent of ideal thrust) than that achieved for a two-dimensional wedge nozzle with a translating shroud, although part of the difference in performance is attributed to internal-performance differences. For the overall range of configurations and conditions, a fixed-cowl terminal boattail angle equal to the wedge half-angle appears to offer the most consistent performance over a wide range of Mach number (up to 2.01) and nozzle pressure ratio (up to about 27). In general, for a constant cowl boattail angle, the highest aeropropulsion performance was attained with the shallowest wedge half-angle (8°) for all test conditions.

INTRODUCTION

Jet aircraft that must operate at both subsonic and supersonic speeds require propulsion exhaust nozzles with variable geometry for high performance over a wide range of engine throttle settings. The most lightweight of such nozzles are axisymmetric and yield high internal performance (i.e., velocity coefficient); therefore, this type of nozzle has been selected for past and current aircraft designs. However, aft-end drag problems have been incurred with many multiengine airplanes because of the round nozzle integration with the airframe and the complex aft-end flow field. (See ref. 1.) These multiengine

configurations inherently have a large boattail "gutter" interfairing, or base region, between the engines or between the nozzles. This interfairing, as well as the nozzle boattail, is subject to adverse interference effects, especially if the flow separates from the afterbody near the nozzle exit. (See refs. 2 and 3.) Addition of empennage surfaces, particularly if mounted on booms which extend aft of the nozzle exits, further aggravates the aft-end drag problem with empennage-boom-nozzle flow interference. (See ref. 4.)

Two-dimensional wedge nozzles properly integrated with the airframe offer improved aeropropulsion performance (thrust minus drag) by eliminating the large boattail gutters between the engines, the nozzles, and/or the tail boom and the nozzle as shown in figure 1. Two-dimensional wedge nozzles are inherently better suited for in-flight thrust reversing or thrust vectoring (with supercirculation lift if the nozzle is properly integrated with the airframe, as discussed in ref. 5) than are conventional nozzles. The wedge centerbody can be used as a carry-through structure for the horizontal tails or wing to reduce airframe weight; it can also be used to suppress infrared radiation.

Because of the potential advantages offered by two-dimensional wedge nozzles, a program has been initiated at the Langley Research Center to evaluate experimentally the performance advantages to be derived from the use of the wedge nozzle. As part of this program, an investigation of an isolated two-dimensional wedge nozzle with a fixed cowl and a simulated variable-geometry centerbody has been conducted in the Langley 16-foot transonic tunnel and the Langley 4-foot supersonic pressure tunnel through a Mach number range up to 2.01. The objectives of the investigation were to determine the aeropropulsion performance (thrust minus drag) of this type of nozzle and to determine the effect of geometric parameters on the aeropropulsion performance. The results of the study are presented and are compared with the performance of an isolated two-dimensional variable-geometry wedge nozzle with translating shroud and collapsing wedge reported in reference 6.

SYMBOLS

A_b effective annular area between metal bellows and surrounding sleeve, m^2

A_e nozzle exit area (measured at end of upper and lower cowl surfaces, station 151.05 cm), m^2

$A_{e,x}$ area of theoretically fully expanded flow at wedge tip, m^2

A_{max} model maximum cross-sectional area, 0.026561 m^2

A_t nozzle throat area, m^2

a half-breadth line, m

b crown (keel) line, m

$C_{F,i}$ ideal thrust coefficient, F_i/qA_{max}

C_p pressure coefficient

D_f external skin friction drag of model between stations 67.31 cm and 126.75 cm, positive downstream, N

d_d internal duct diameter, m

d_t throat diameter, m

$F_{a,n}$ total-nozzle axial force (drag at $\alpha = 0^o$) on model aft of station 126.75 cm, positive downstream, N

$F_{a,ap}$ total-nozzle pressure axial force (pressure drag for $\alpha = 0^o$) on model aft of station 126.75 cm (friction drag removed), positive downstream, N

F_{bal} axial force indicated by balance, positive downstream, N

F_i ideal isentropic gross thrust, N

F_j gross thrust, positive upstream, N

l_d transition duct length from circular cross section to two-dimensional throat, m

l_w wedge length from leading edge to throat, m

M free-stream Mach number

$\dot{m}_i$ ideal mass-flow rate, kg/sec

$\dot{m}_j$ measured nozzle mass-flow rate, kg/sec

n	order of elliptical equation
$p_{b,d}$	pressure acting on downstream bellows, Pa
$p_{b,u}$	pressure acting on upstream bellows, Pa
p_{cav}	model internal-cavity pressure, Pa
p_j	jet static pressure, Pa
$p_{t,j}$	jet total pressure, Pa
p_∞	free-stream static pressure, Pa
q	free-stream dynamic pressure, Pa
r	radius, m
r_t	nozzle throat radius, m
r_β	circular-arc radius of boattail, m
x	distance along model center line from start of nozzle boattail, positive downstream, m
x/ℓ	ratio of x to overall length from start of nozzle boattail to nozzle terminus
y	lateral distance from plane passing through nozzle crown line and center line, m
z	vertical distance from plane passing through nozzle maximum half-breadth line and center line, m
α	angle of attack, deg
β	local boattail angle, deg
β_c	cowl boattail angle, deg

β_w wedge half-angle, deg

Abbreviations:

ASME American Society of Mechanical Engineers

EPR engine-operating pressure ratio (stagnation to free stream)

L.E. leading edge

Sta. model station

APPARATUS AND METHODS

Wind Tunnels

This investigation was conducted in the Langley 16-foot transonic tunnel and in the Langley 4-foot supersonic pressure tunnel. The Langley 16-foot transonic tunnel is a single-return, continuous-flow, atmospheric wind tunnel with a slotted octagonal test section. A constant test-section airspeed can be maintained over a range of Mach number from 0.20 to 1.30. A detailed description of the 16-foot transonic tunnel is given in reference 7. The Langley 4-foot supersonic pressure tunnel is a single-return, continuous-flow wind tunnel with a stagnation-pressure range from 27.58 kPa to 206.84 kPa and a stagnation-temperature range from 310 K to 322 K. By use of flexible tunnel-nozzle walls fitted to a calibrated contour, the tunnel Mach number can be varied from 1.25 to 2.20. A brief description of the 4-foot supersonic pressure tunnel is given in reference 8.

Model and Support System

General arrangement.- Shown in figure 2 are photographs of the air-powered nacelle model with the two-dimensional wedge nozzle installed in the Langley 16-foot transonic tunnel and in the Langley 4-foot supersonic pressure tunnel. The overall model, illustrated in detail in figure 3, is composed of four major sections:

	Model station, cm
Nose forebody	0 to 67.31
Low-pressure plenum	67.31 to 104.01
Instrumentation	104.01 to 126.75
Nozzle	126.75 to 175.34

In this test the nose forebody was nonmetric and all other major sections were parts of the metric afterbody. The fixed forebody provided a smooth transition from the circular nose to the rectangular maximum cross-sectional area of the model; the maximum area occurred forward of the metric break. The metric break is indicated in figure 2(a) by the double lines near the "midfuselage" station. A low-friction seal was inserted in the metric break to eliminate cross flow through the metric-nonmetric interface and to stabilize the internal-cavity pressure without transmission of axial force at the metric-nonmetric interface.

Internal air supply.- Inside the model, dry high-pressure air, at a stagnation temperature of about 300 K, entered the high-pressure plenum in the nose forebody through six supply lines in the support strut. The high-pressure air was then introduced, perpendicular to the model axis, into the low-pressure plenum which was supported by the balance as shown in figure 3. The decelerated airflow in the low-pressure plenum was diffused by bullet fairing over the balance. The airflow was then straightened forward of the instrumentation section by a 75-percent-open baffle plate. The holes in the baffle plate had a length-to-diameter ratio of 2.5. The air passed through the instrumentation section, where the stagnation conditions were measured, and was exhausted through the test nozzle (that portion of the model aft of the single line in fig. 2(a)).

Force-balance—air system.- Air passage from the high-pressure plenum to the low-pressure plenum was through eight sonic nozzles equally spaced around the axis of the high-pressure plenum. Since the high-pressure air was introduced radially to the model axis and an opposing nozzle canceled each jet impingement, the resultant tare forces and moments were minimal. Therefore, the balance measured only the gross thrust developed by the rearward acceleration of the air and the effect of external aerodynamic forces. The low-pressure plenum was sealed by a set of flexible metal bellows having similar spring constants, which served to compensate for the axial force caused by pressurization of the bellows.

Model support system.- The model was supported in the Langley 16-foot transonic tunnel by a sting-strut support with the nose of the model attached to the strut as shown in figures 2(a) and 3. The center line of the model was located on the wind-tunnel center line with the center line of the sting, which supports the strut, 55.88 cm below that level. (See fig. 3.) The sting portion of the support system was 5.08 cm by 10.16 cm in cross section with the top and bottom capped by half-cylinders with a 2.54-cm radius. The strut was 5 percent thick with a 50.8-cm chord in the streamwise direction. The strut leading and trailing edges were swept 45°. Flow interference, which is considered small for this model support system, is discussed in reference 9. Only the modified strut support was used in the Langley 4-foot supersonic pressure tunnel as shown in figure 2(b). The blade strut which was attached to the tunnel side wall was extended so that the model and tunnel center lines were alined.

Nozzle configurations.- Four circular-arc cowls with terminal boattail angles of 6°, 10°, 14°, and 18° are shown in figure 4. The cowls were tested with interchangeable wedges which simulated wedge geometry variation. Cowl boattail variations were restricted to the upper and lower external surfaces of the cowl, while the external surface on each side of the cowl had an approximate terminal boattail angle of 6°. (In subsequent discussions the cowl boattail variations are called the 6° boattail cowl, the 10° boattail cowl, etc.)

External and internal contours of these nonaxisymmetric nozzles were designed by use of "super-ellipse" cross sections. Smooth surfaces were defined mathematically by three control curve equations: (1) maximum half-breadth (width) line a, (2) crown (keel) line b, and (3) exponent (section shape) curve n. The general equation for the control curves for a and b is expressed in conic form as a function of length by

$$a(x) \quad \text{or} \quad b(x) = Px + Q + \sigma(Rx^2 + Sx + T)^{1/2}$$

where P, Q, σ, R, S, and T are coefficients shown in figure 5. The control curve for n is a curve fit. Each control curve is evaluated at a specific station. The cross section at that station is described by the coordinates y and z derived by substituting the values of a, b, and n into the super-ellipse expression $(z/a)^n + (y/b)^n = 1$. A typical cowl external contour and the corresponding control curve equations are shown in figure 5. The aft cowl "cutout" was determined by the base-line wedge geometry which dictated the cowl internal contours. The cowl internal contours were generated to achieve a generalized ratio A_t/A_{max} typical of modern aircraft. Typical cowl internal contours also generated by the super-ellipse equation are illustrated in figure 6. The transition geometry was selected from the data of reference 10 which indicate the optimum transition for this geometry to be $l_d/d_d = 1.10$ and $l_w/d_d = 0.50$. The internal area distribution for this nozzle can be obtained from reference 10.

Interchangeable wedge centerbodies used to vary the ratio of internal exit area to throat area (internal expansion area ratio) are shown in figure 7. All nozzles tested had throat areas representative of a dry power throttle setting. The interchangeable wedges provided internal expansion area ratios from 1.00 to 2.00. Figure 8 shows three wedge centerbodies, each designed with an internal $A_e/A_t = 1.10$ but with external wedge half-angles β_w of 8°, 10°, and 13.3°. The length of these wedges was varied because of the half-angle variation. For $\beta_w = 10^{\circ}$ the base-line wedge (wedge tip station, 175.34 cm) was used. For $\beta_w = 8^{\circ}$ the wedge was 16.5 percent longer than base line (wedge tip station, 181.53 cm), and for $\beta_w = 13.3^{\circ}$ the wedge was 16.5 percent shorter (wedge tip station, 169.16 cm). These wedges were tested with cowl such as the 10° boattail cowl shown in figure 8. Base-line wedge geometry was used with all configurations, unless otherwise noted.

All wedge-cowl combinations were not tested. Sketches of configurations tested are presented in figures 9 to 12. (Configurations with $A_e/A_t = 1.30$ had internal and external wedge half-angles of 4.5^o and 9^o, respectively; i.e., $\beta_w = 4.5^o/9^o$.) In addition to variations of internal expansion area ratio, configurations were tested to study the effects of a wedge leading-edge profile similar to the one reported in reference 6 (see fig. 10(b)) and of a reduction in wedge sideplate area (see fig. 11). Only the nozzle configuration with $A_e/A_t = 1.10$ and $\beta_c = 14^o$ was modified to study the effect of reducing sideplate area. The modification consisted of trimming the sideplate along a line that was a continuation of the local cowl slope ($\beta_c = 14^o$) at the nozzle exit (see fig. 11). The sideplate area reduction was about 65 percent of the base-line exposed sideplate area. Total elimination of the sideplate would have resulted in a large base region at the nozzle exit and thus would have required extensive recontouring of the nozzle afterbody.

Instrumentation

A six-component strain-gage balance was used to measure the forces and moments on the model downstream of the metric break. (See fig. 3.) Individual pressure transducers were used to measure the jet total pressures and tare-force pressures (such as internal-cavity and differential bellows pressures). A total of 12 jet total pressures, 15 internal-cavity pressures, and 2 bellows pressures were measured. A thermocouple was used to measure the jet total temperature, and an electronic turbine flowmeter was used to measure the mass flow of the high-pressure air.

Tests

Tests were conducted in the Langley 16-foot transonic tunnel at Mach numbers from 0 to 1.20. Tests were also conducted in the Langley 4-foot supersonic pressure tunnel statically and at a Mach number of 2.01 at a stagnation pressure of 124.1 Pa and a stagnation temperature of 316.5 K. The angle of attack was set at a nominally constant value of 0^o during the entire investigation. The Reynolds number based on model length varied from approximately 18.3×10^6 at $M = 0.60$ to 21.9×10^6 at $M = 1.20$ in the Langley 16-foot transonic tunnel and was approximately 20.8×10^6 at $M = 2.01$ in the Langley 4-foot supersonic pressure tunnel. The ratio of jet total pressure to free-stream static pressure (referred hereafter as nozzle pressure ratio) was varied from jet-off to about 27 depending on Mach number. Boundary-layer transition was fixed on the model by a 0.254-cm-wide strip of No. 100 grit placed 2.54 cm from the nose in accordance with the techniques described in references 11 and 12.

Data Reduction

Wind-tunnel data recorded on magnetic tape were used to compute standard force and pressure coefficients. All force data in this report are referenced to the body axes through the center line of the model.

The basic performance parameter used for the presentation of results is the aeropropulsion thrust ratio $\left(F_j - F_{a,n}\right)/F_i$ where

$$F_j - F_{a,n} = F_{bal} + \left(p_{cav} - p_\infty\right)A_{max} + \left(p_{b,d} - p_{b,u}\right)A_b + \Delta K_b + D_f$$

The term F_{bal} is the axial force indicated by the balance, corrected for weight tares and balance interactions. The term $\left(p_{cav} - p_\infty\right)A_{max}$ is a tare-force correction for a pressure difference between the inside and outside of the model. The cavity pressure was measured at 15 locations within the model, and the average pressure was assumed to act on the maximum cross-sectional area A_{max}. The term $\left(p_{b,d} - p_{b,u}\right)A_b$ is a bellows dynamic (jet-on) tare correction which by design should be essentially zero. However, when the internal velocities are high, a small pressure difference between the ends of the bellows exists. In this investigation, the maximum bellows dynamic tare correction was less than 0.5 percent of the ideal thrust. The term ΔK_b is a bellows static tare correction which also by design should be zero. However, differences in the spring constants of the forward and aft bellows can cause a slight tare force as the bellows are pressurized. In this investigation, the bellows static tare correction was essentially zero for the test in the Langley 16-foot transonic tunnel and less than 0.5 percent of the ideal thrust for the test in the Langley 4-foot supersonic pressure tunnel. The term D_f is the calculated skin friction drag on the portion of the model with constant cross section between the metric break at station 67.31 cm and the start of the nozzle at station 126.75 cm. For static tests, where $M = 0$, the external nozzle axial force $F_{a,n}$ is considered zero and the aeropropulsion thrust ratio reduces to F_j/F_i, or the internal-performance thrust ratio.

In an attempt to aid performance estimates for aircraft with this type of nozzle installed, all friction drag on the external wetted area of the nozzle has been subtracted and the performance is presented as the ratio of thrust minus axial pressure force to ideal thrust $\left(F_j - F_{a,ap}\right)/F_i$. This term reflects only the external pressure drag and the internal performance of the nozzle. The wedge and internal sideplate friction drag was charged to the nozzle internal performance.

After the complete model was installed in the wind tunnel, a check force-balance calibration was made to assure minimum restraints to the force balance. No tare

corrections were found to be necessary. Repeated calibration checks were made throughout the testing period to insure faithful force measurement.

To check the operation of the force-balance and airflow system and the resulting tare corrections, an axisymmetric convergent nozzle (configuration 3 of ref. 9) was tested statically to determine whether the system would repeat the static internal performance determined in reference 9. The internal contour of the "reference" convergent nozzle was essentially an ASME long-throat nozzle with a throat area of 45.16 cm^2. The result of the convergent nozzle static performance test is shown in figure 13. The present data agreed well with the data of reference 9 and indicated that the repeatability of static internal performance F_j/F_i and mass-flow ratio was within 0.5 percent for nozzle pressure ratios above 2.0. The reference convergent nozzle was tested randomly throughout the investigation to verify the data repeatability of the system.

RESULTS AND DISCUSSION

Since the external flow affects the internal performance of plug- and ejector-type nozzles, a complete evaluation of these nozzle types must be made at the flight Mach number and the engine-operating nozzle pressure ratio. The internal performance F_j/F_i is important for static take-off condition, but the aeropropulsion performance, or thrust minus drag, of the nozzle must be determined to evaluate plug and ejector nozzles at forward flight speeds.

Static Take-Off Performance

The static internal-performance characteristics of several two-dimensional wedge nozzle configurations are shown in figure 14. The mass-flow ratio $\dot{m}_j/\dot{m}_i$ and the thrust ratio F_j/F_i are shown as a function of nozzle pressure ratio $p_{t,j}/p_\infty$ for configurations with $\beta_c = 6^\circ$. The different test-point symbols shown on the plots represent repeat tests for the configuration. Similar plots for cowl boattail angles of 10°, 14°, and 18° are presented in figures 15, 16, and 17, respectively. Thrust ratios from repeat tests varied generally within 0.5 to 1 percent of ideal thrust. A 0.5 percent F_i difference in thrust ratios from repeat tests was observed for the reference metal convergent nozzle as shown in figure 13. The larger difference in thrust ratio (up to 1 percent F_i) for the two-dimensional wedge nozzles with identical internal geometry may be partially attributed to their plastic construction which may have resulted in slightly different internal geometry because of the hand fairing technique. However, repeatability of 1 percent is acceptable considering the data accuracy and geometric variations possible.

For axisymmetric nozzles operating at low values of nozzle pressure ratio (i.e., $p_{t,j}/p_\infty \approx 2.0$), the highest thrust ratio F_j/F_i is achieved with an expansion area ratio

of 1, or a convergent nozzle. (See ref. 6.) However, the data of figure 14 for the two-dimensional wedge nozzle indicate that the performance of the wedge nozzle with $A_e/A_t = 1.00$ did not yield the highest thrust ratio. For all cowl-wedge configurations a maximum thrust ratio of approximately 0.96 was attained with an internal area ratio A_e/A_t equal to 1.05. This peak value was attained for $p_{t,j}/p_\infty = 2.5$, which corresponds to the design nozzle pressure ratio (for which $p_j/p_\infty = 1.0$) for $A_e/A_t = 1.05$. At larger internal expansion area ratios the characteristics of the two-dimensional wedge nozzle are similar to those for axisymmetric converging-diverging nozzles; namely, the peak of thrust ratio is shifted to higher values of $p_{t,j}/p_\infty$ by increasing the internal expansion area ratio A_e/A_t.

Aeropropulsion Performance

In order to evaluate the aeropropulsion performance of the two-dimensional wedge nozzles of this investigation, data were acquired at each test Mach number to bracket the typical schedule of pressure ratio with flight Mach number for an advanced engine as shown in figure 18. This engine-operating pressure ratio (EPR) schedule is referred to periodically in the following discussion. Note that the typical schedule yields at $M = 0$, a $p_{t,j}/p_\infty$ of 2.5 that corresponds approximately to the nozzle pressure ratio at which the configurations for $A_e/A_t = 1.05$ attained their maximum static thrust.

In an attempt to aid performance estimates for aircraft with this type of nozzle installed, all friction drag on the external wetted area of the nozzle has been subtracted and the resulting thrust minus pressure drag ratio $(F_j - F_{a,ap})/F_i$ is presented in the appendix. Ideal thrust coefficients $C_{F,i}$ are also presented in the appendix for most configurations at all test Mach numbers.

Effect of cowl boattail.- The effect of cowl boattail angle on the aeropropulsion performance $(F_j - F_{a,n})/F_i$ of a two-dimensional wedge nozzle is presented for internal expansion area ratios of 1.00, 1.05, 1.10, 1.30, and 1.53 in figures 19, 20, 21, 22, and 23, respectively.

For an internal expansion area ratio A_e/A_t of 1.00, data were obtained only for cowl boattail angles of 6° and 10°. The wedge half-angle for these configurations was 10°. The nozzle with a 10° boattail cowl generally had as much as 2 percent F_i higher performance than the one with a 6° boattail cowl at typical EPR for flight conditions. (See fig. 19.) The higher performance for $\beta_c = 10^\circ$ is attributed to a favorable external-internal flow interaction effect on the wedge pressures, because the larger cowl boattail angle increased turning of the external flow toward the wedge.

Data were obtained for cowl boattail angles of 6°, 10°, and 14° for $A_e/A_t = 1.05$ (fig. 20). Again, the wedge half-angle was 10°. These data indicate that for subsonic speeds up to about $M = 0.90$, the nozzle with a 14° boattail cowl generally had the highest performance (up to 1.5 percent F_i greater at $M = 0.90$). This higher nozzle performance is probably because of a favorable external-internal flow interaction effect on the wedge pressures. As the free-stream Mach number approaches sonic conditions (i.e., $M = 0.95$), the drag for $\beta_c = 14^{\circ}$ increases greatly causing the performance $\left(F_j - F_{a,n}\right)/F_i$ to be lower for nozzle pressure ratios up to about 5. This drag increase is probably caused by a trailing (lambda) shock located on the blunt 14° boattail cowl surface. The trailing shock is due to the sudden recompression of the flow along the afterbody at the 14° boattail. The boundary-layer flow is unable to negotiate the high pressure gradient and separates from the body. As free-stream Mach number increases, this trailing shock moves rearward on the model until it is located near the cowl exit. Trailing shocks for axisymmetric circular-arc boattails are discussed in reference 13. Shadowgraphs in reference 13 show no trailing shock formation on a shallow boattail (5.6°) surface. The no-shock situation does not separate the flow and may account for the higher aeropropulsion performance of the 6° and 10° boattail cowls at $M = 0.95$ and 1.20 shown in figure 20. The much higher performance for $\beta_c = 6^{\circ}$ at $M = 0.95$ up to $p_{t,j}/p_{\infty} = 5$ could be because the boundary-layer flow has not become critical as have most possibly the boundary-layer flows for $\beta_c = 10^{\circ}$ and 14°. As nozzle pressure ratio increases above 2.5, the jet begins to plume as depicted in the following sketch. Increase in nozzle pressure ratio was shown in reference 14 to drive the trailing shock upstream and cause an increase in pressure gradient on the boattail as illustrated in the pressure trend in the sketch. The increase in pressure gradient causes the boundary-layer flow to separate from the boattail surface at a point upstream of the original point undisturbed by the jet. The increased cowl boattail pressure is probably due to the boundary-layer flow separation from the afterbody as the exhaust jet pluming increases; and since the pressure acts on a rearward-facing area, a reduction in the cowl drag of the 14° boattail resulted. This cowl drag reduction and possible change of interference on the wedge surface result in the higher aeropropulsion performance at $M = 0.95$ and 1.20 above a nozzle pressure ratio of about 5.5 as shown in figure 20.

Figure 21 presents data obtained for cowl boattail angles of 6°, 10°, 14°, and 18° for $A_e/A_t = 1.10$. The wedge half-angle for these configurations was 10°. Although the wedge half-angle is the same and the ratio A_e/A_t only slightly larger than for the two configurations previously discussed, the configuration with $A_e/A_t = 1.10$ yields higher performance at $M = 0.95$ and 1.20. The difference is that the nozzle throat has been transferred inside the cowl as was shown in figures 7 and 9, so that some of the exhaust

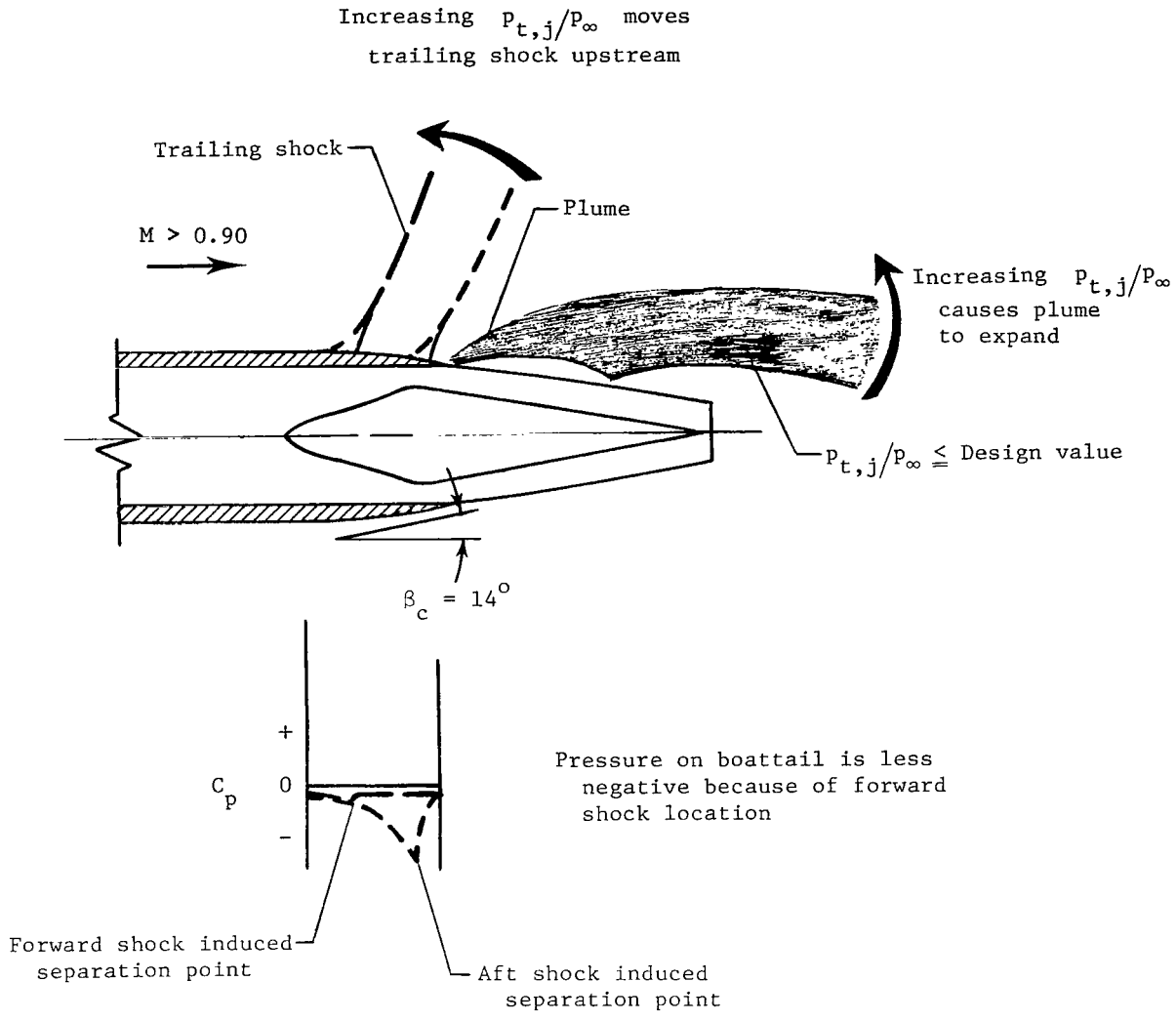

flow expansion now occurs internally. The internal wedge half-angle from the throat is approximately 1.5^o with a 10^o external expansion surface. The data of figure 21 indicate that for this configuration the cowl boattail angle should be equal to the external wedge half-angle (10^o) to achieve the highest nozzle performance at all test Mach numbers at typical EPR. Up to $M = 0.90$, the nozzle with a 14^o boattail cowl had approximately the same performance as the one with a 10^o boattail cowl; however, at $M = 0.95$, the performance of the 14^o boattail nozzle was about 1 percent F_i lower near flight conditions than that for the 10^o boattail nozzle. The 6^o boattail nozzle exhibited the same performance as the 10^o boattail nozzle at $M = 1.20$ but was generally about 1 percent F_i lower at EPR for subsonic test Mach numbers. The 18^o boattail cowl was inferior at all test conditions.

Data shown in figure 22 were obtained for cowl boattail angles of 6°, 10°, 14°, and 18° for $A_e/A_t = 1.30$. The internal and external wedge half-angles for this configuration were 4.5° and 9°, respectively. Data of figure 22 indicate that the highest aeropropulsion performance $\left(F_j - F_{a,n}\right)/F_i$ was obtained with the 6° boattail cowl, a result which is anomalous with the results at other expansion area ratios. This anomaly may be because the 6° cowl boattail angle more closely matches the combination $4.5^{\circ}/9^{\circ}$ wedge half-angle. On the basis of previous data, the match of cowl boattail angle and wedge half-angle could yield a favorable external-internal flow interaction effect on the wedge pressures as well as take advantage of the lower drag for the 6° boattail cowl. At $M = 0.95$ and 1.20, the 6° boattail cowl with $A_e/A_t = 1.30$ is clearly superior to the other cowl boattail configurations.

Figure 23 presents data for configurations with $A_e/A_t = 1.53$ and cowl boattail angles of 6°, 10°, and 14°. The wedge half-angle for these configurations was 8° for both internal and external expansion surfaces. The data indicate that the 10° boattail nozzle has higher performance up to $M = 0.95$ and that the 6° boattail nozzle has higher performance above $M = 0.95$. The results for $\beta_c = 6^{\circ}$ and 10° at $A_e/A_t = 1.53$ are consistent with the previous results except for data at $A_e/A_t = 1.30$. At subsonic speeds ($M < 0.90$), the performance of the 14° boattail nozzle compared with that of the 10° boattail nozzle was lower (approximately 1 percent F_i for flight conditions). This is probably because of the greater difference between the wedge half-angle (8°) and the cowl boattail angle (14°) for the $A_e/A_t = 1.53$ configuration, which may have resulted in a flow disturbance and adversely affected wedge pressures.

Figure 24 summarizes the effect of cowl boattail angle on two-dimensional wedge nozzle performance at the scheduled nozzle pressure ratio shown in figure 18. Since the effect of cowl boattail angle on aeropropulsion performance appears to be a function of A_e/A_t (i.e., nozzle exit Mach number), the discussion of cowl boattail effects is divided into low values of $A_e/A_t = 1.00$, 1.05, and 1.10 (fig. 24(a)) and higher values of $A_e/A_t = 1.30$ and 1.53 (fig. 24(b)).

Figure 24(a) presents data for configurations with $A_e/A_t = 1.00$, 1.05, and 1.10 (all with wedge half-angles of 10°) as well as comparable two-dimensional wedge nozzle data from reference 6. Each different internal expansion area ratio will of course have a different level of performance. For $M \leq 0.90$, cowl boattail angles ranging from 6° to 18° had a relatively small effect on aeropropulsion performance (increment less than 1.5 percent F_i); cowl boattail angles in the range from 10° to 14° generally resulted in slightly higher performance with the wedge half-angle of 10°. For the same conditions the 6° boattail cowl consistently had the lowest performance. For $M = 0.95$ and 1.20, cowl boattail angles ranging from 6° to 18° did affect aeropropulsion performance by as

much as 3.5 percent F_i. It should be noted that, on the basis of axisymmetric converging-diverging nozzle characteristics, the A_e/A_t ratios shown in figure 24(a) may not be desirable above $M \geq 0.95$ in order to achieve maximum nozzle performance.

To obtain the two-dimensional wedge nozzle performance data from reference 6, a translating shroud was used to vary the internal expansion area ratio. The solid circles shown in figure 24(a) represent data of reference 6 for $A_e/A_t = 1.05$ (shroud retracted), $\beta_w = 10^o$, and $\beta_c = 12^o$. Data comparisons indicate that the performance of the fixed-cowl, variable-centerbody nozzle with $A_e/A_t = 1.05$ is about 0.7 percent F_i lower for $M \leq 0.90$ than its translating-shroud counterpart and 2 to 3 percent F_i lower at $M = 0.95$ and 1.20. Part of the performance difference is attributed to lower internal performance as observed for $M = 0$.

Figure 24(b) presents data for configurations with $A_e/A_t = 1.30$ and 1.53 (wedge half-angles of $4.5^o/9^o$ and 8^o, respectively) as well as comparable two-dimensional wedge nozzle data from reference 6. For $M \leq 0.90$, no trend could be well established since the performance levels for all cowl boattail configurations varied only about 1 percent F_i and inconsistent trends were noted for the two configurations tested. These data indicate that for $M \leq 0.90$ and high values of A_e/A_t (i.e., high supersonic exit Mach numbers), the cowl boattail angle has little or no effect. This no-effect result is academic since for $M \leq 0.90$ significantly higher nozzle performance can be achieved with $A_e/A_t < 1.30$; however, the no-effect result is probably because of the absence of exhaust plume for these conditions. At $M = 0.95$ and 1.20 where values of A_e/A_t of 1.30 and 1.53 may be desirable, the configuration with the lowest cowl boattail angle (6^o) had the highest performance. Thus, a shallow boattail cowl may be desirable at near-sonic and supersonic speeds. Comparison of data from reference 6 with current data for $A_e/A_t = 1.53$ indicates that the performance of the fixed-cowl, variable-centerbody nozzle is consistently about 1.4 percent F_i lower at all test Mach numbers than that of the wedge nozzle with a translating shroud.

Effect of internal expansion area ratio.- Figure 25 presents the effect of internal expansion area ratio on the performance of a two-dimensional wedge nozzle at the EPR schedule for several Mach numbers. Aeropropulsion performance $(F_j - F_{a,n})/F_i$ is presented as a function of internal expansion area ratio. The data indicate performance characteristics (i.e., nozzle peak performance shifted to higher values of $p_{t,j}/p_\infty$ with increase in internal A_e/A_t) similar to those for axisymmetric converging-diverging nozzles with the exception of the performance for $A_e/A_t = 1.00$, which should theoretically result in the highest performance at static ($M = 0$) conditions. The lower performance for $A_e/A_t = 1.00$ emphasizes the importance of throat and exit locations with respect to wedge geometry. The lower performance at this expansion area ratio was probably caused by a distortion of the nozzle sonic line which causes a cocking of the upper and

lower thrust vectors and results in a loss of axial thrust. As free-stream Mach number increases, the scheduled EPR also increases as does nozzle drag. The combined result is that as Mach number increases the internal expansion area ratio must increase to shift the peak performance to a nozzle pressure ratio to match the EPR schedule shown in figure 18. The data of figure 25 indicate that for $M < 0.90$ the internal expansion area ratio can be fixed as low as a value of 1.05. At $0.90 \leq M \leq 1.20$, the data indicate that higher internal expansion area ratios $\left(\text{up to } A_e/A_t = 1.53 \text{ at } M = 1.20\right)$ would be required for maximum performance.

In a subsequent test at the Langley 4-foot supersonic pressure tunnel, cowl boattail angles of 6° and 10° were tested with internal expansion area ratios of 1.53, 1.70, and 2.00. The results of this are shown in figure 26. As expected, an increase in internal expansion area ratio results in an increase in aeropropulsion performance. Increasing A_e/A_t from 1.53 to 2.00 resulted in about a 2 percent F_i increase at a nozzle pressure ratio of 25 for both test cowl boattail angles. The 6° boattail nozzle had a slightly higher aeropropulsion performance than the 10° boattail nozzle with comparable values of A_e/A_t. The superiority of the 6° boattail nozzle is probably because cowl drag at supersonic speeds is lower for $\beta_c = 6^\circ$ than for $\beta_c = 10^\circ$. The effect of lower cowl drag is more evident at lower nozzle pressure ratios. For example, at $p_{t,j}/p_\infty = 11$, the aeropropulsion performance of the 6° boattail nozzle is generally about 1 percent F_i higher than the 10° boattail nozzle. At $p_{t,j}/p_\infty = 25$, the 6° boattail nozzle performance is higher only by about 0.3 percent F_i. The lower percentage of F_i at the higher pressure ratio $\left(\text{i.e., } p_{t,j}/p_\infty = 25\right)$ indicates that the cowl drag increment $\left(\text{between } \beta_c = 6^\circ \text{ and } 10^\circ\right)$ is approximately constant with pressure ratio and therefore represents a smaller fraction of ideal thrust as F_i increases.

With the 10° boattail cowl, a parabolic leading-edge wedge profile was also investigated. This modification is illustrated in the sketch of figure 10(b). The data (fig. 26(b)) indicate a slight performance increase of approximately 0.5 percent F_i for $p_{t,j}/p_\infty < 13$ with the parabolic profile compared with the reflexed profile.

Effect of wedge half-angle.- Figure 27 presents the effect of wedge half-angle on the performance of a two-dimensional wedge nozzle with $A_e/A_t = 1.10$ and $\beta_c = 10^\circ$. The data show that the wedge half-angle significantly affects two-dimensional wedge nozzle performance, especially at Mach numbers above $M = 0.80$. At $M = 0.90$ and 0.95, the exhaust flow probably separates from the steeper wedge $\left(\beta_w = 13.3^\circ\right)$ at a nozzle pressure ratio between 4.0 and 5.0 causing a decrease in nozzle performance at pressure ratios above 4.0. At $M = 1.20$ and $p_{t,j}/p_\infty = 6.0$, the two-dimensional wedge nozzle with a 13.3° half-angle wedge had about 4 percent F_i lower aeropropulsion performance than that for the nozzle with the 10° half-angle base-line wedge.

Figure 28 presents similar data for $A_e/A_t = 1.10$ and $\beta_c = 18^o$. The difference in aeropropulsion performance for the nozzles with 10^o and 13.3^o half-angle wedges at $M \leq 0.8$ was not as great as with the 10^o boattail configuration (see fig. 27) because of the influence of cowl boattail angle on nozzle aeropropulsion performance. As discussed previously, the effect of using the 18^o boattail cowl with the 10^o half-angle wedge is probably to increase cowl drag and thereby reduce nozzle aeropropulsion performance. On the 13.3^o half-angle wedge the 18^o boattail cowl probably has a more favorable or less detrimental external-internal flow interaction and thereby increases the aeropropulsion performance as compared with a 10^o boattail cowl. The result of the influence of cowl boattail angle is to narrow the difference in aeropropulsion performance up to $M = 0.8$. However, above $M = 0.8$ the performance of the two-dimensional wedge with a 13.3^o half-angle is significantly lower than the aeropropulsion performance of the 10^o half-angle configuration. Because of the significant effect of wedge half-angle on two-dimensional wedge aeropropulsion performance, a shallower wedge half-angle of 8^o was tested with $\beta_c = 18^o$ and $A_e/A_t = 1.10$. As shown in figure 28, a significant increase in nozzle performance was attained at all Mach numbers and nozzle pressure ratios tested. Even with the increase in friction drag resulting from increased wetted area, the nozzle with a longer, shallower half-angle wedge had higher performance (about 2 percent subsonically and 3 percent supersonically) than the nozzle with the 10^o half-angle wedge.

Figure 29 summarizes the effect of wedge half-angle on two-dimensional wedge nozzle performance for two cowl boattail angles. The internal expansion area ratio for these comparisons was 1.10. These data indicate incremental results for wedge half-angle variations similar to those discussed previously for figures 27 and 28. However, for the configurations tested the data indicate the trend that the shallowest wedge half-angle incorporating an equal or slightly greater cowl boattail angle will have the highest two-dimensional wedge nozzle performance.

Effect of sideplate reduction.- A reduction or elimination of sideplate surface area is desirable to reduce the amount of cooling required for the nozzle parts exposed to the hot exhaust of the nozzle. Reference 15 shows that total elimination of the sideplates of a flight two-dimensional wedge nozzle, with secondary air being used to ventilate the base created by the sideplate removal, actually resulted in about a 1 percent F_i increase in performance at flight conditions. A modification was made to the configuration with $A_e/A_t = 1.10$ and $\beta_c = 14^o$ to reduce sideplate area about 65 percent as discussed in the "Apparatus and Methods" section for figure 11. Performance results of this configuration are compared in figure 30 with those for the base-line configuration. This comparison indicates that the 65 percent reduction in sideplate area had little or no effect on two-dimensional wedge nozzle performance at all test Mach numbers near flight EPR.

SUMMARY OF RESULTS

A wind-tunnel investigation has been conducted in the Langley 16-foot transonic tunnel and the Langley 4-foot supersonic pressure tunnel on a two-dimensional wedge nozzle with a fixed cowl and variable-geometry wedge centerbody. The investigation was conducted statically and at simulated flight speeds up to a Mach number of 2.01 at an angle of attack of 0°. The ratio of jet exhaust total pressure to free-stream static pressure was varied up to 27 depending on Mach number.

The results of the investigation indicate the following:

1. For static take-off and low subsonic Mach numbers, the aeropropulsion performance of the fixed-cowl, variable-wedge nozzle was slightly lower (less than 0.7 percent of ideal thrust) at a comparable internal expansion area ratio, than the performance of a similar two-dimensional wedge nozzle with a translating shroud. Part of the 0.7-percent difference is attributed to internal-performance differences. At supersonic speeds, for dry power operation, the performance of the fixed-cowl variable-wedge nozzle was about 1.4 percent of ideal thrust lower than that for the nozzle with a translating shroud.

2. At subsonic speeds (Mach numbers less than 0.9), cowl boattail angle (ranging from 6° to 18°) had a small effect on aeropropulsion performance, with cowl boattail angles in the range from 10° to 14° (equal to or slightly greater than the wedge half-angle) being only slightly superior.

3. At near-sonic and supersonic speeds the highest aeropropulsion performance was attained with a shallow boattail cowl design, either a 6° or 10° boattail angle for the configurations tested.

4. In general, for a constant cowl boattail angle, the highest aeropropulsion performance was attained with the shallowest wedge half-angle for all test conditions.

5. For the overall range of configurations and conditions, a fixed-cowl terminal boattail angle equal to the wedge half-angle appears to offer the most consistent performance over a wide range of Mach numbers (up to 2.01) and nozzle pressure ratios (up to about 27).

6. For Mach numbers less than 0.90, an internal expansion area ratio of 1.05 resulted in consistently high performance at engine-operating nozzle pressure ratios. At near-sonic and supersonic speeds an increase in internal expansion area ratio is desirable. At Mach numbers of 1.20 and 2.01, the highest aeropropulsion performance was obtained with the highest internal area ratios tested, 1.53 and 2.00, respectively.

7. A large reduction in sideplate surface area (approximately 65 percent) had little or no effect on aeropropulsion performance.

Langley Research Center
National Aeronautics and Space Administration
Hampton, VA 23665
May 20, 1976

APPENDIX

AIDS TO AIRCRAFT PERFORMANCE ESTIMATES

In order to facilitate estimates of the performance of aircraft using the two-dimensional nozzle concept presented in this report, the following figures are presented for reference. The variation of the thrust minus axial pressure force ratio $\left(F_j - F_{a,ap}\right)/F_i$ with nozzle pressure ratios for several internal expansion area ratios is presented in figures 31 to 35. As discussed in the section "Data Reduction," the term $\left(F_j - F_{a,ap}\right)/F_i$ does not include the nozzle external friction drag. The results of figures 31 to 35 are similar to the results discussed for figures 19 to 23.

Similar plots of $\left(F_j - F_{a,ap}\right)/F_i$ as a function of $p_{t,j}/p_\infty$ are presented for nozzles with 10^o and 18^o boattail cowls for $A_e/A_t = 1.10$ in figures 36 and 37, respectively. The results of figures 36 and 37 are similar to the results presented for figures 27 and 28.

The variation of the aerodynamic ideal thrust coefficient with the nozzle pressure ratio for most configurations is presented in figure 38 for all test Mach numbers.

REFERENCES

1. Runckel, Jack F.: Interference Between Exhaust System and Afterbody of Twin-Engine Fuselage Configurations. NASA TN D-7525, 1974.

2. Galigher, Lawrence L.: Performance of Various Twin-Nozzle Afterbody Configurations of an Air Superiority Fighter-Type Model at Mach Numbers From 0.6 to 2.5. AEDC-TR-72-17, U.S. Air Force, Feb. 1972. (Available from DDC as AD 891 242L.)

3. Berrier, Bobby L.: Effect of Empennage Interference on Single-Engine Afterbody/Nozzle Drag. AIAA Paper No. 75-1296, Sept.-Oct. 1975.

4. Mercer, Charles E.; and Berrier, Bobby L.: Effect of Afterbody Shape, Nozzle Type, and Engine Lateral Spacing on the Installed Performance of a Twin-Jet Afterbody Model. NASA TM X-1855, 1969.

5. Capone, Francis J.: Supercirculation Effects Induced by Vectoring a Partial-Span Rectangular Jet. AIAA Paper No. 74-971, Aug. 1974.

6. Maiden, Donald L.: Performance of an Isolated Two-Dimensional Variable-Geometry Wedge Nozzle With Translating Shroud and Collapsing Wedge at Speeds Up to Mach 2.01. NASA TN D-7906, 1975.

7. Corson, Blake W., Jr.; Runckel, Jack F.; and Igoe, William B.: Calibration of the Langley 16-Foot Transonic Tunnel With Test Section Air Removal. NASA TR R-423, 1974.

8. Schaefer, William T., Jr.: Characteristics of Major Active Wind Tunnels at the Langley Research Center. NASA TM X-1130, 1965.

9. Reubush, David E.; and Runckel, Jack F.: Effect of Fineness Ratio on the Boattail Drag of Circular-Arc Afterbodies Having Closure Ratios of 0.50 With Jet Exhaust at Mach Numbers Up to 1.30. NASA TN D-7192, 1973.

10. Goetz, G. F.; and Petit, J. E.: Integrated Nozzle Development Program, Transition Study Test Report No. D180-15443 (Contract No. N00140-73-C-0027), Boeing Co.

11. Braslow, Albert L.; and Knox, Eugene C.: Simplified Method for Determination of Critical Height of Distributed Roughness Particles for Boundary-Layer Transition at Mach Numbers From 0 to 5. NACA TN 4363, 1958.

12. Braslow, Albert L.; Hicks, Raymond M.; and Harris, Roy V., Jr.: Use of Grit-Type Boundary-Layer Transition Trips on Wind-Tunnel Models. NASA TN D-3579, 1966.

13. Silhan, Frank V.; and Cubbage, James M., Jr.: Drag of Conical and Circular-Arc Boattail Afterbodies at Mach Numbers From 0.6 to 1.3. NACA RM L56K22, 1957.

14. Swihart, John M.; Mercer, Charles E.; and Norton, Harry T., Jr.: Effect of Afterbody-Ejector Configurations on the Performance at Transonic Speeds of a Pylon-Supported Nacelle Model Having a Hot-Jet Exhaust. NASA TN D-1399, 1962.

15. Johns, Albert L.: Flight Investigation of Installation Effects on a Wedge Nozzle Installed on an Underwing Nacelle. NASA TM X-3207, 1975.

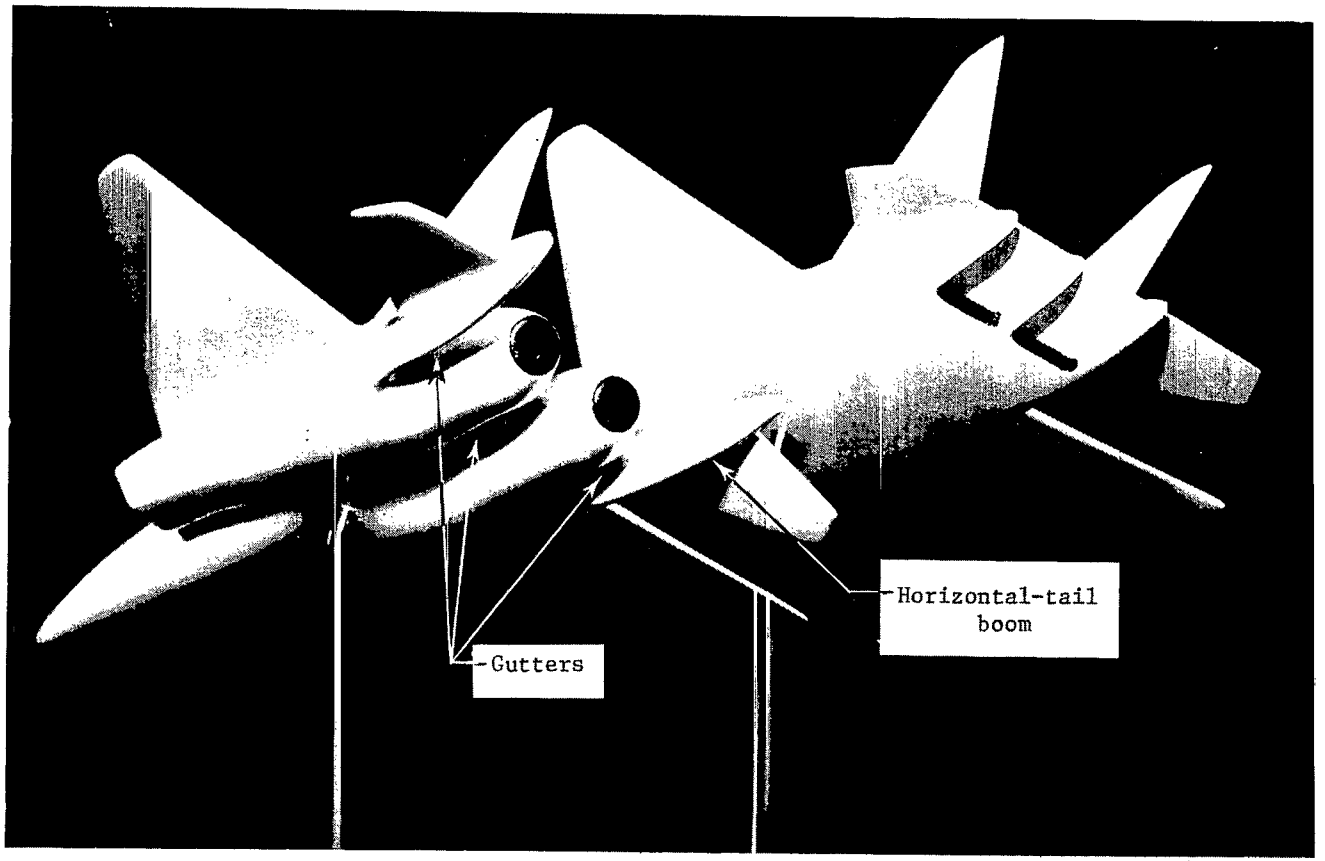

L-74-3691.1

Figure 1.- Conventional axisymmetric nozzle integration and two-dimensional wedge nozzle integration concept.

L-74-3209

(a) In Langley 16-foot transonic tunnel.

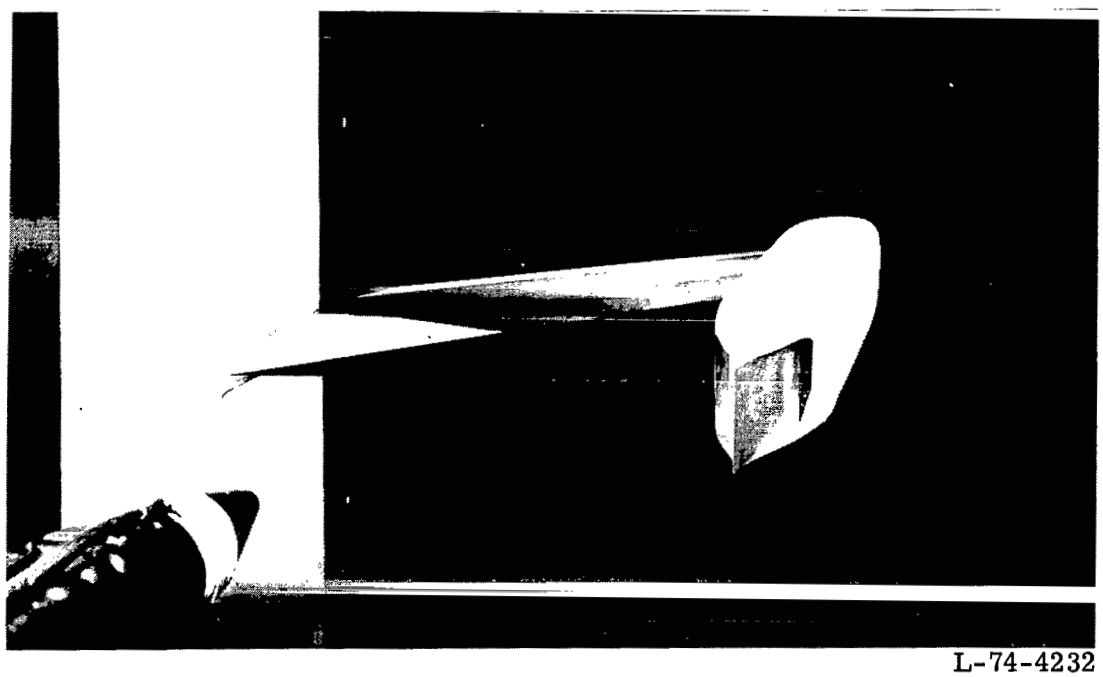

L-74-4232

(b) In Langley 4-foot supersonic pressure tunnel.

Figure 2.- Isolated air-powered nacelle installations.

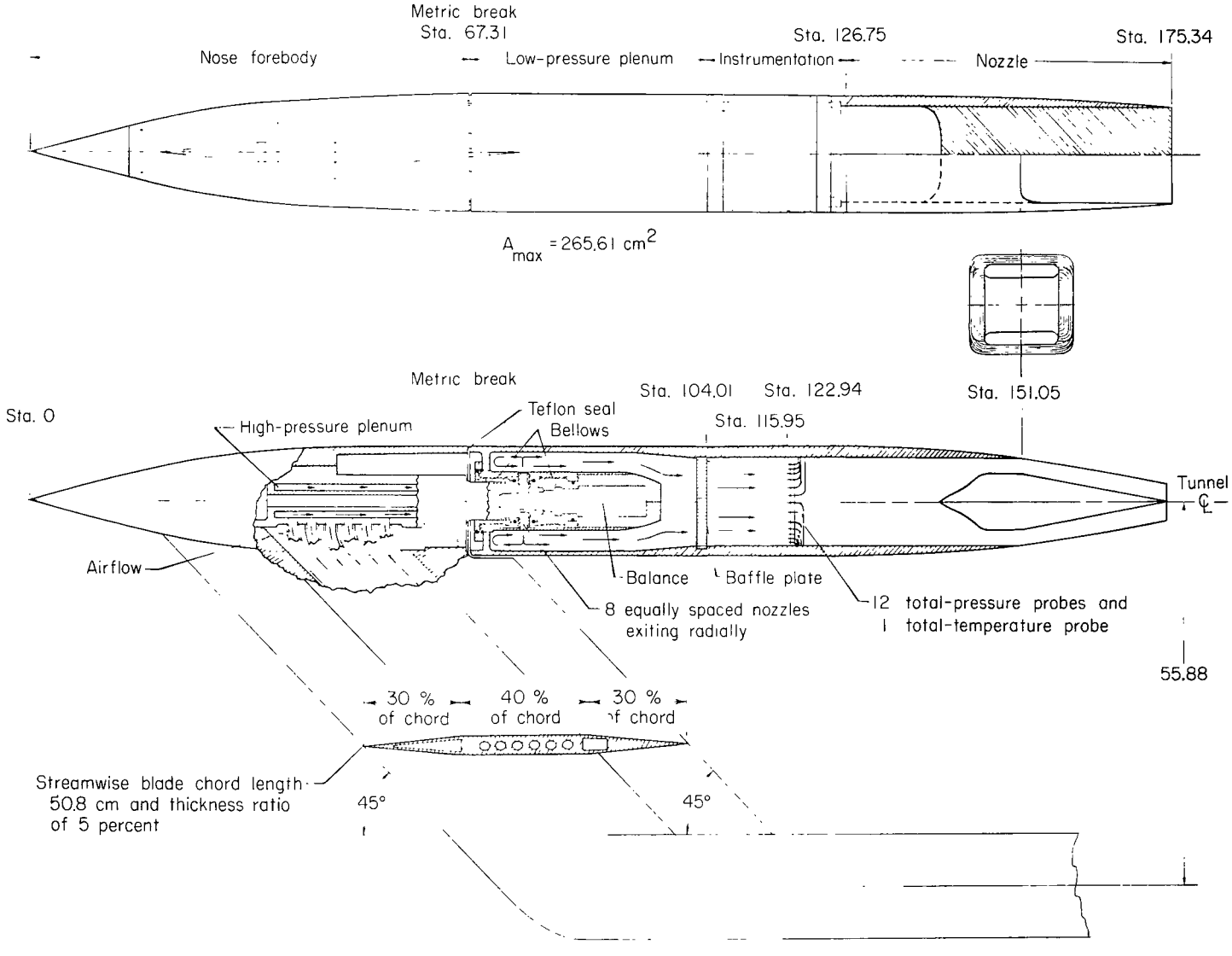

Figure 3.- Sketch of air-powered nacelle model with two-dimensional wedge nozzle installed in the Langley 16-foot transonic tunnel. All dimensions and stations are in centimeters unless otherwise noted.

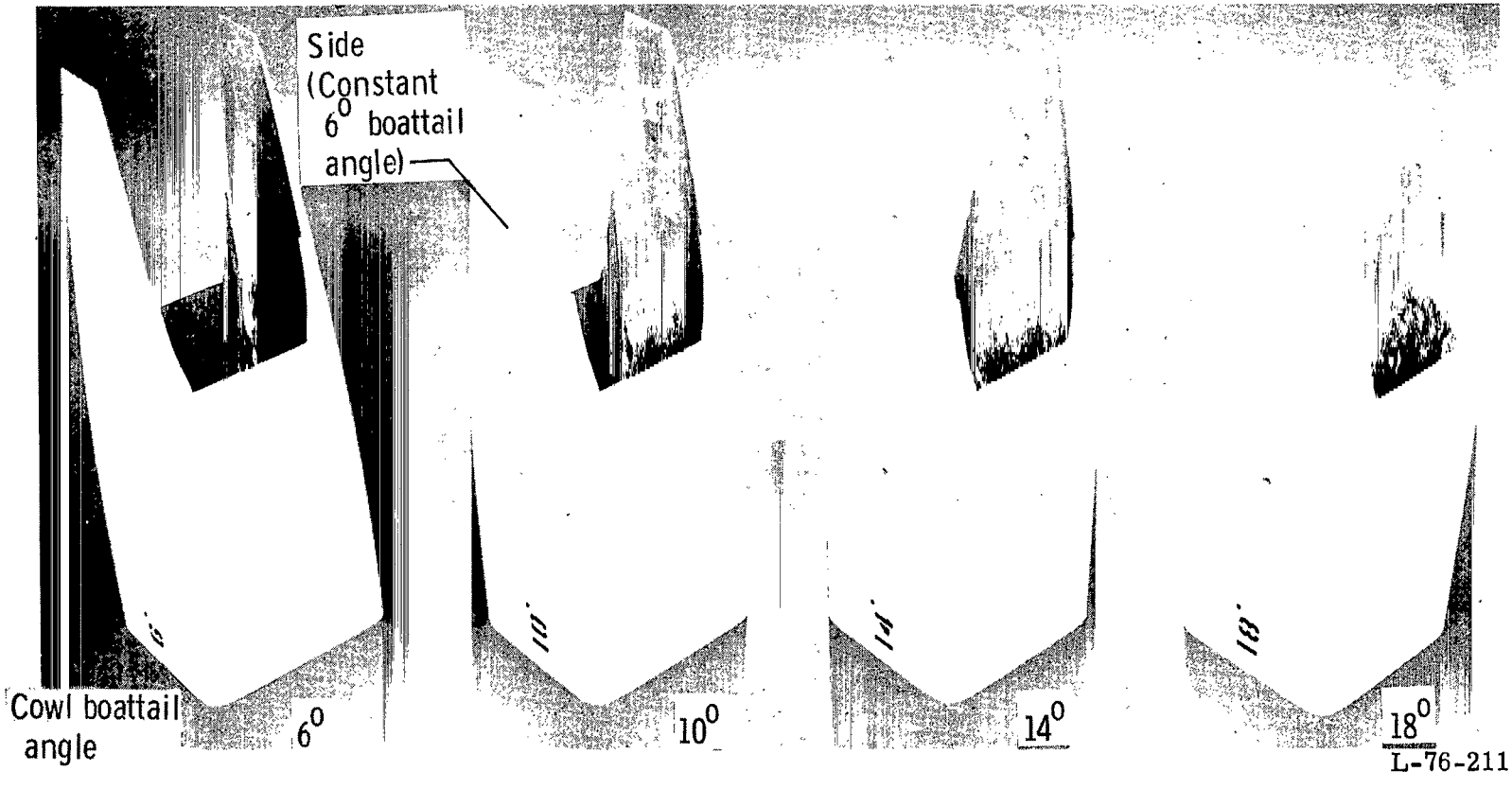

Figure 4.- Circular-arc cowls.

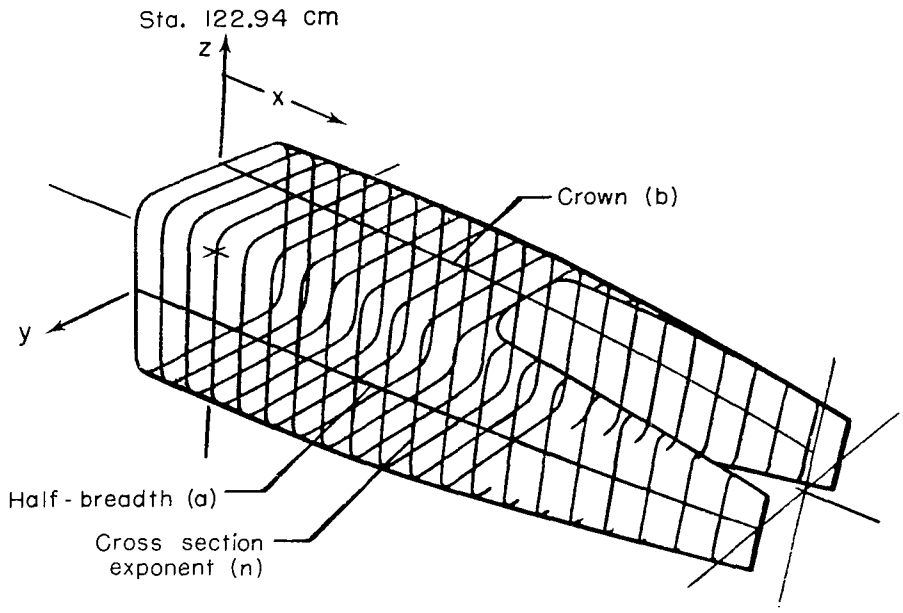

Perspective of a 6° boattail cowl

Super-Ellipse Equation

$$\left(\frac{z}{a}\right)^n + \left(\frac{y}{b}\right)^n = 1$$

where

$$a = -0.0173x + 6.601 - (0.0016x^2 - 0.203x + 15.910)^{1/2}$$

$$b = -102.776 + (-0.155x^2 + 38.11x + 8867.175)^{1/2}$$

If $122.94 \leqq x \leqq 151.05$ and $\frac{x}{l} = \frac{x - 122.94}{151.05 - 122.94}$

$$n = 9 + 3\frac{x}{l}$$

If $151.05 \leqq x \leqq 175.76$ and $\frac{x}{l} = \frac{x - 151.05}{175.76 - 151.05}$

$$n = 12 + 4\left[1 + \sin \pi\left(\frac{x}{l} + 1.5\right)\right]$$

Figure 5.- Typical computer-generated contour.

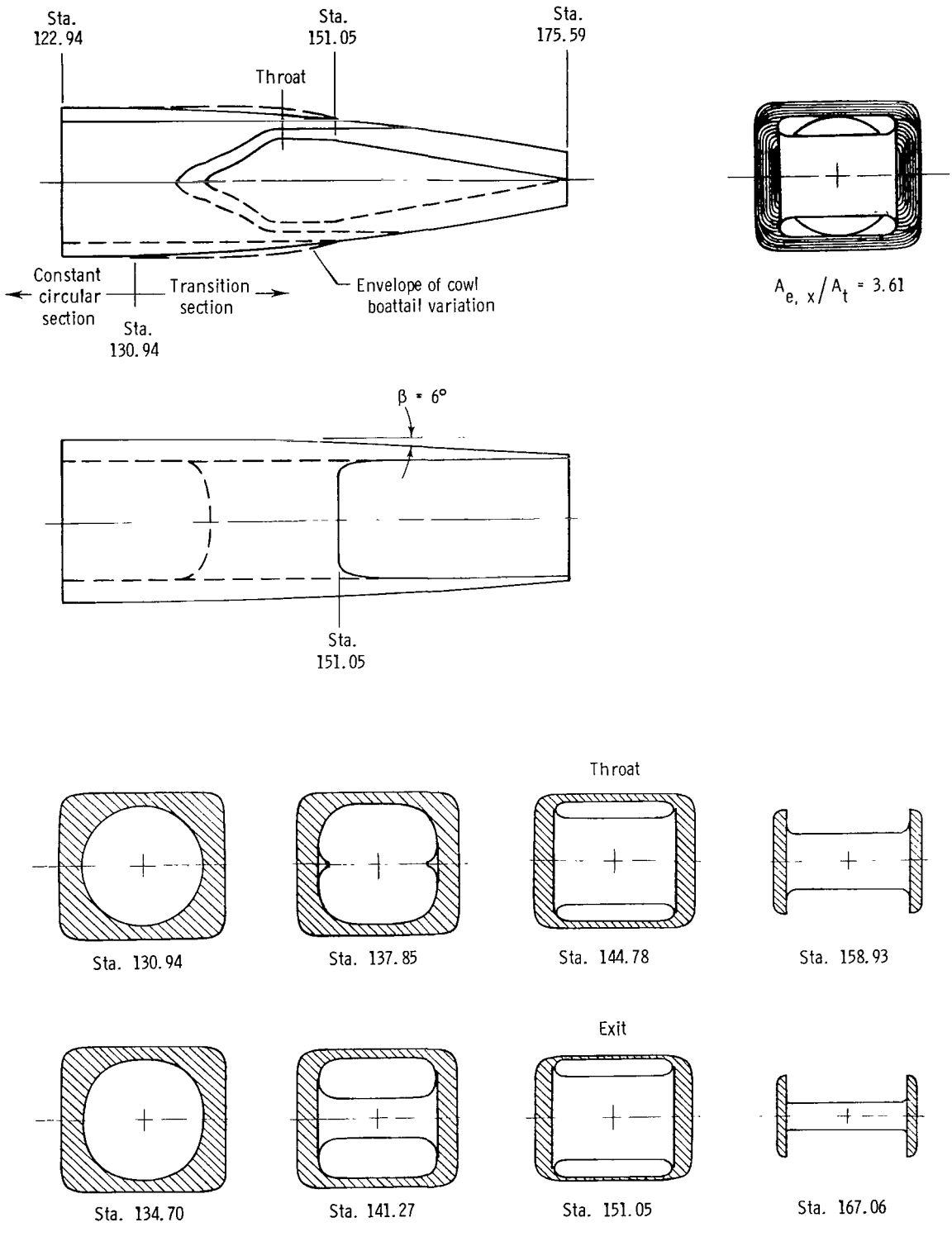

Figure 6.- Typical internal contours generated by super-ellipse equation. Dimensions and stations are given in centimeters.

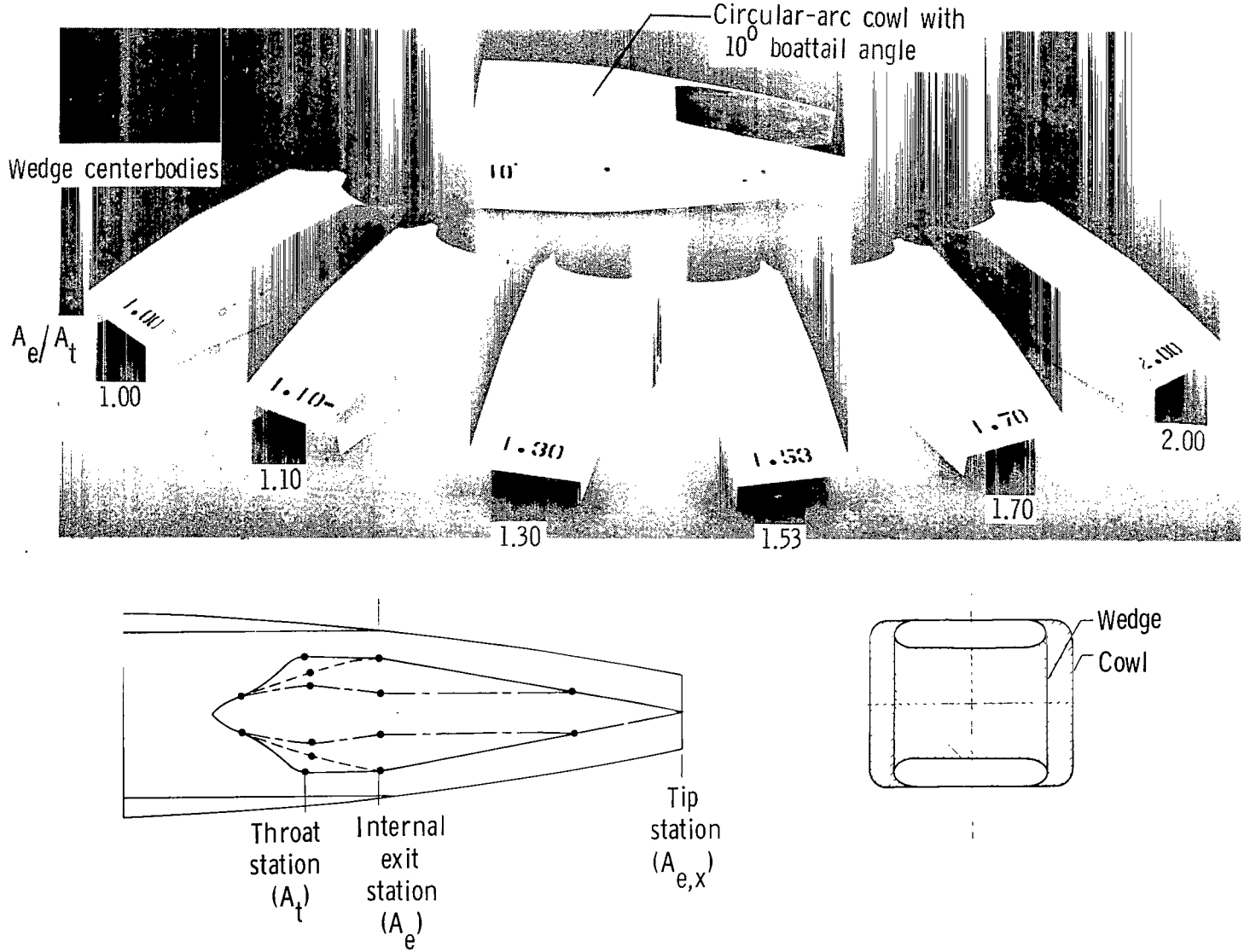

L-76-212

Figure 7.- Typical cowl and wedge centerbodies used to change internal expansion area ratio.

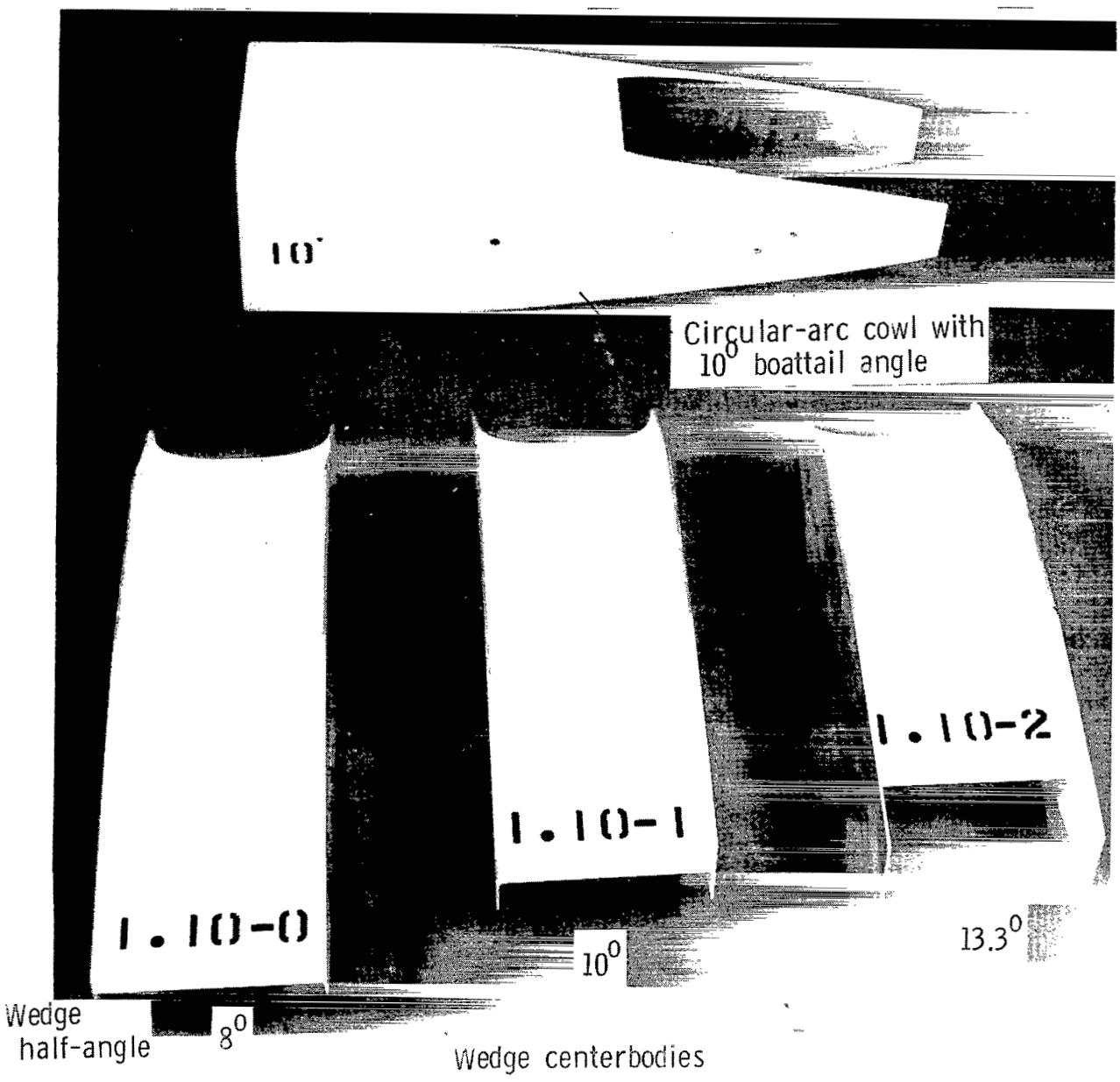

L-76-213

Figure 8.- Typical cowl and wedge centerbodies used to change wedge half-angle. $A_e/A_t = 1.10$.

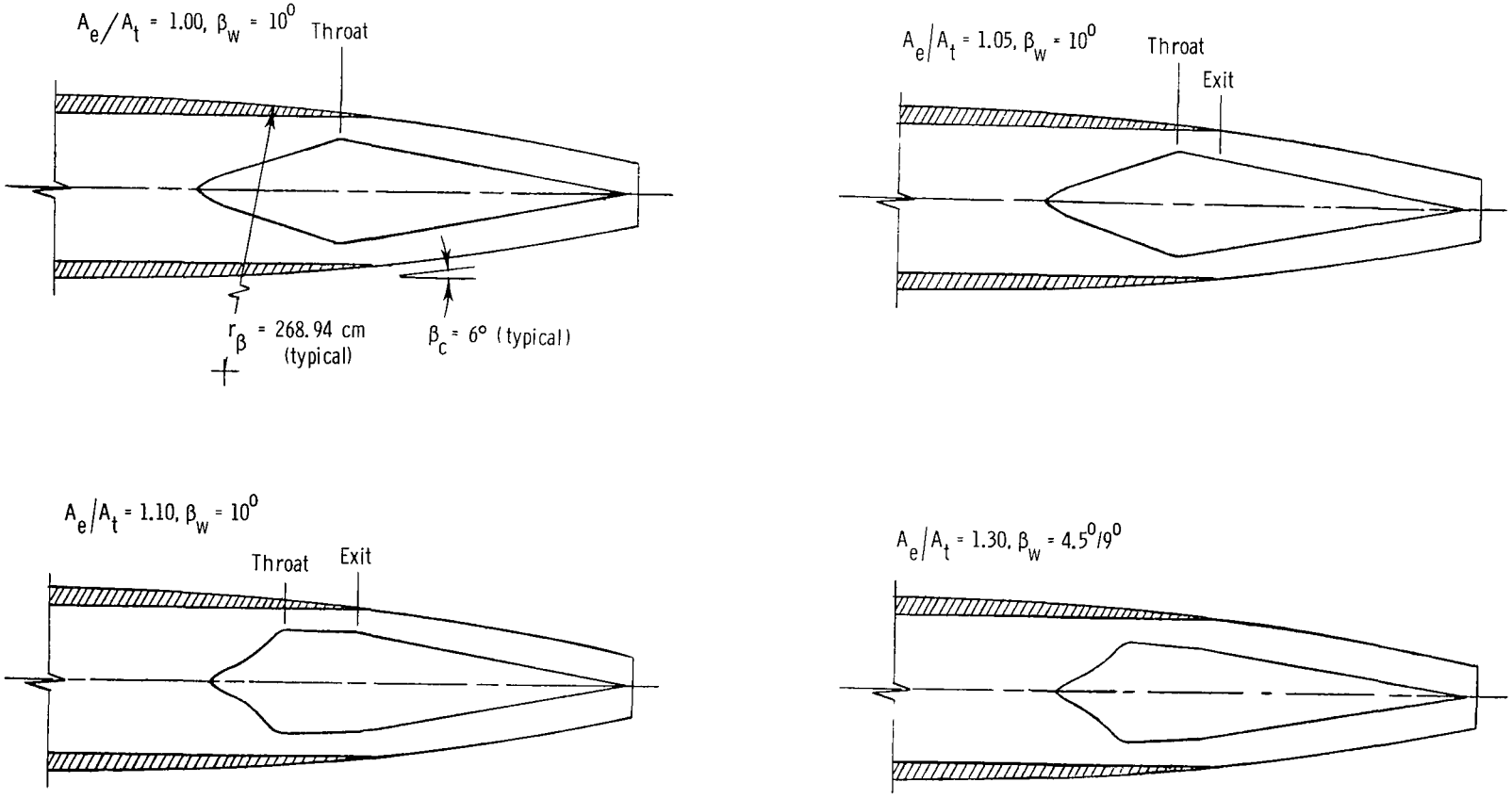

(a) Configurations with various internal expansion area ratios.

Figure 9.- Sketch of two-dimensional wedge nozzle configurations with 6° boattail cowl. $A_{e,x}/A_t = 3.61$.

$A_e/A_t = 1.53, \beta_w = 8^0$

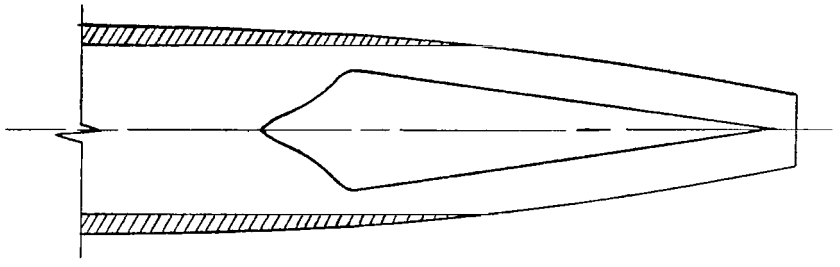

$A_e/A_t = 1.70$

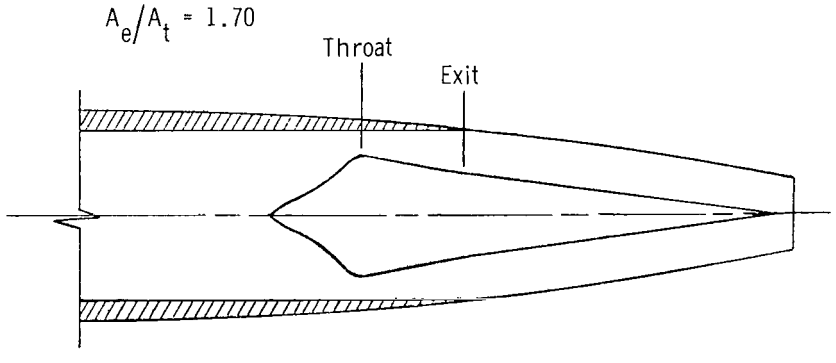

$A_e/A_t = 2.00$

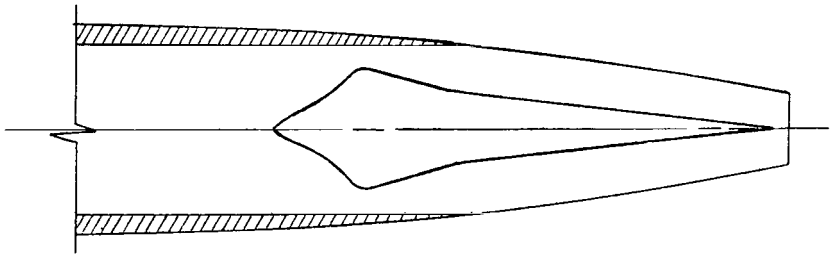

(a) Concluded.

Figure 9.- Continued.

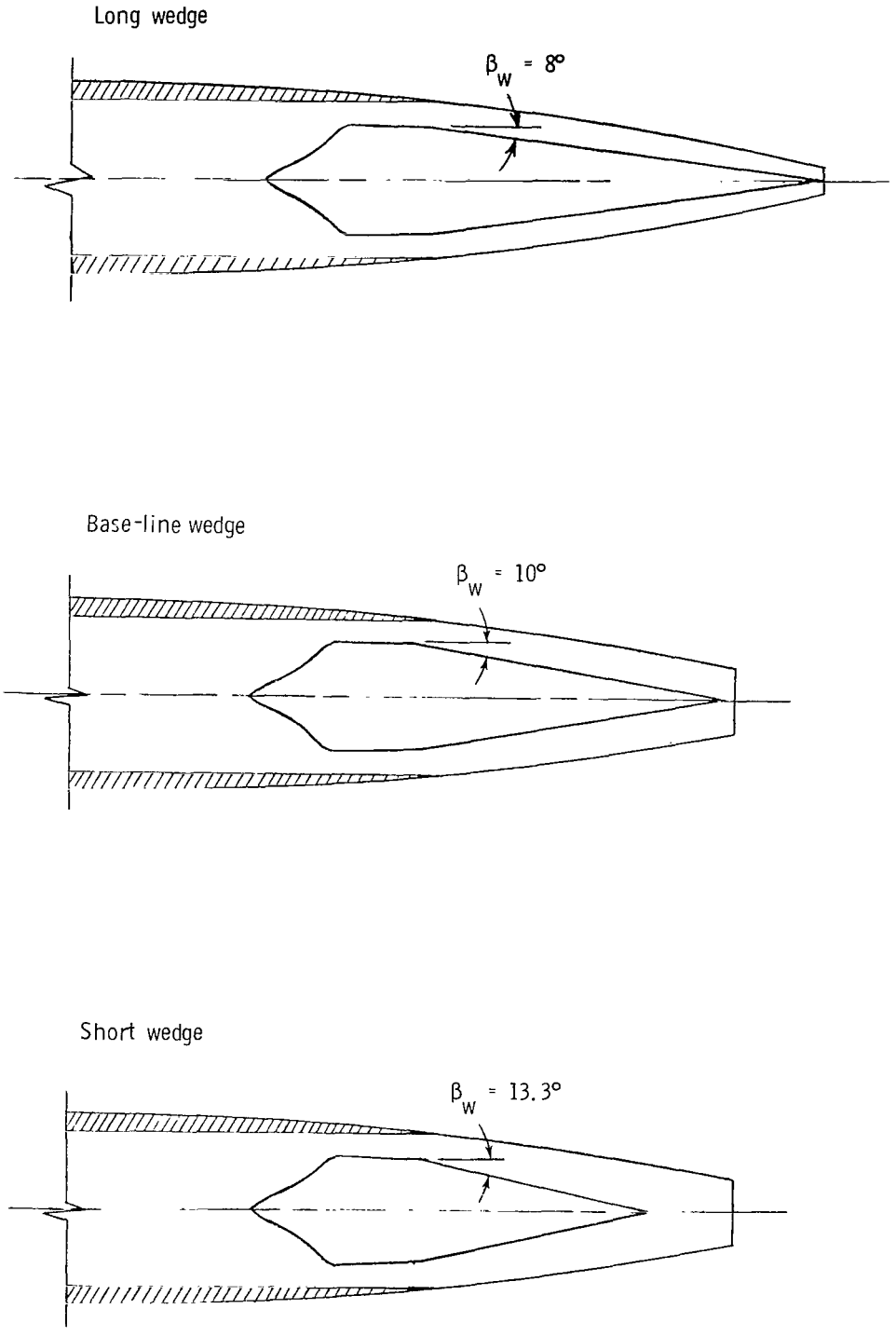

(b) Configurations with various wedge half-angles for $A_e/A_t = 1.10$.

Figure 9.- Concluded.

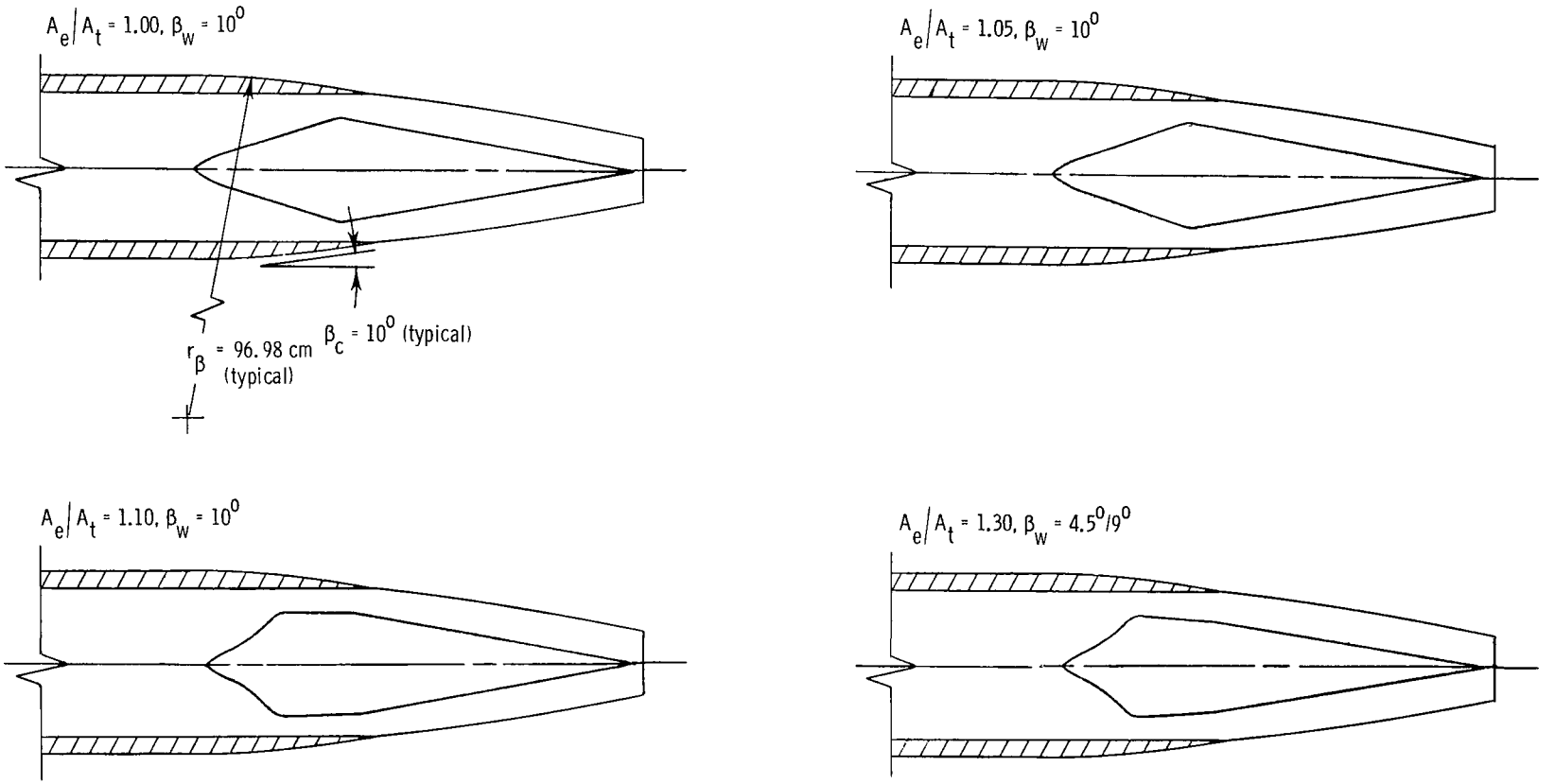

(a) Configurations with various expansion area ratios.

Figure 10.- Sketch of two-dimensional wedge nozzle configurations with 10^0 boattail cowl. $A_{e,x}/A_t = 3.61$.

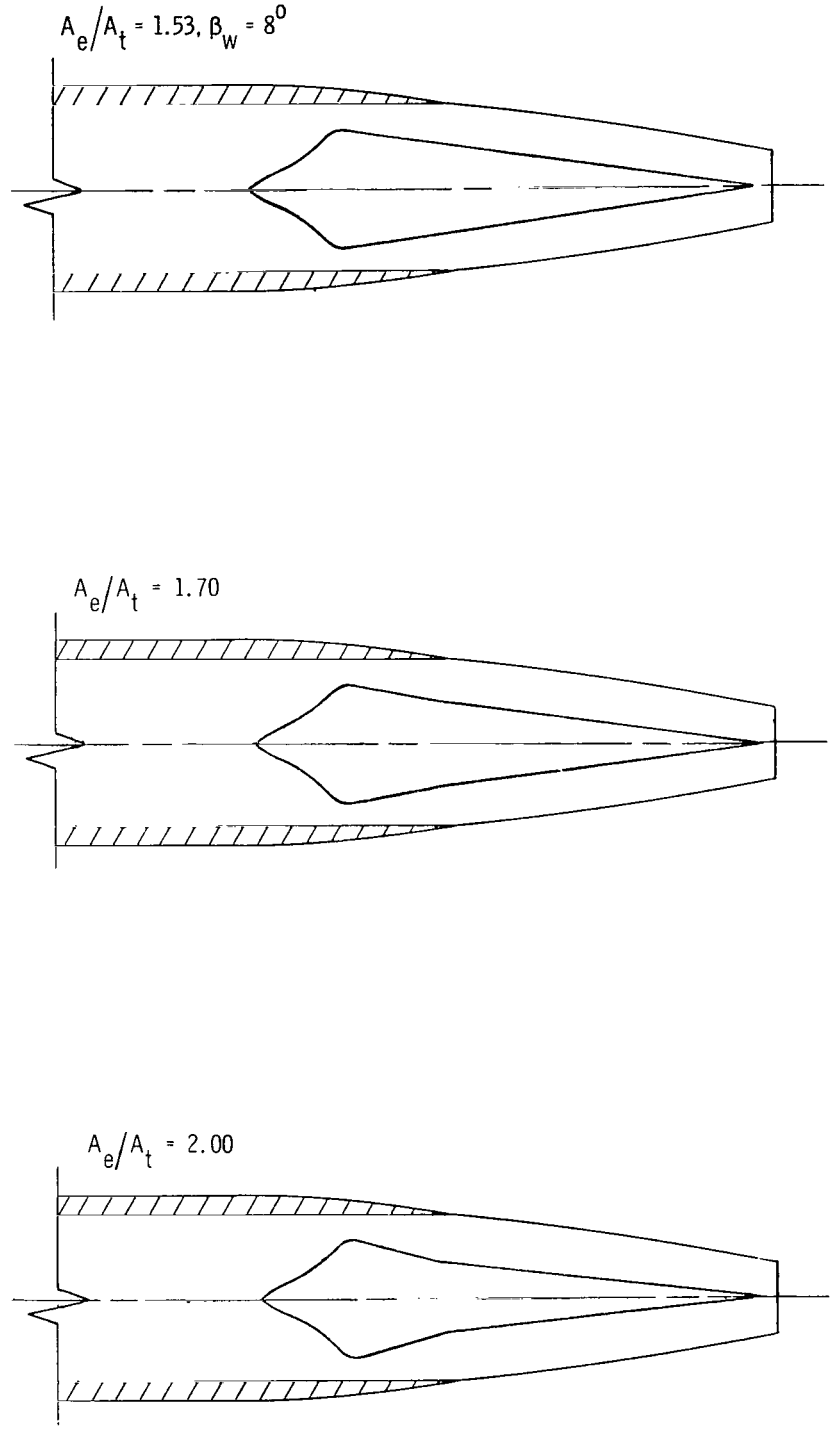

(a) Concluded.

Figure 10.- Continued.

A_e/A_t = 1.10, short wedge

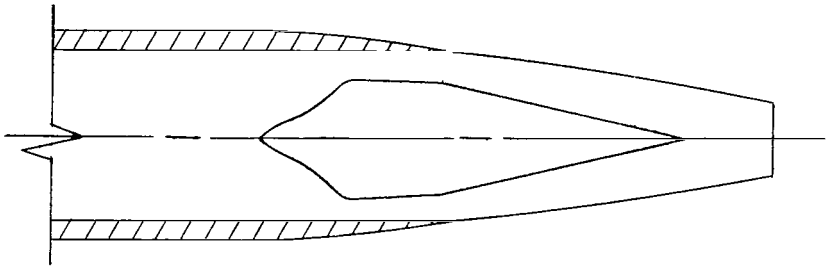

A_e/A_t = 1.53, parabolic L.E. wedge profile

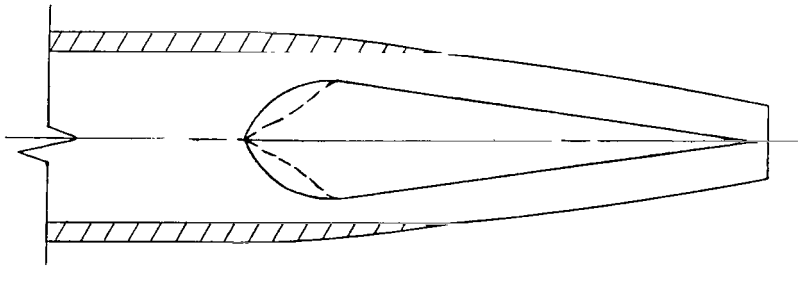

(b) Configurations with wedges other than base line.

Figure 10.- Concluded.

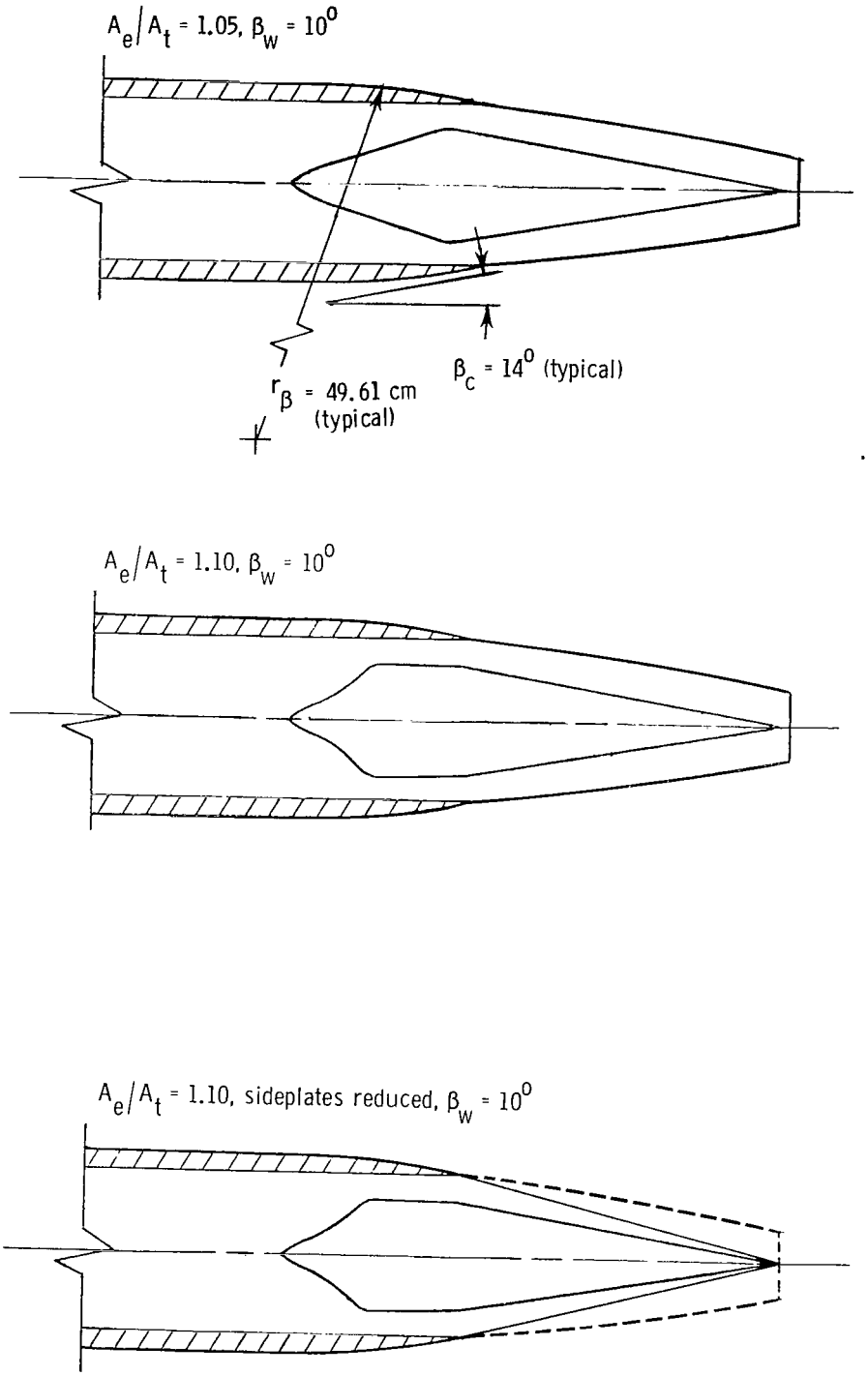

Figure 11.- Sketch of two-dimensional wedge nozzle configurations with 14° boattail cowl. $A_{e,x}/A_t$ = 3.61.

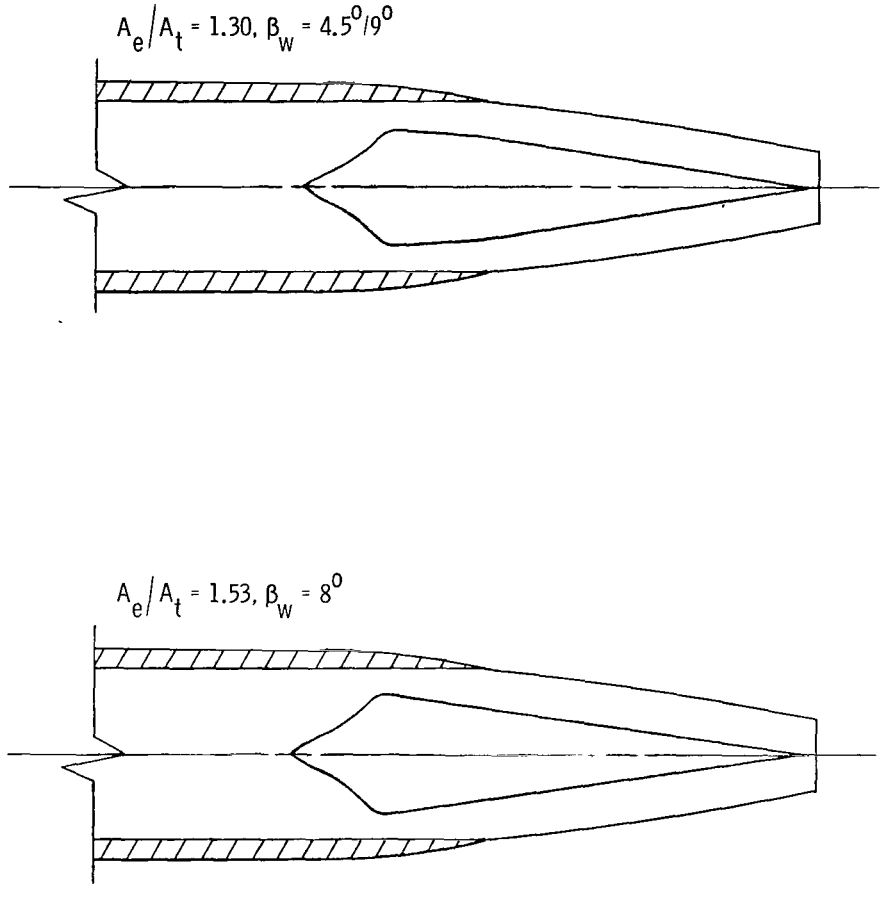

Figure 11.- Concluded.

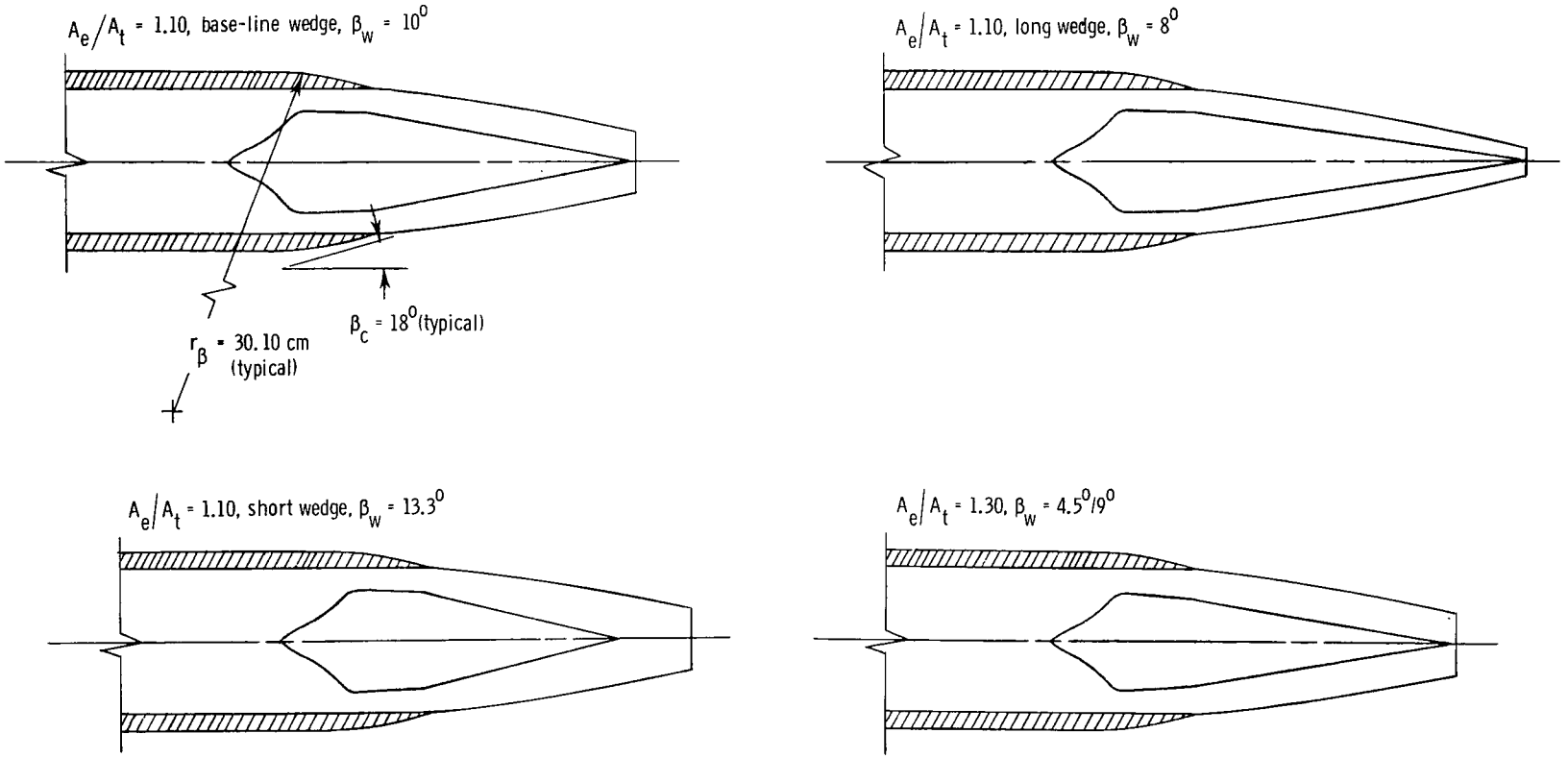

Figure 12.- Sketch of two-dimensional wedge nozzle configurations with 18° boattail cowl. $A_{e,x}/A_t$ = 3.61.

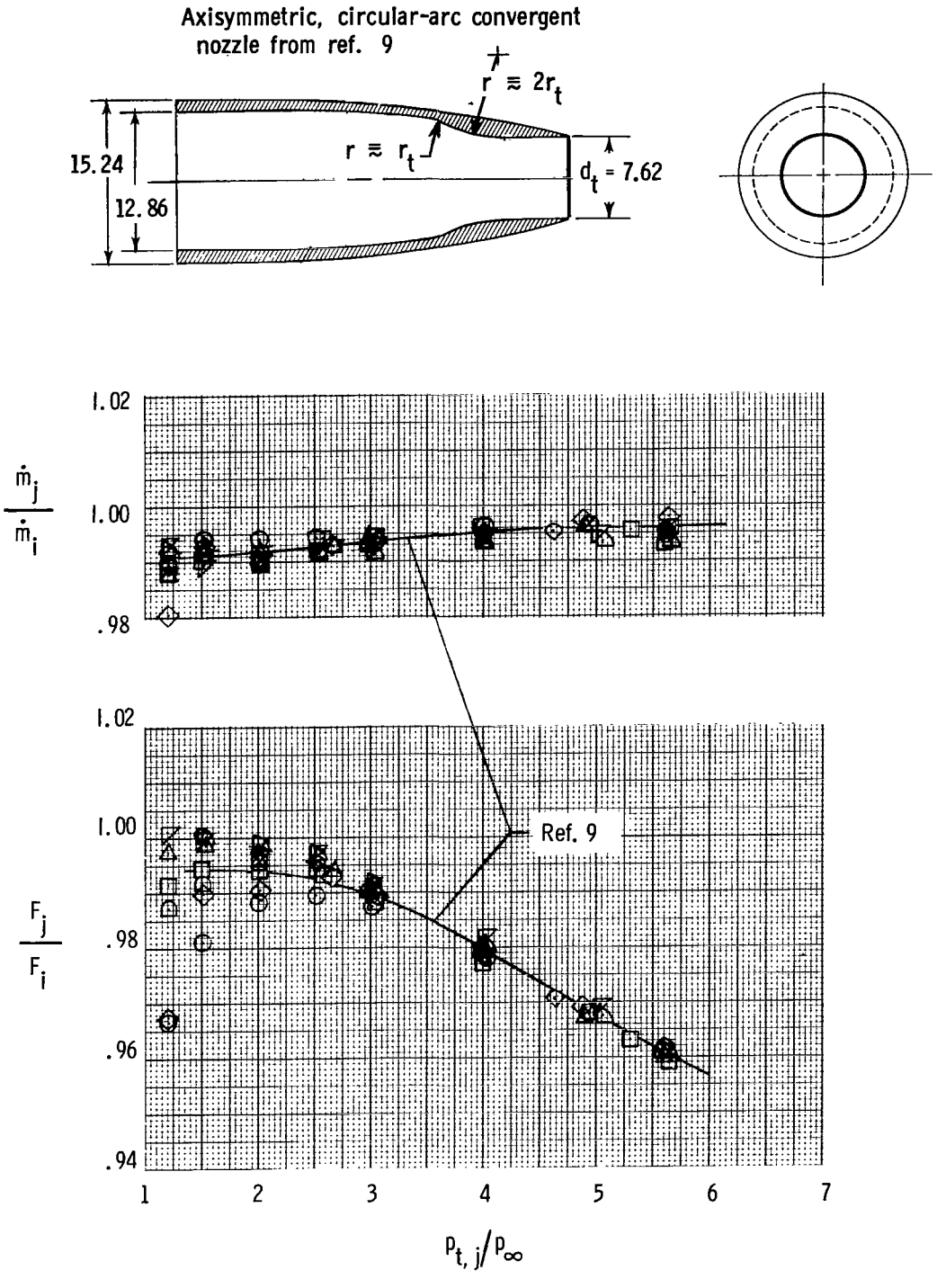

(a) Installed in Langley 16-foot transonic tunnel.

Figure 13.- Static performance of convergent nozzle used as calibration for air-powered nacelle. All dimensions are in centimeters. Test-point symbols denote repeat tests.

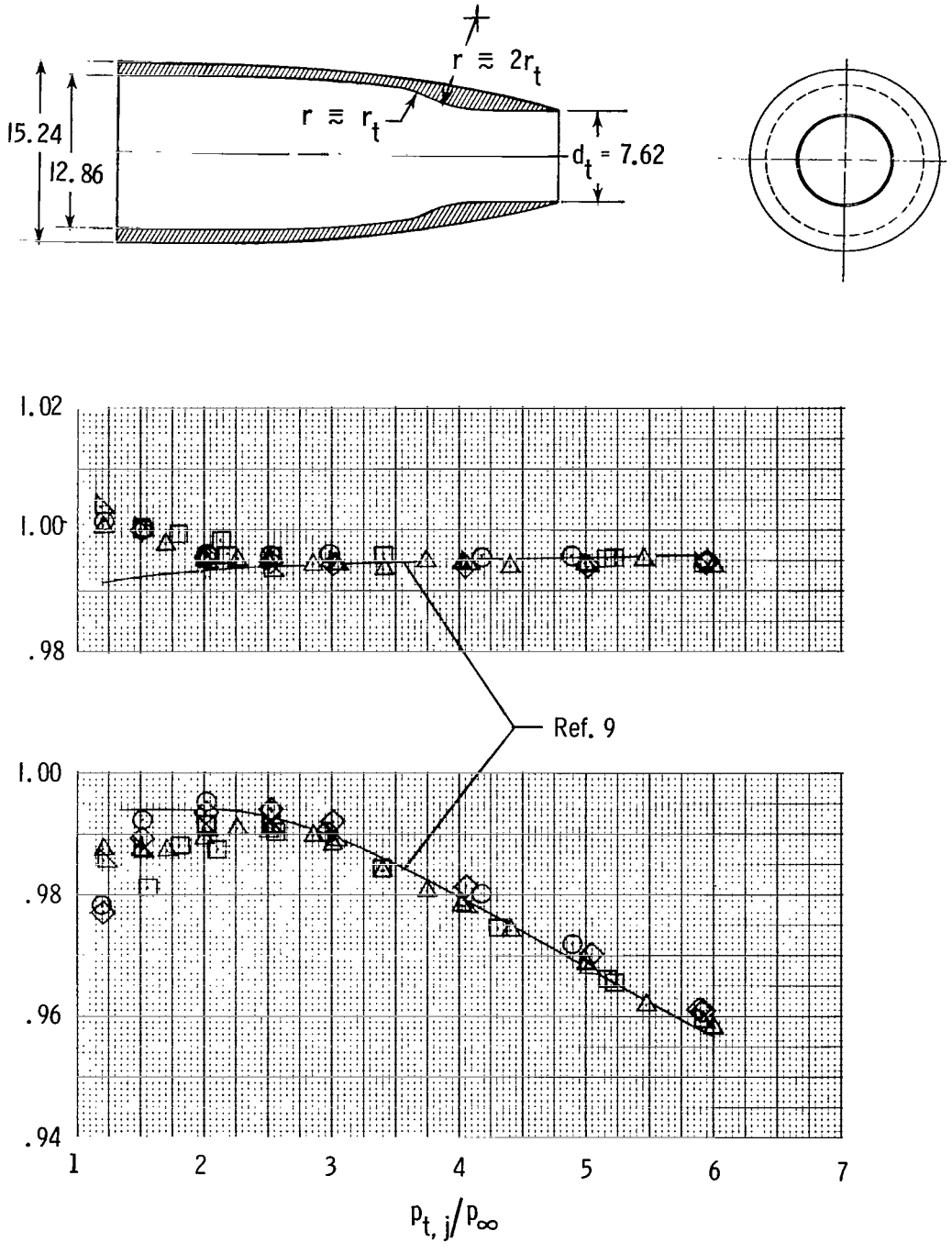

(b) Installed in Langley 4-foot supersonic pressure tunnel.

Figure 13.- Concluded.

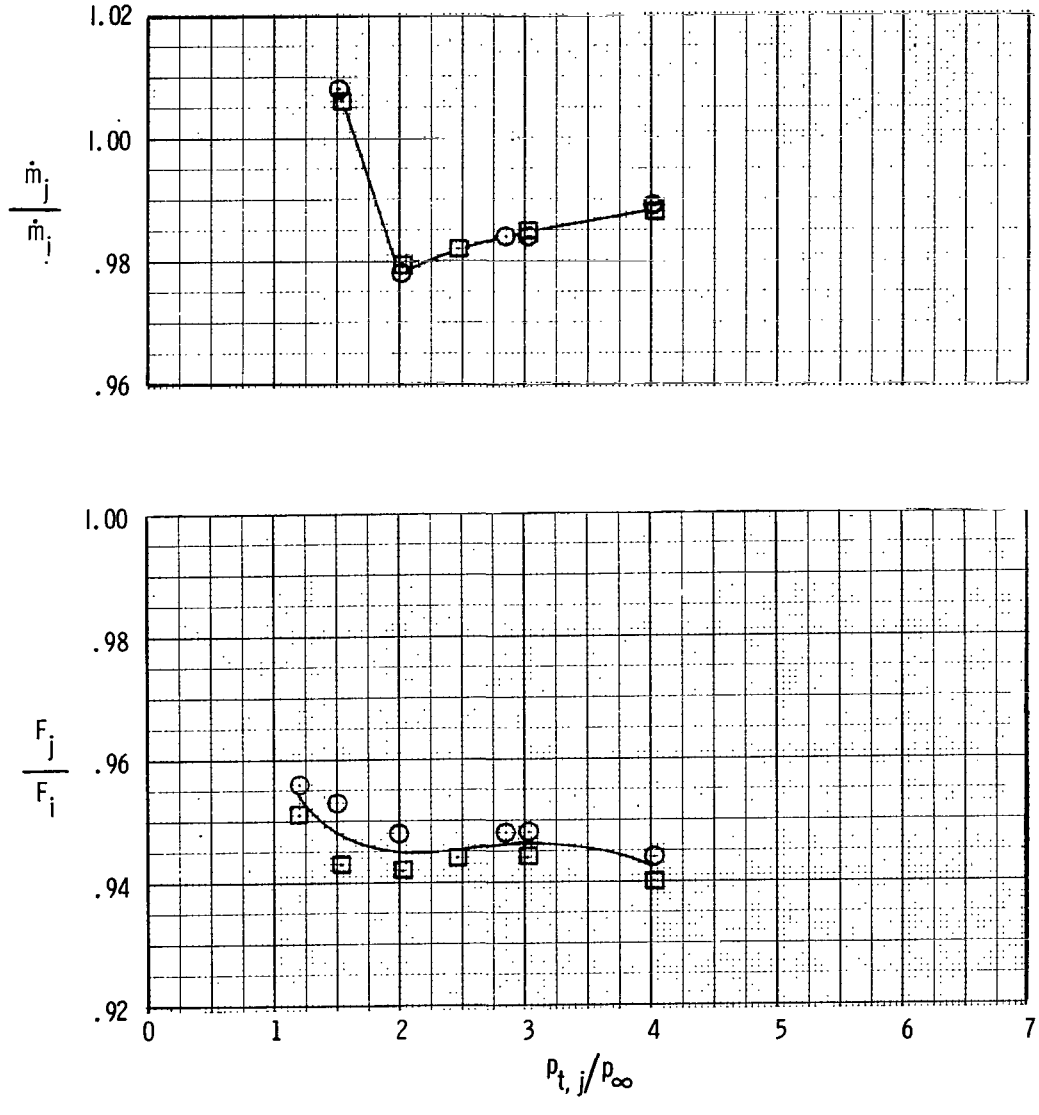

(a) $A_e/A_t = 1.00$; $\beta_w = 10^o$.

Figure 14.- Static performance characteristics of configurations with 6^o boattail cowl. Test-point symbols denote repeat tests.

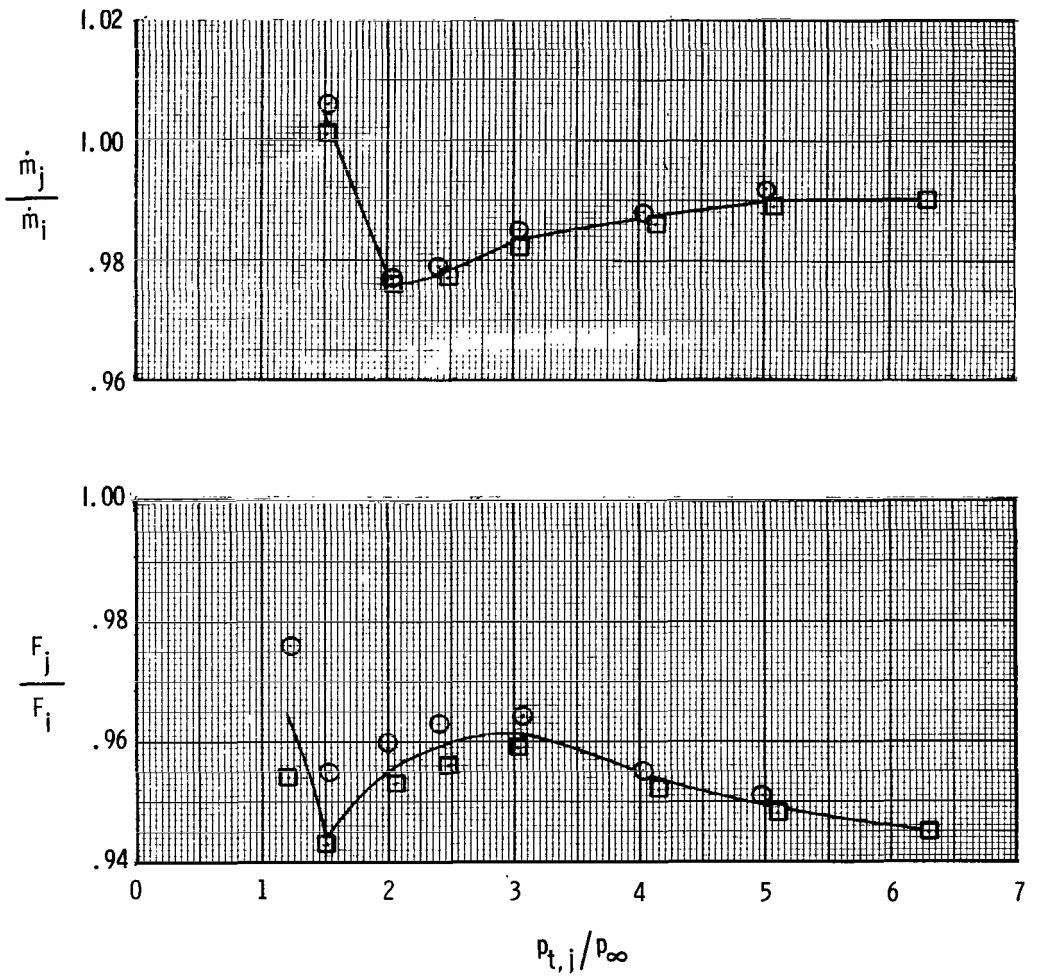

(b) $A_e/A_t = 1.05$; $\beta_w = 10^o$.

Figure 14.- Continued.

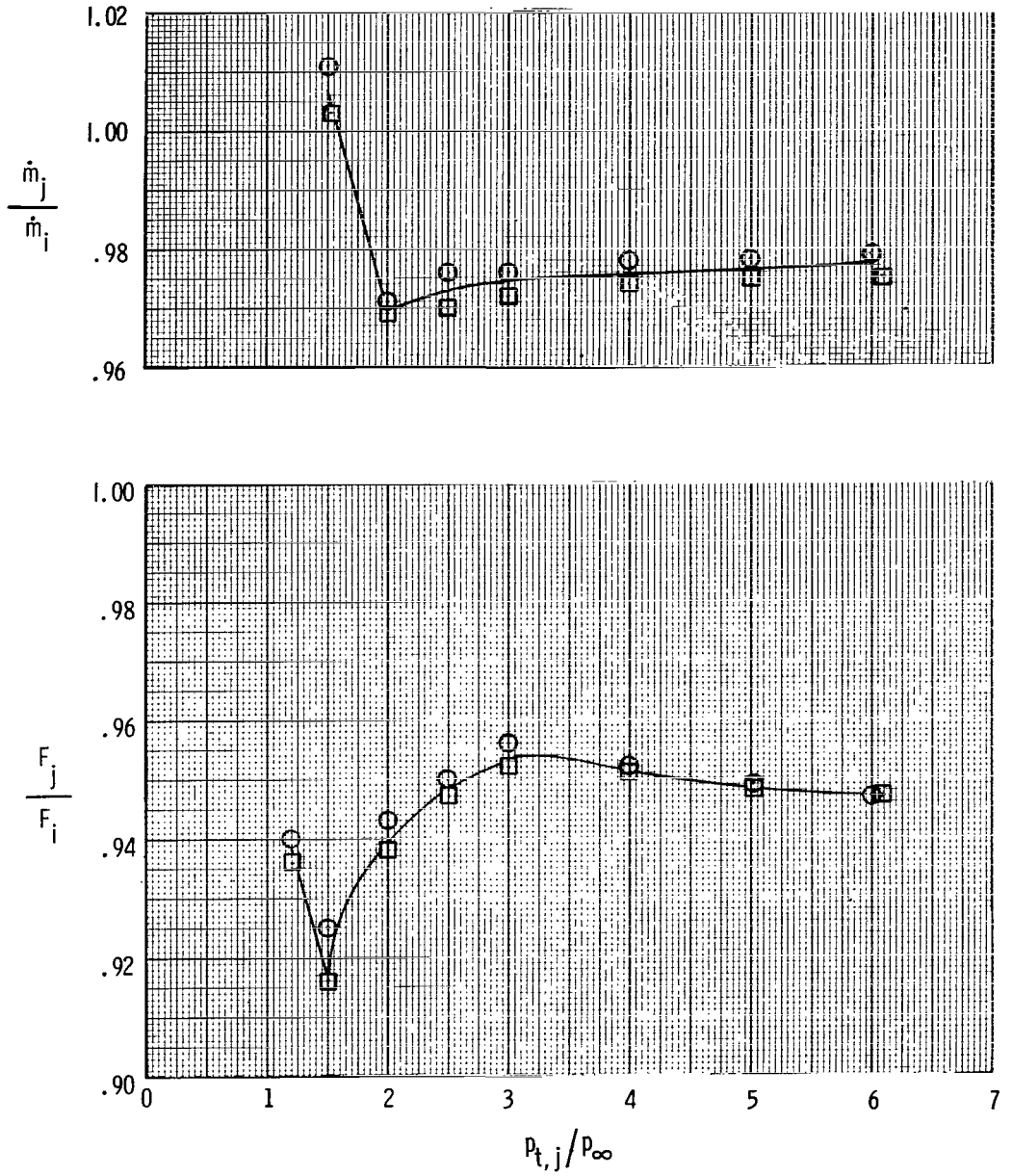

(c) $A_e/A_t = 1.10$; base-line wedge; $\beta_w = 10^o$.

Figure 14.- Continued.

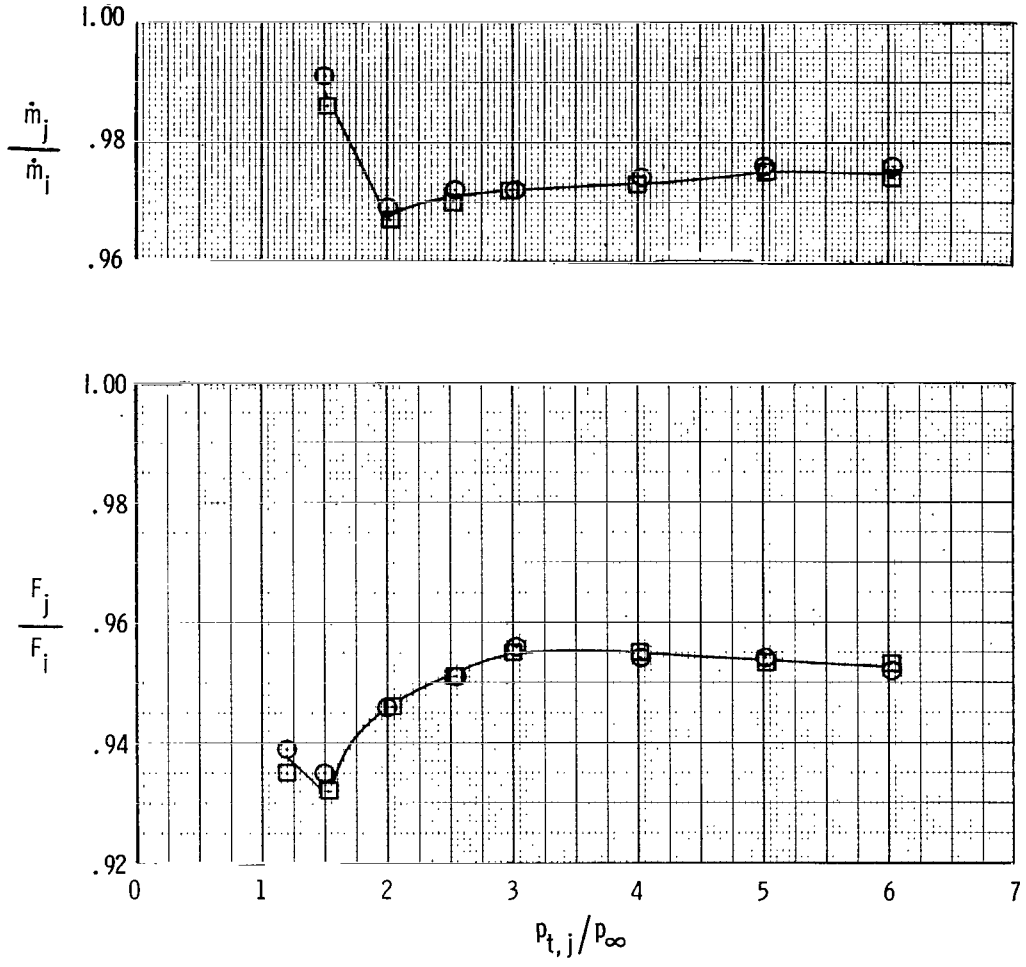

(d) $A_e/A_t = 1.10$; long wedge; $\beta_w = 8^o$.

Figure 14.- Continued.

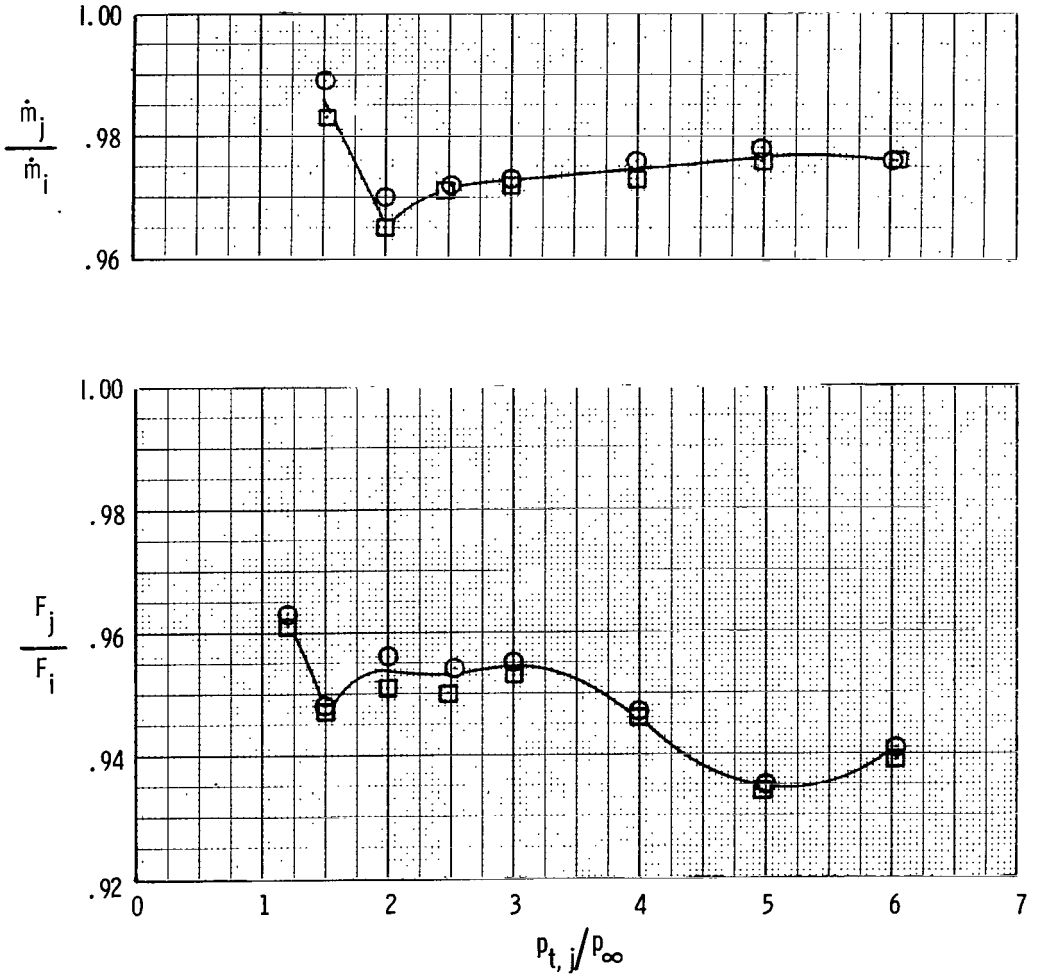

(e) $A_e/A_t = 1.10$; short wedge; $\beta_w = 13.3^o$.

Figure 14.- Continued.

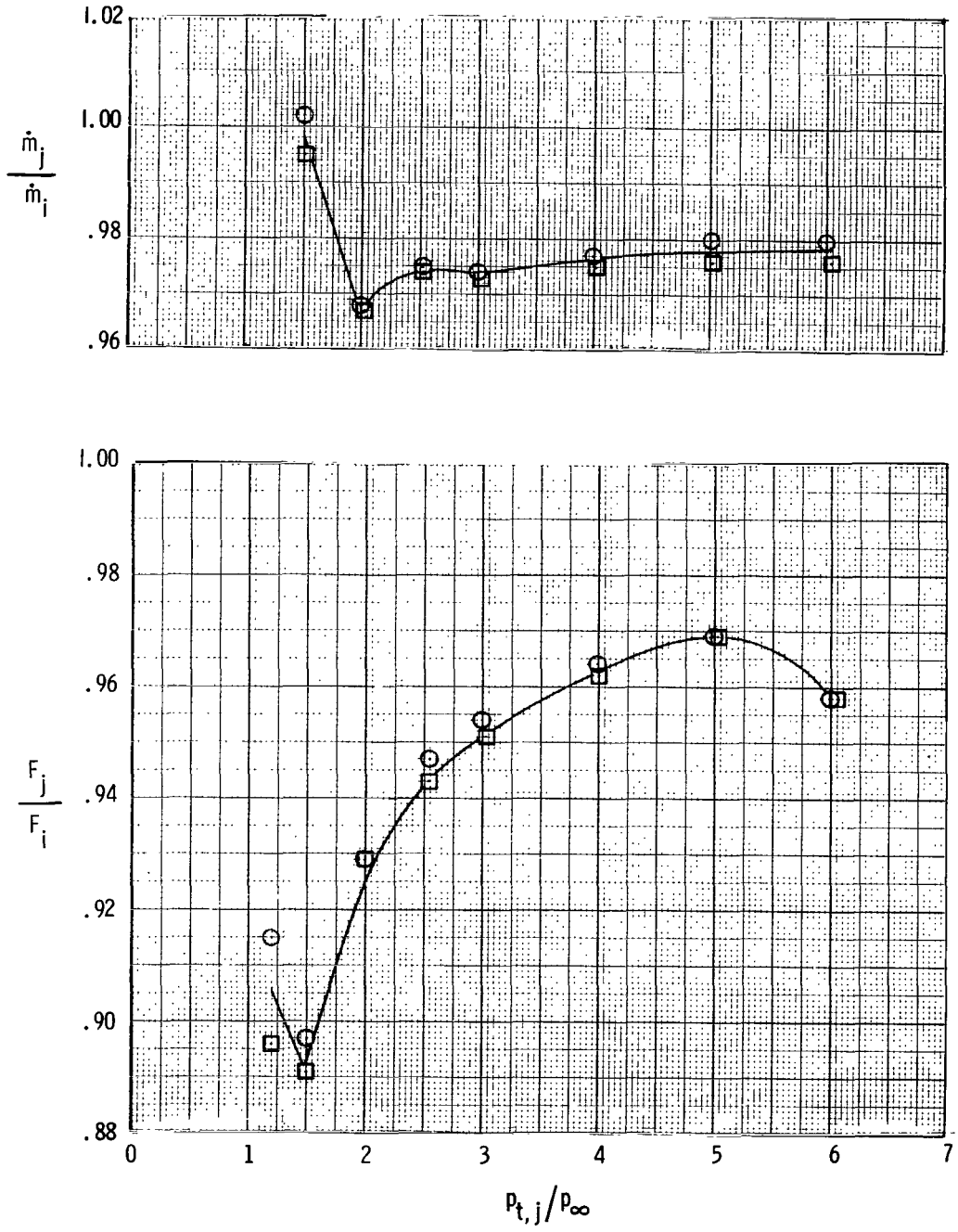

(f) $A_e/A_t = 1.30$; $\beta_w = 4.5^o/9^o$.

Figure 14.- Continued.

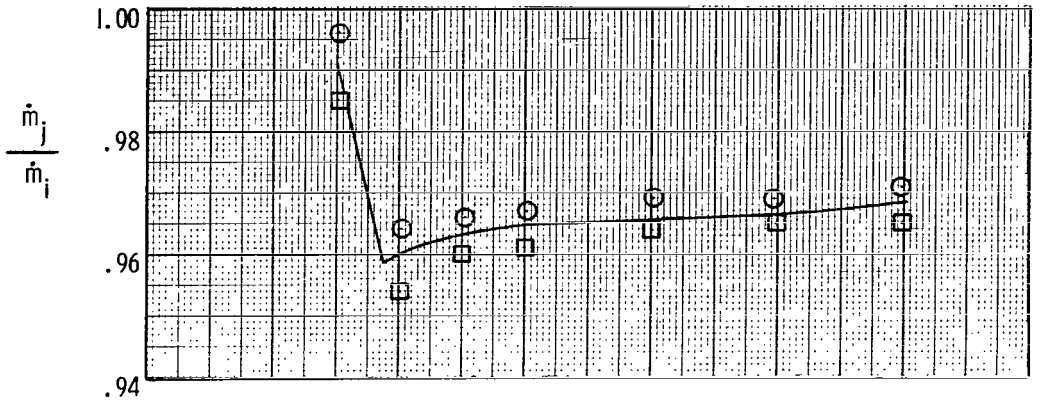

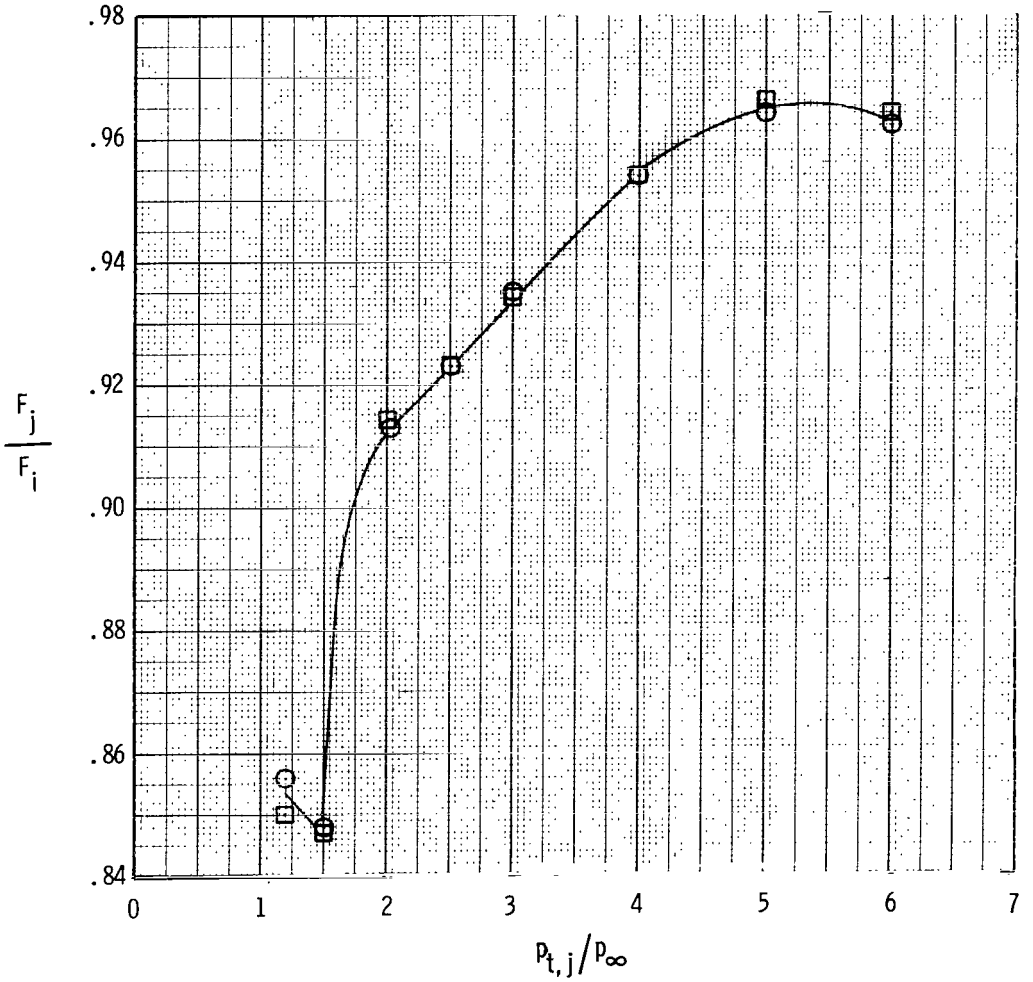

(g) $A_e/A_t = 1.53$; $\beta_w = 8^o$.

Figure 14.- Concluded.

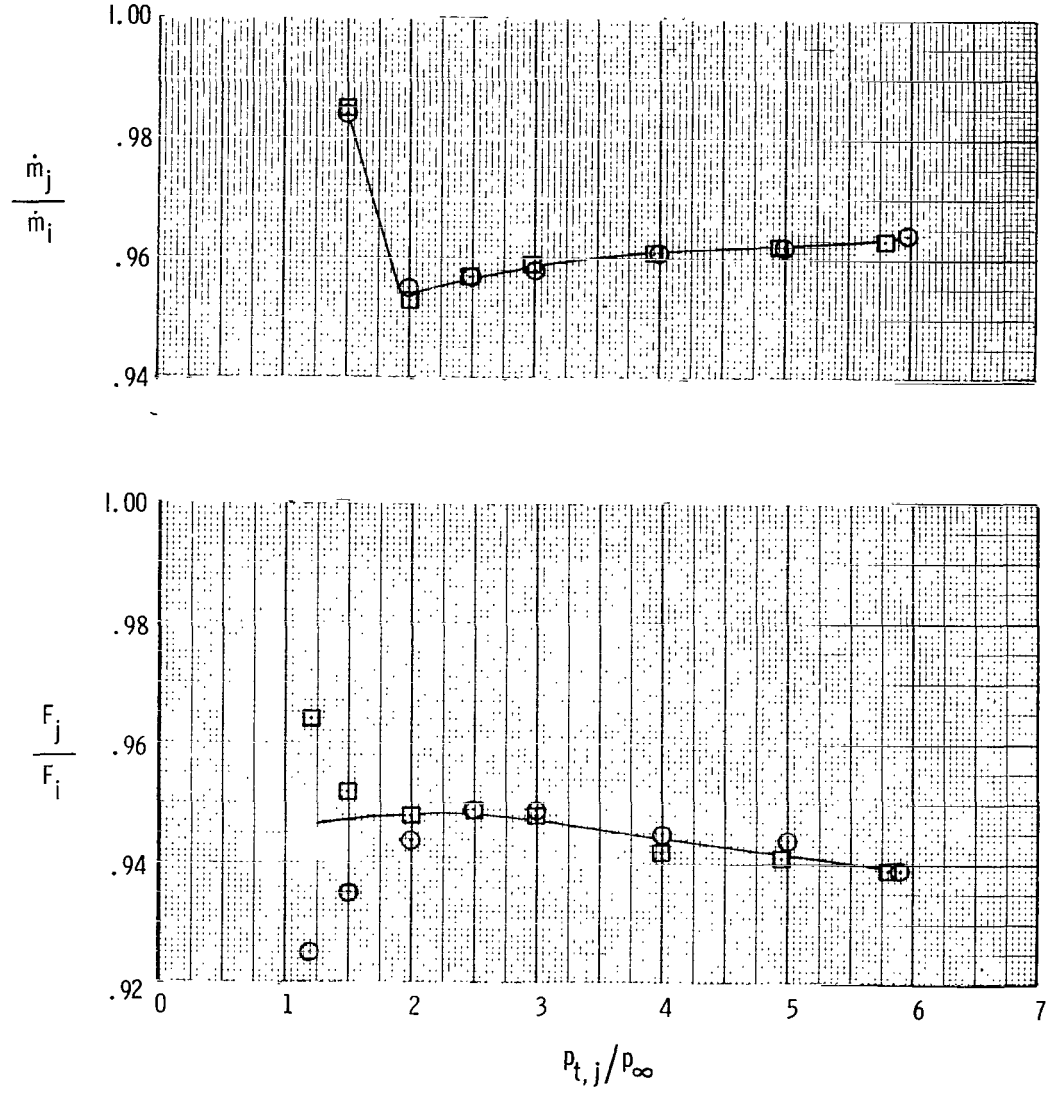

(a) $A_e/A_t = 1.00$; $\beta_w = 10^o$.

Figure 15.- Static performance characteristics of configurations with 10^o boattail cowls. Test-point symbols denote repeat tests.

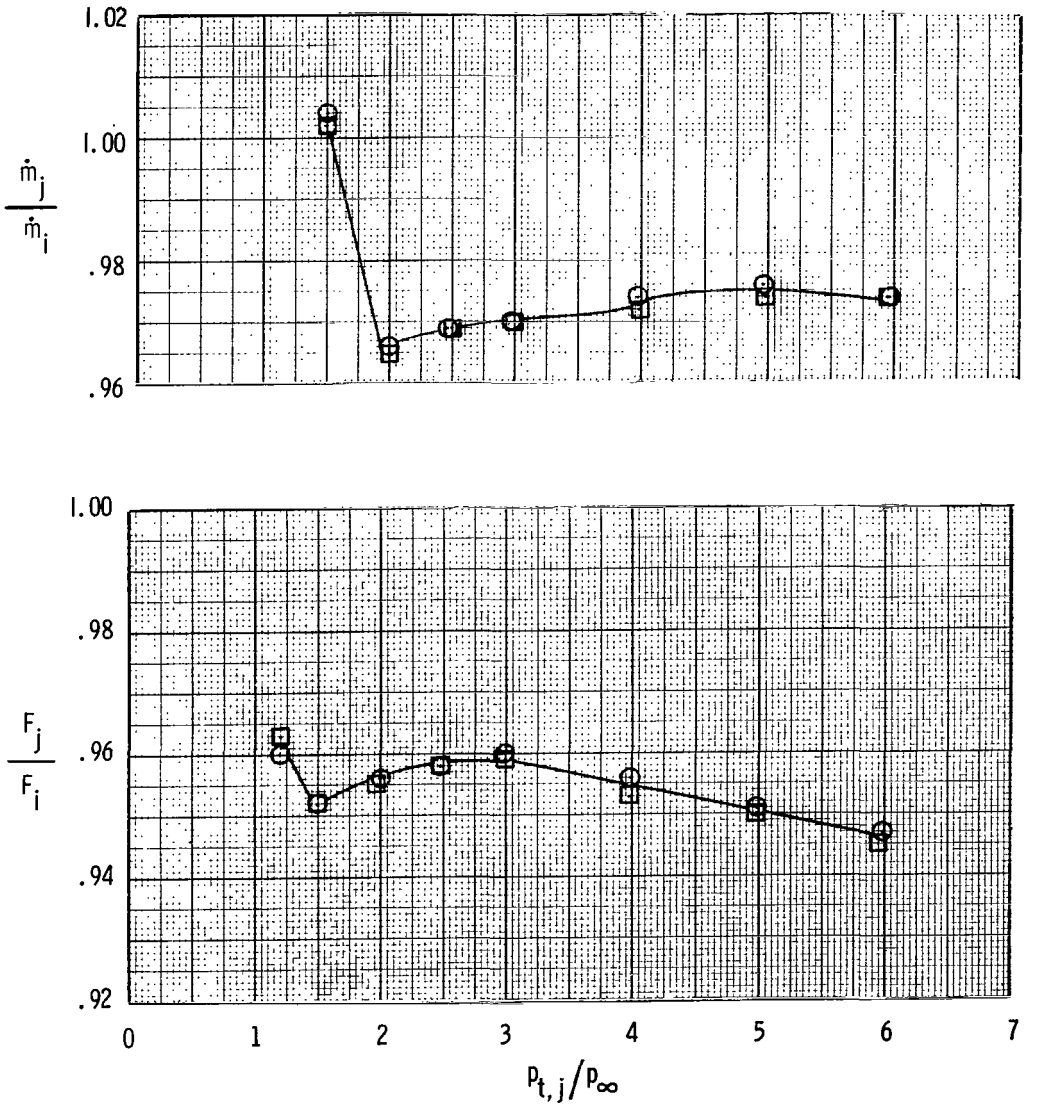

(b) $A_e/A_t = 1.05$; $\beta_w = 10^o$.

Figure 15.- Continued.

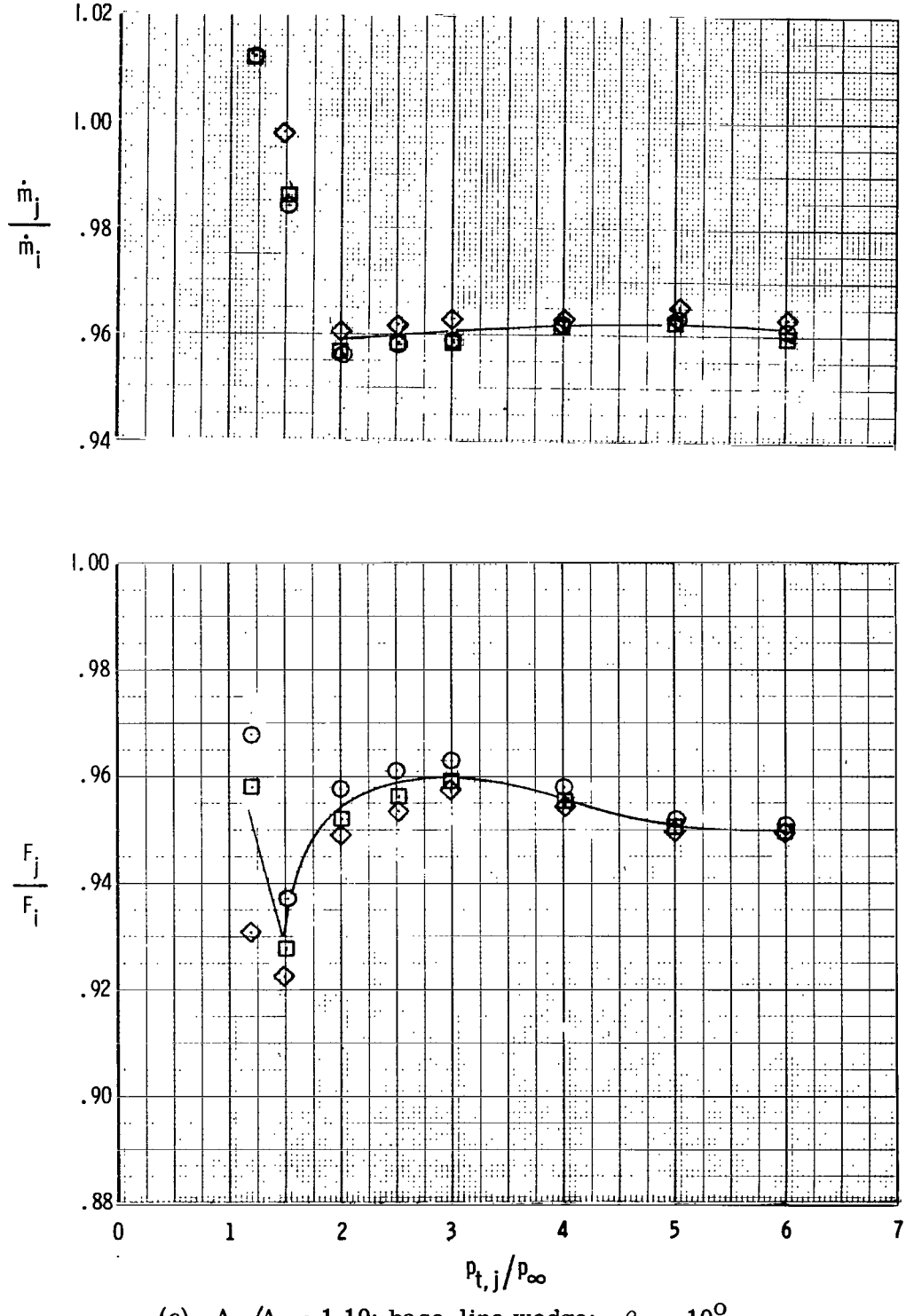

(c) $A_e/A_t = 1.10$; base-line wedge; $\beta_w = 10^o$.

Figure 15.- Continued.

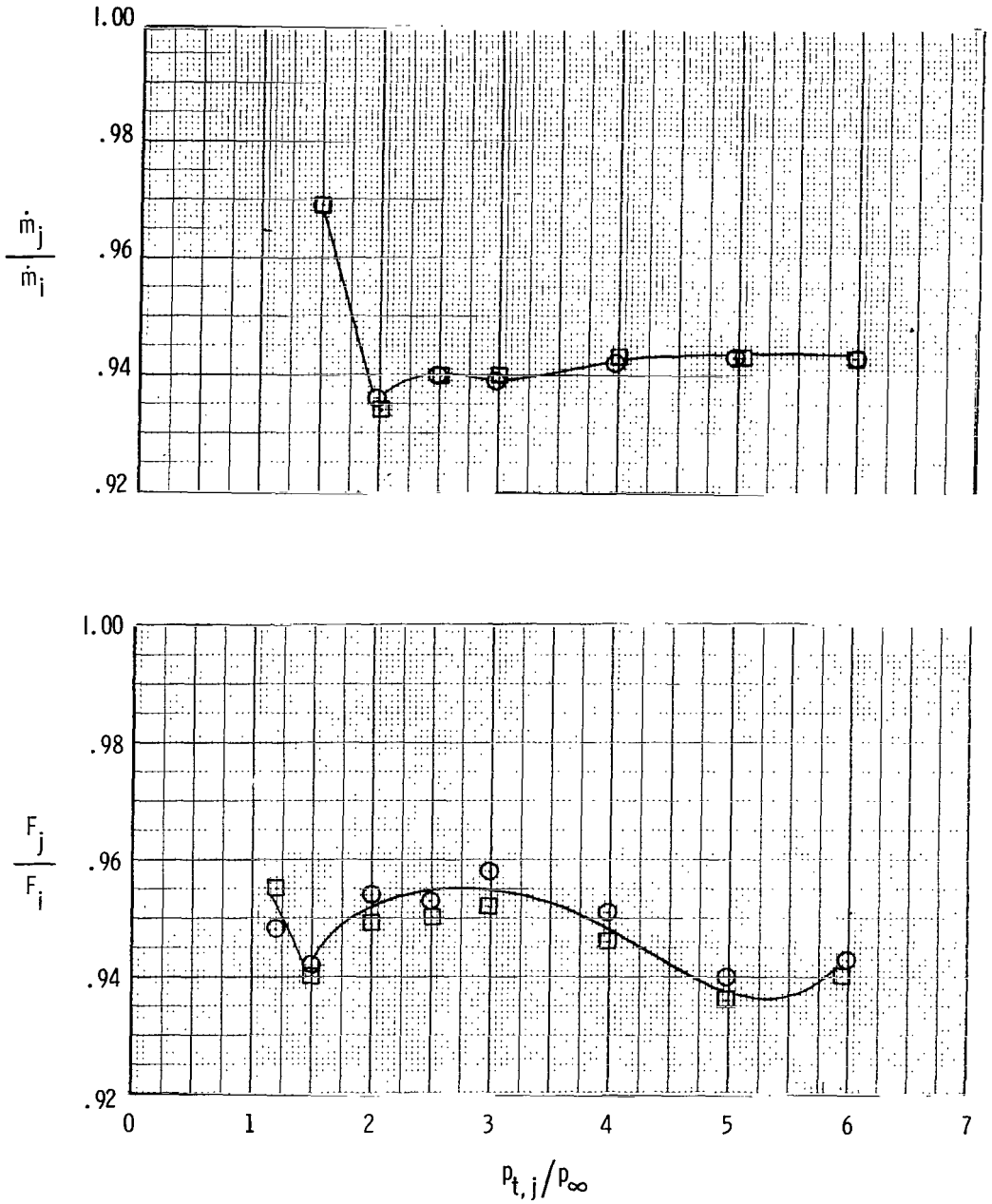

(d) $A_e/A_t = 1.10$; short wedge; $\beta_w = 13.3^o$.

Figure 15.- Continued.

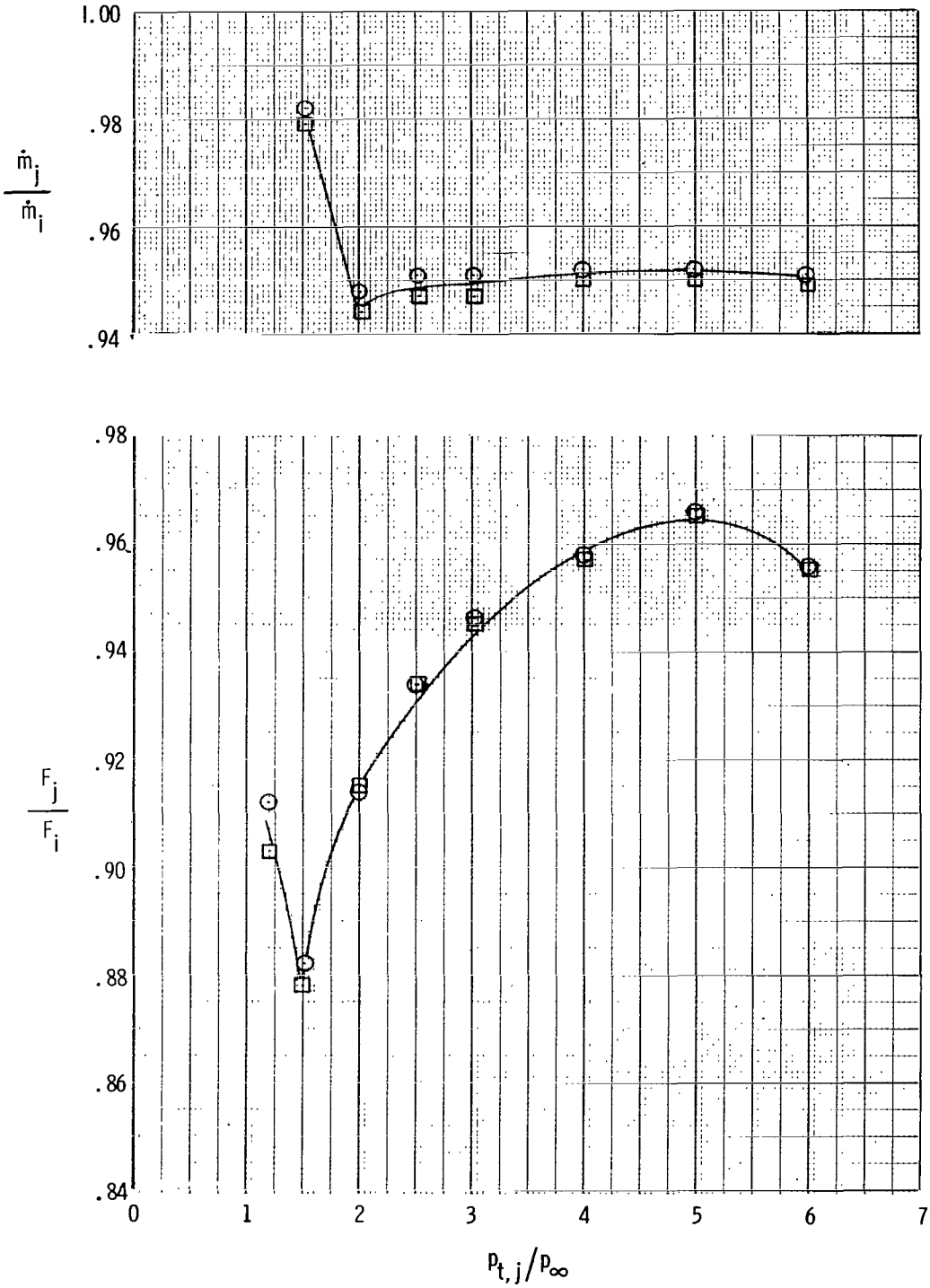

(e) $A_e/A_t = 1.30$; $\beta_w = 4.5^o/9^o$.

Figure 15.- Continued.

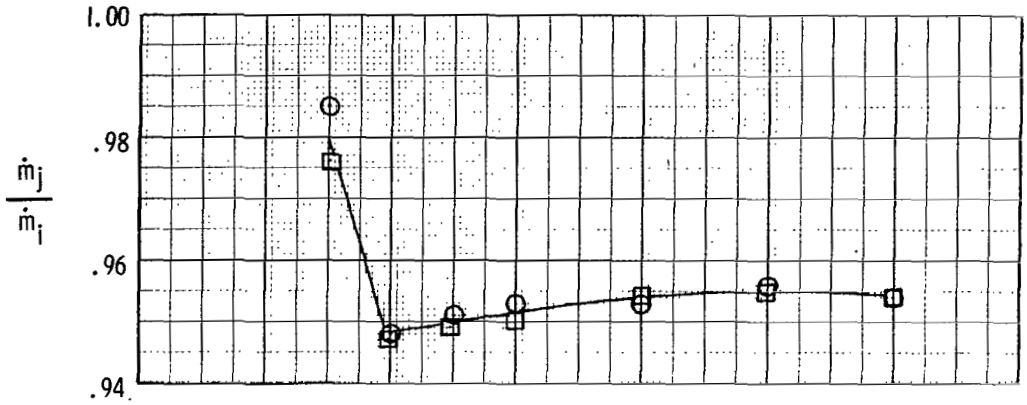

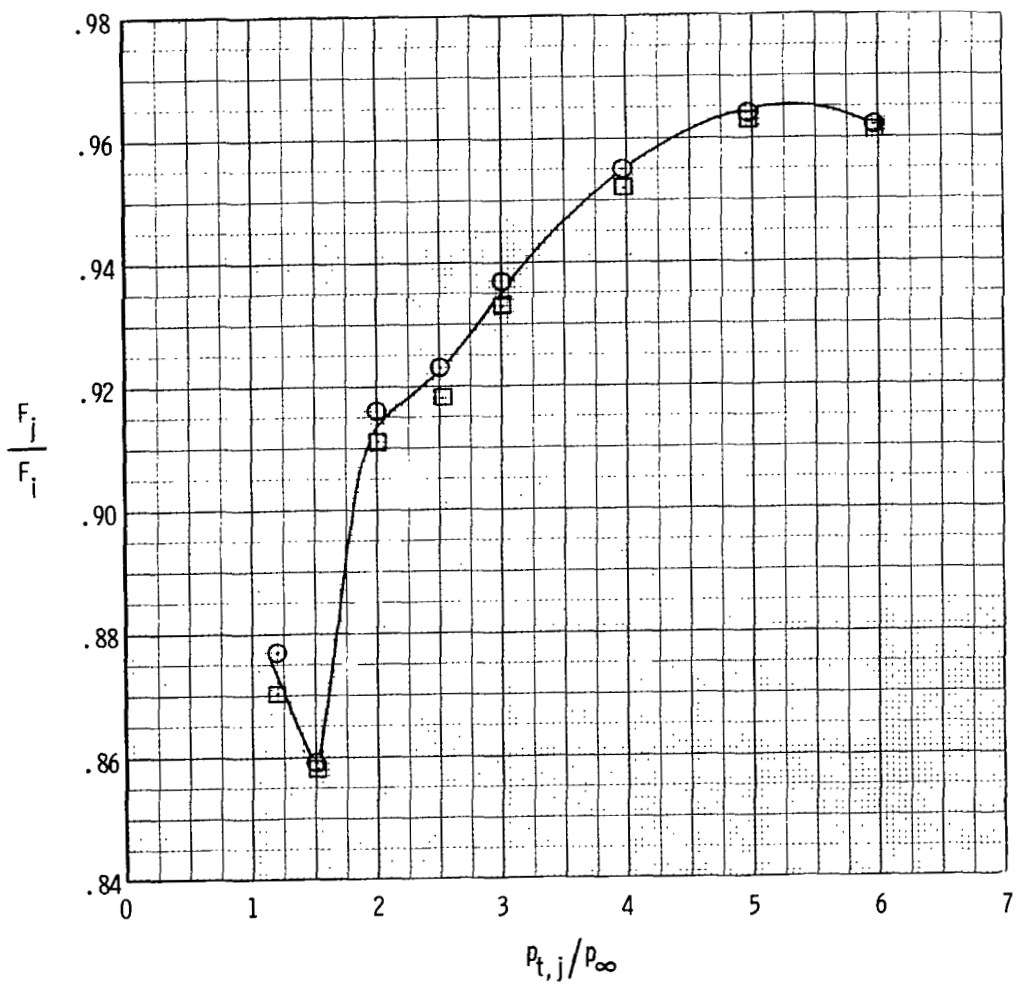

(f) $A_e/A_t = 1.53$; $\beta_w = 8^o$.

Figure 15.- Concluded.

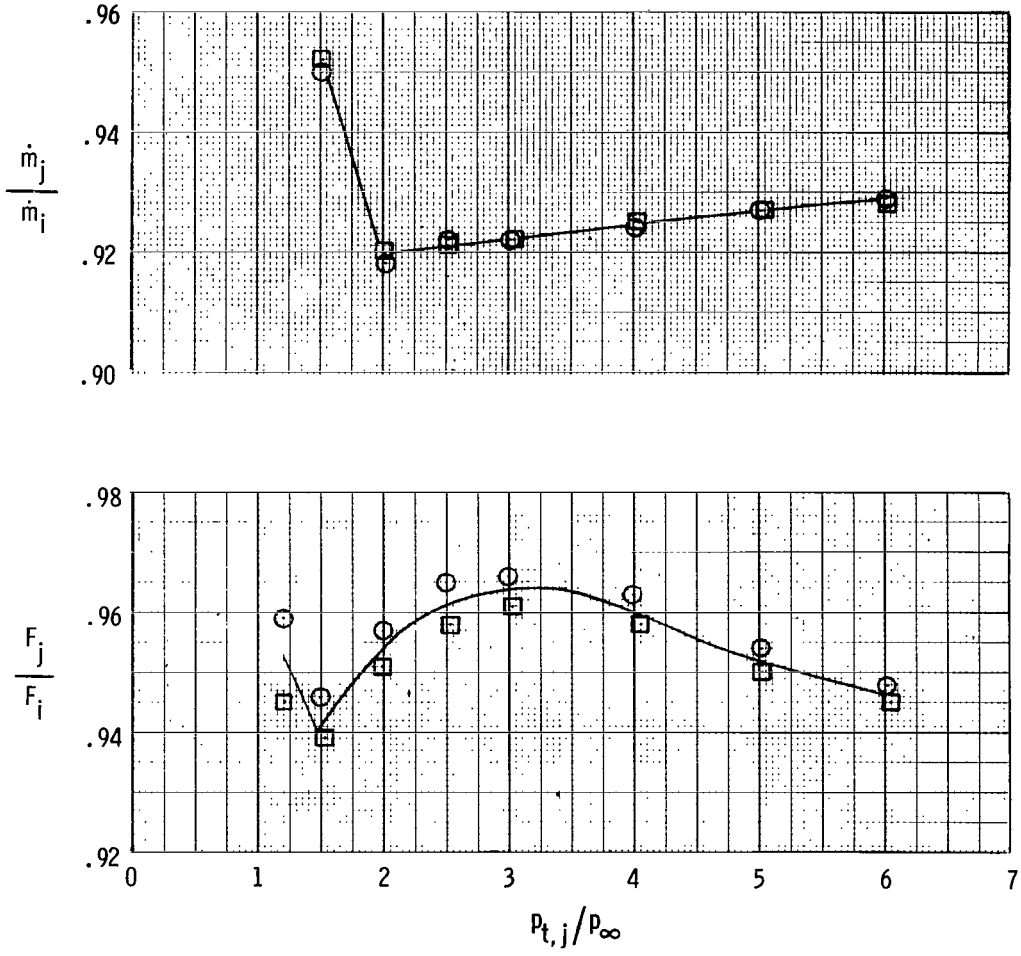

(a) $A_e/A_t = 1.05$; $\beta_w = 10^o$.

Figure 16.- Static performance characteristics of configurations with 14^o boattail cowls. Test-point symbols denote repeat tests.

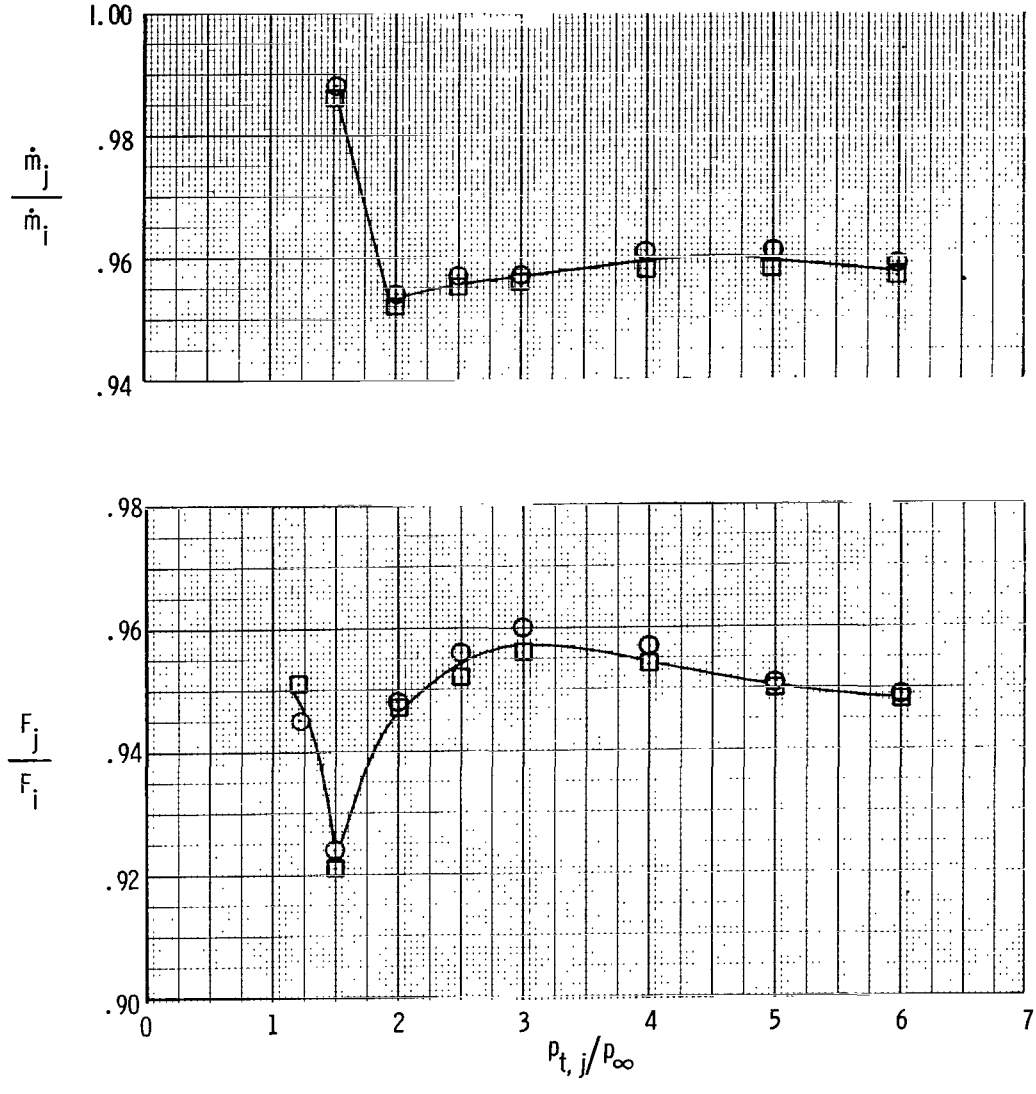

(b) $A_e/A_t = 1.10$; no sideplate reduction; $\beta_w = 10^o$.

Figure 16.- Continued.

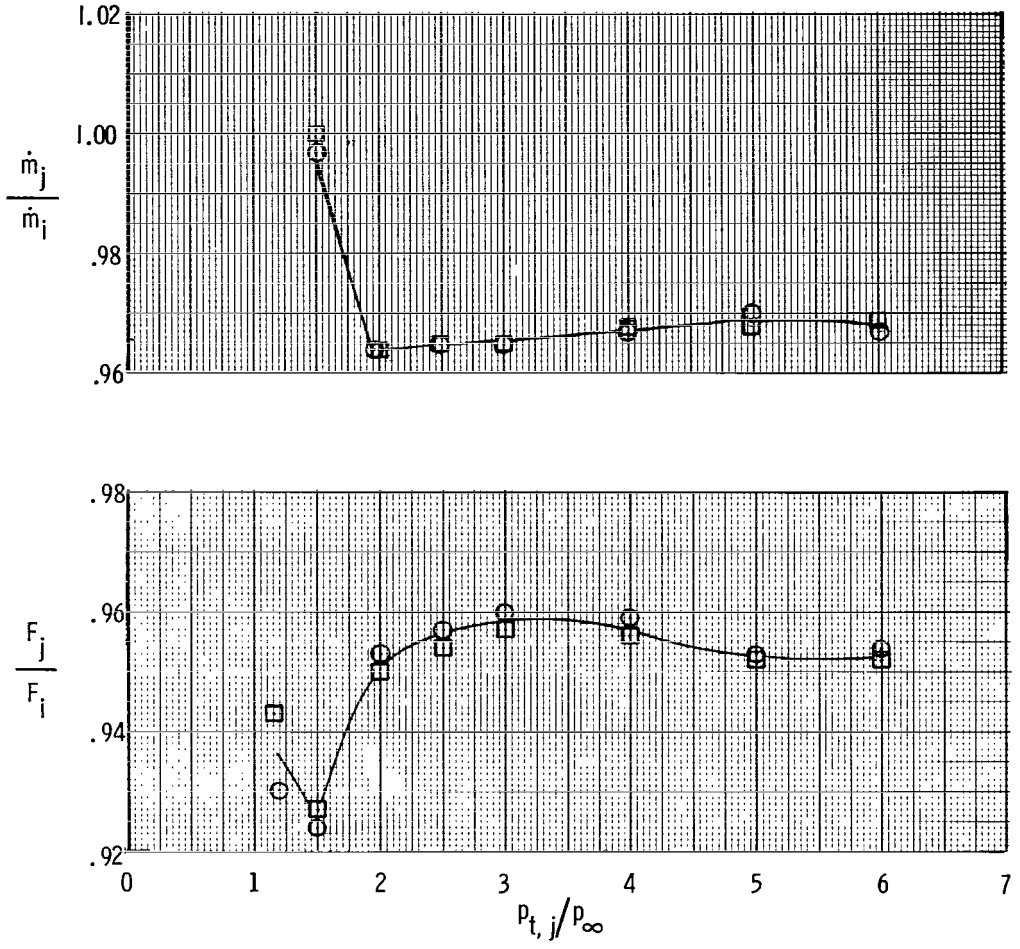

(c) $A_e/A_t = 1.10$; sideplates reduced; $\beta_w = 10^o$.

Figure 16.- Continued.

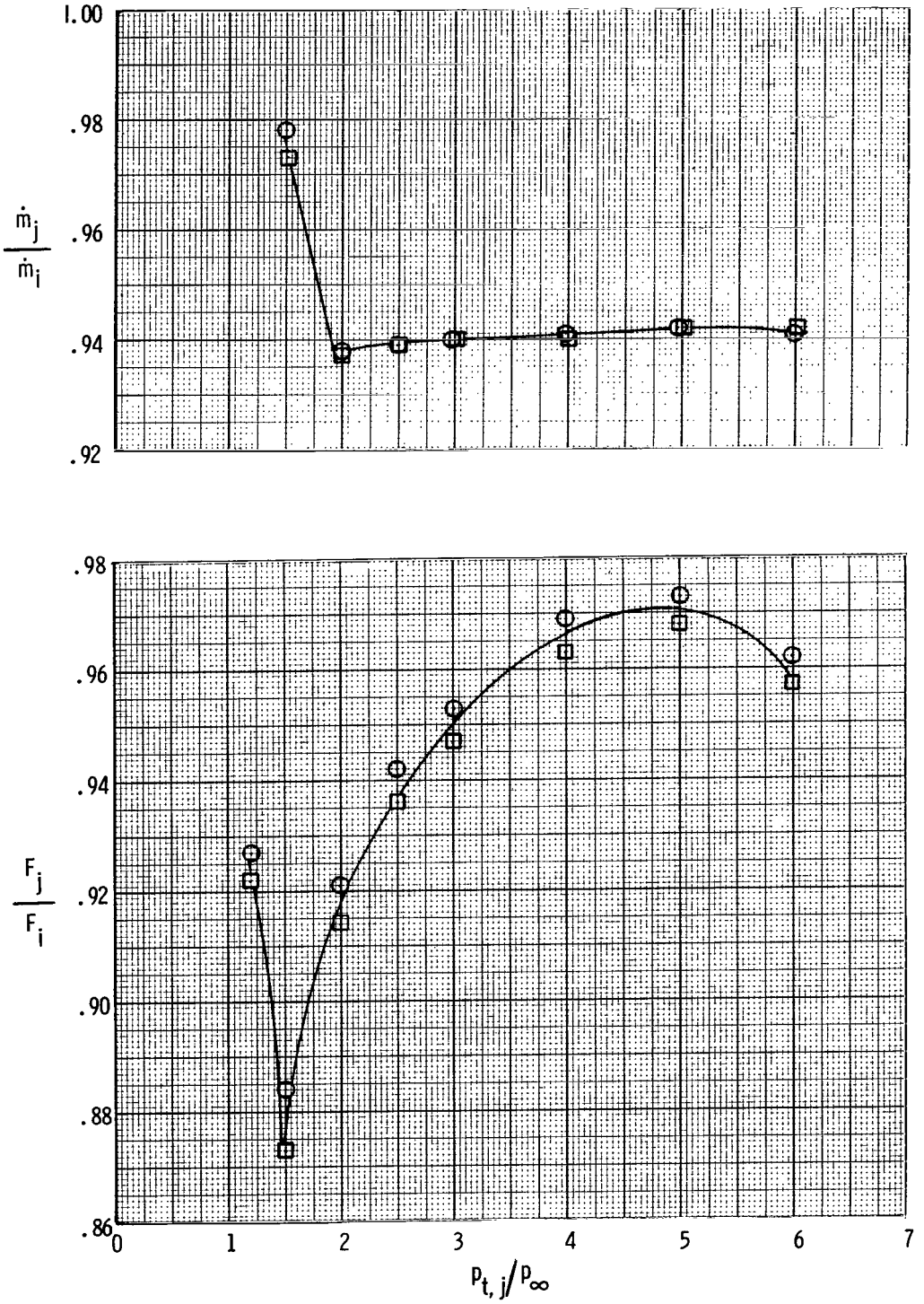

(d) $A_e/A_t = 1.30$; $\beta_w = 4.5^o/9^o$.

Figure 16.- Continued.

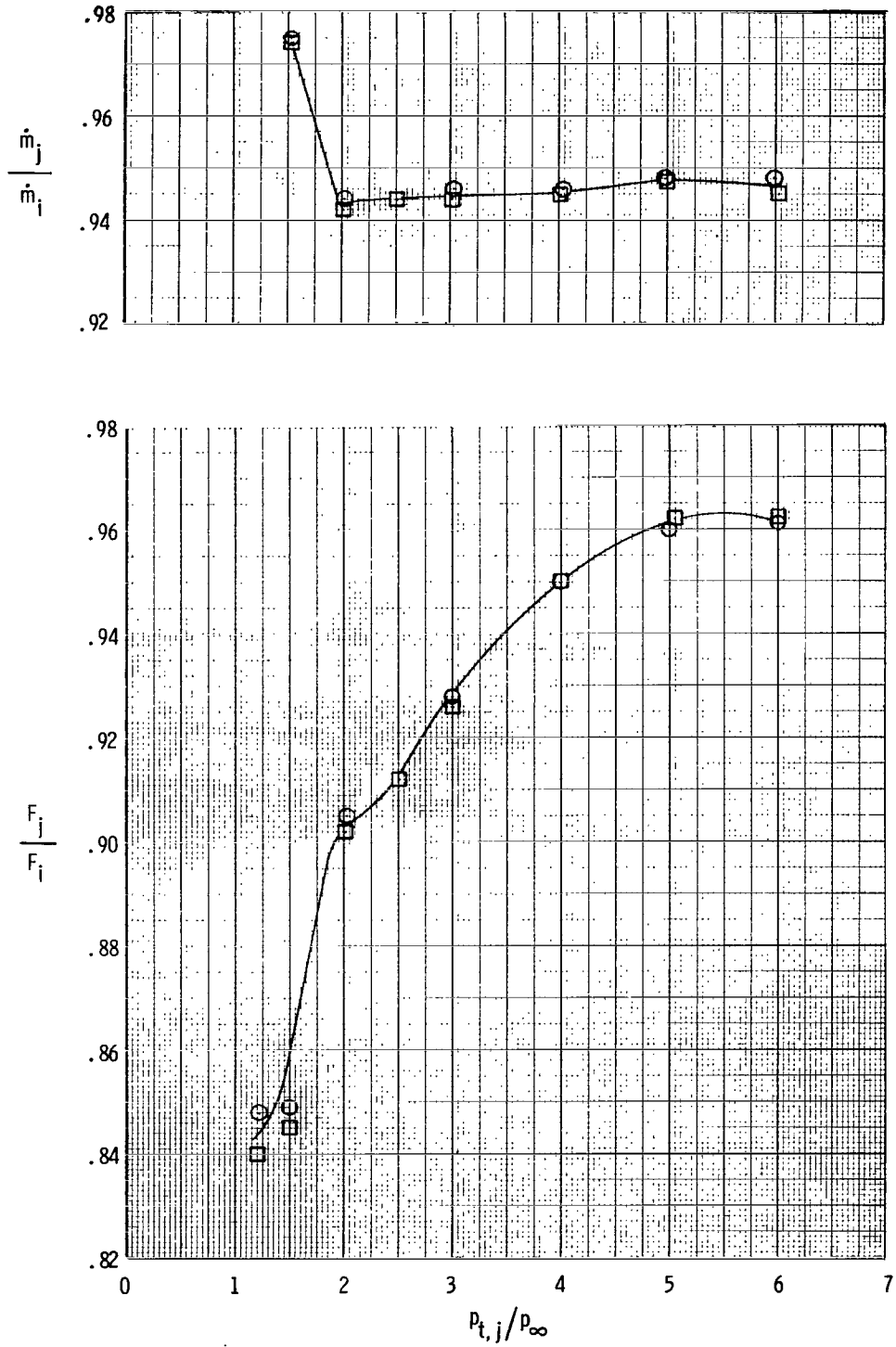

(e) $A_e/A_t = 1.53$; $\beta_w = 8^o$.

Figure 16.- Concluded.

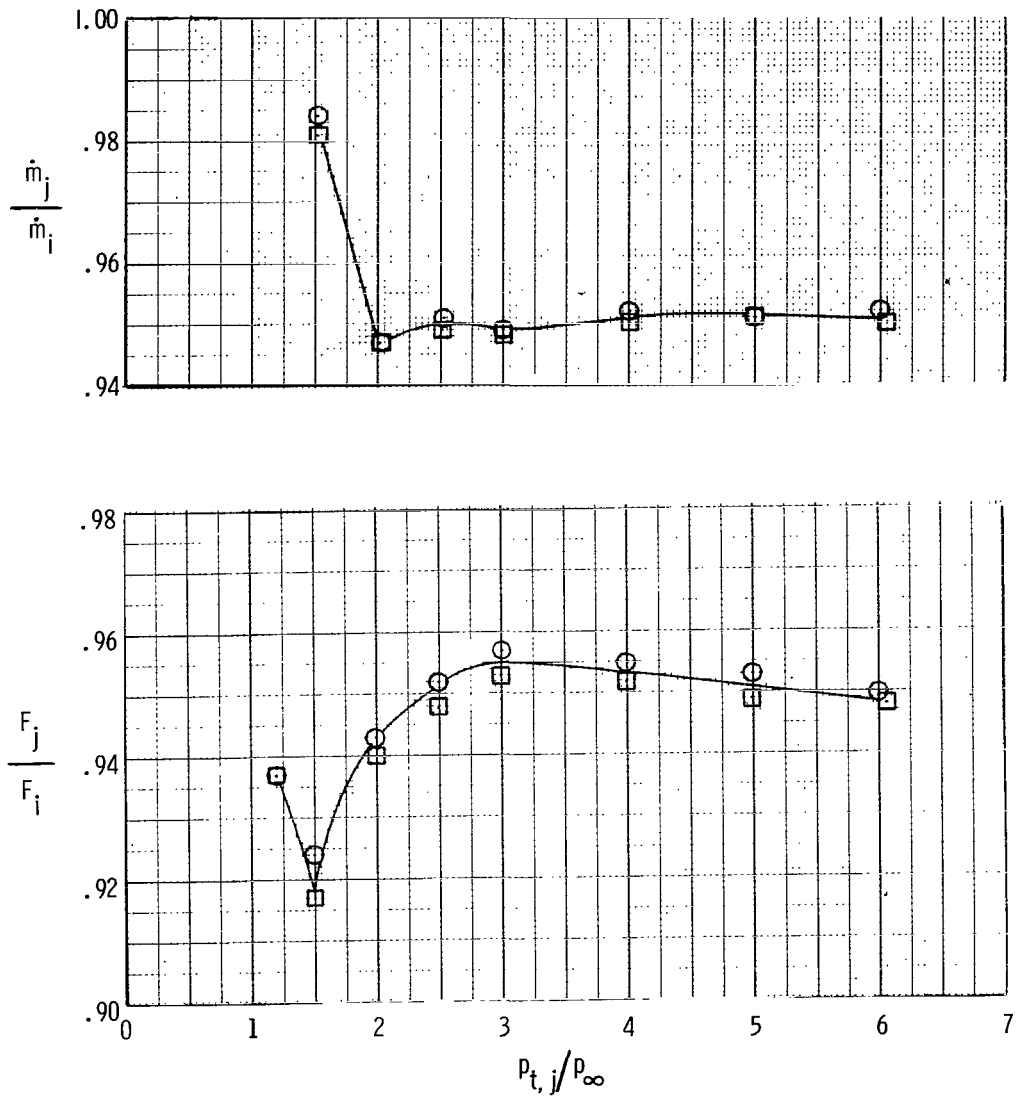

(a) $A_e/A_t = 1.10$; base-line wedge; $\beta_w = 10^o$.

Figure 17.- Static performance characteristics of configurations with 18^o boattail cowls. Test-point symbols denote repeat tests.

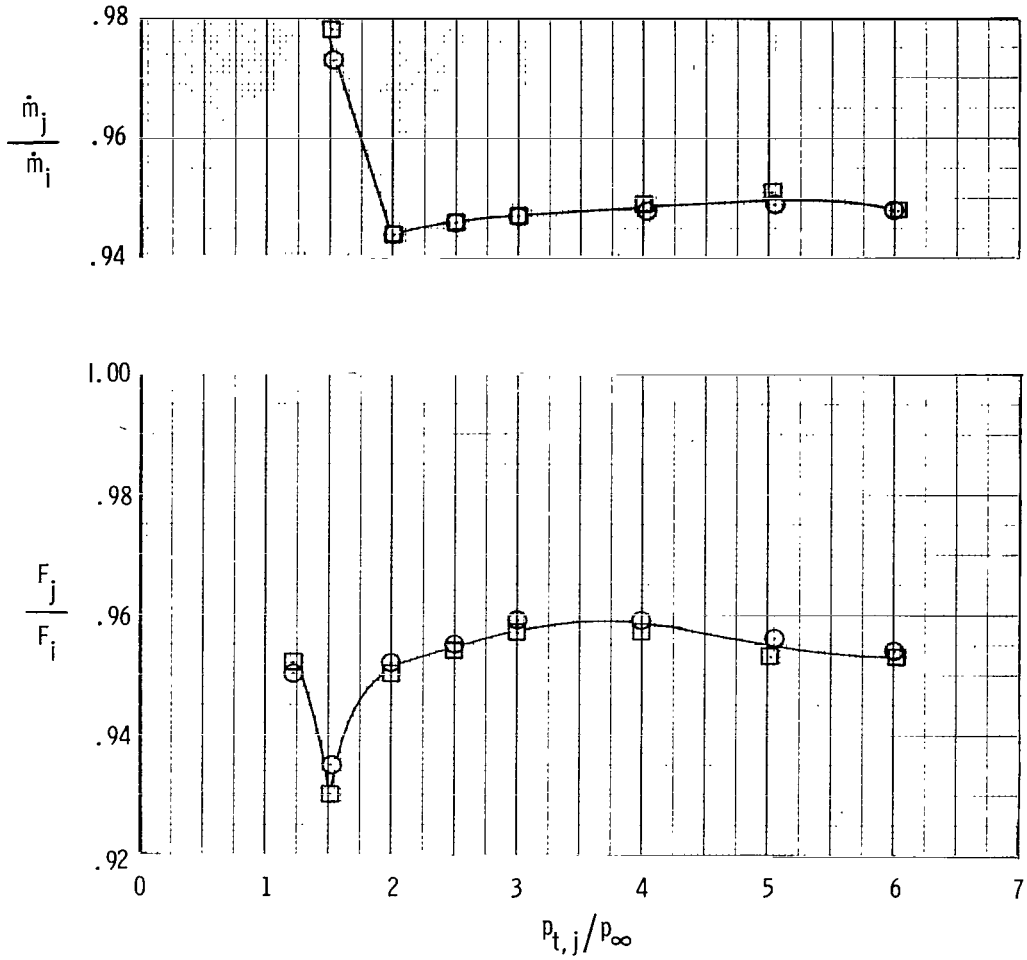

(b) $A_e/A_t = 1.10$; long wedge; $\beta_w = 8^o$.

Figure 17.- Continued.

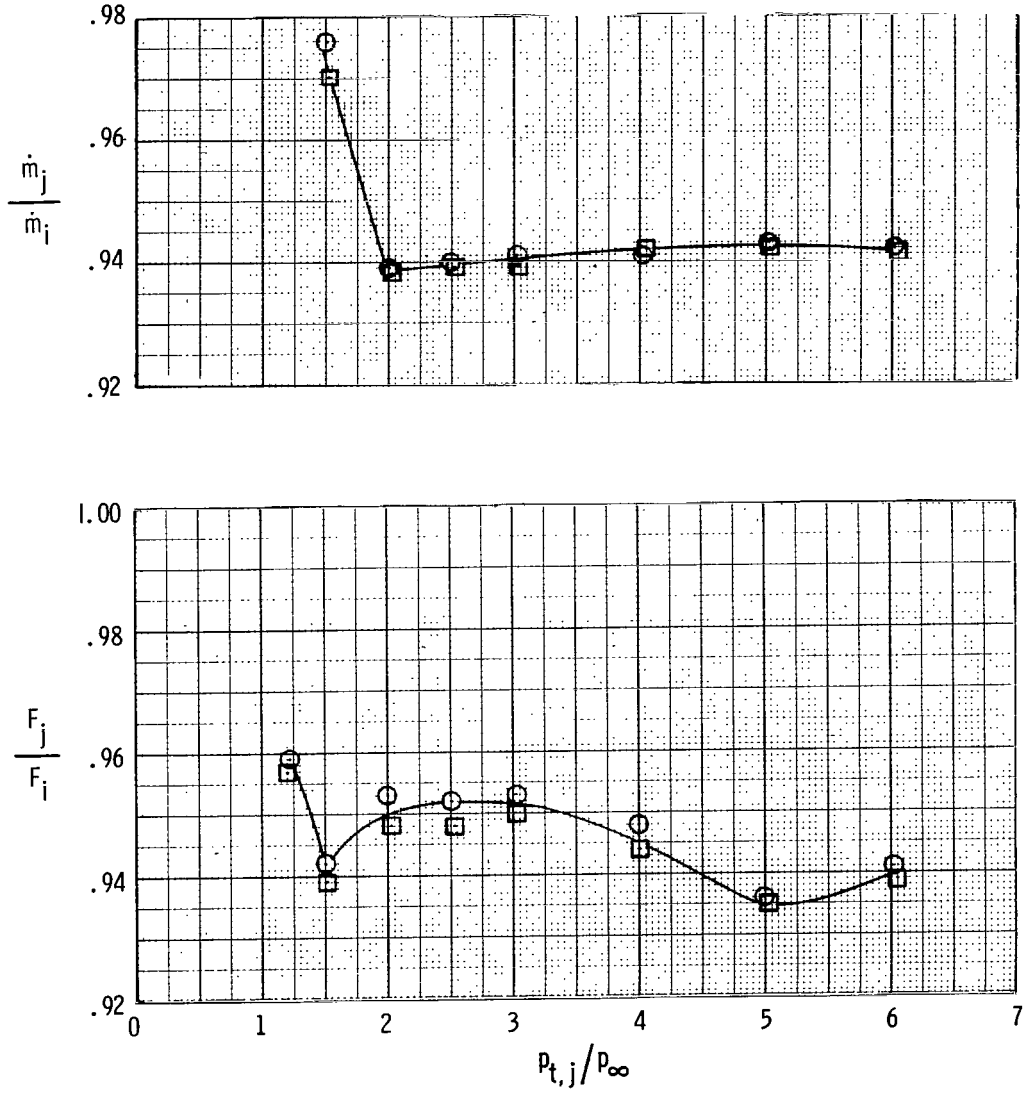

(c) $A_e/A_t = 1.10$; short wedge; $\beta_w = 13.3^o$.

Figure 17.- Continued.

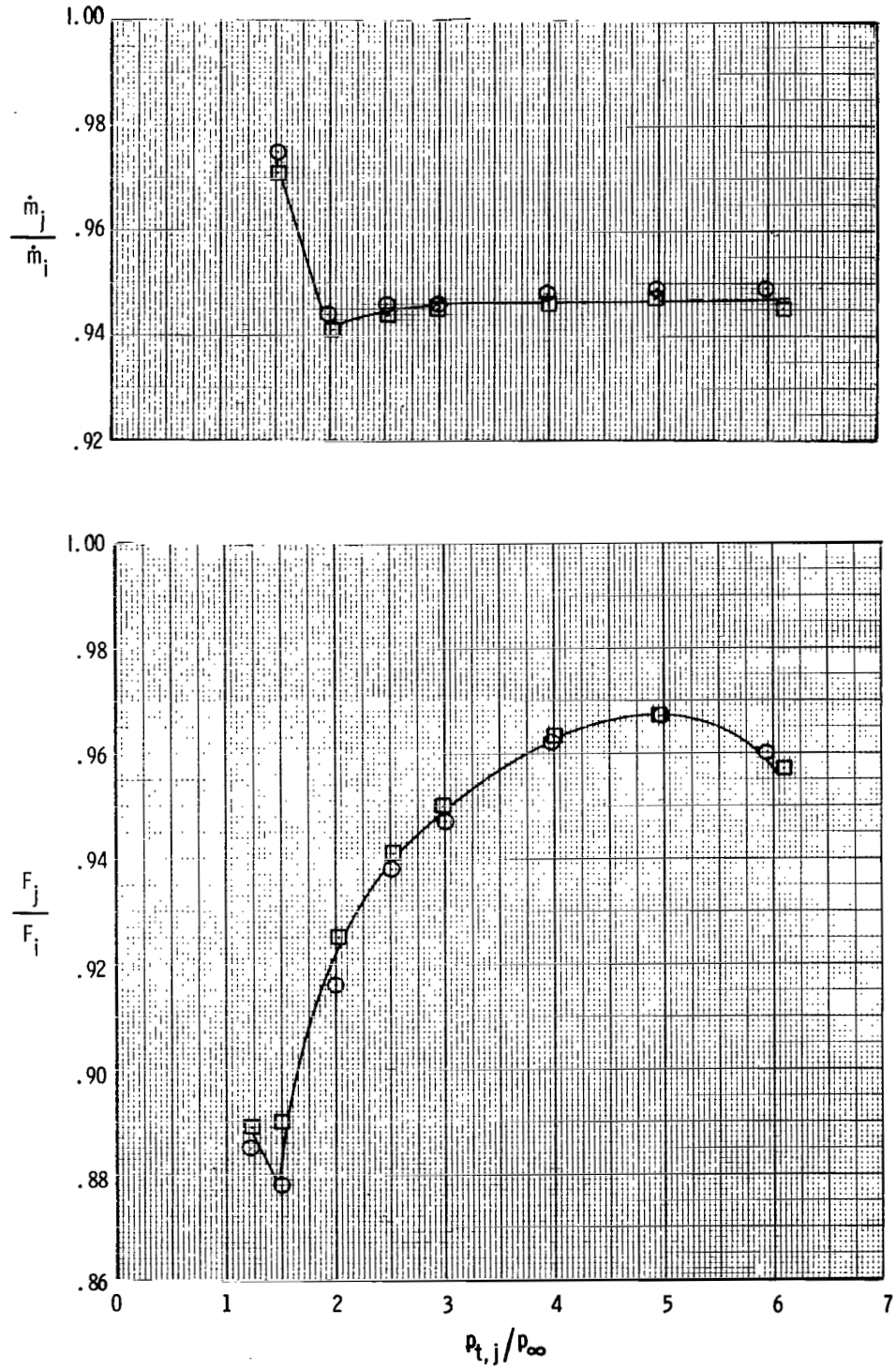

(d) $A_e/A_t = 1.30$; $\beta_w = 4.5^o/9^o$.

Figure 17.- Concluded.

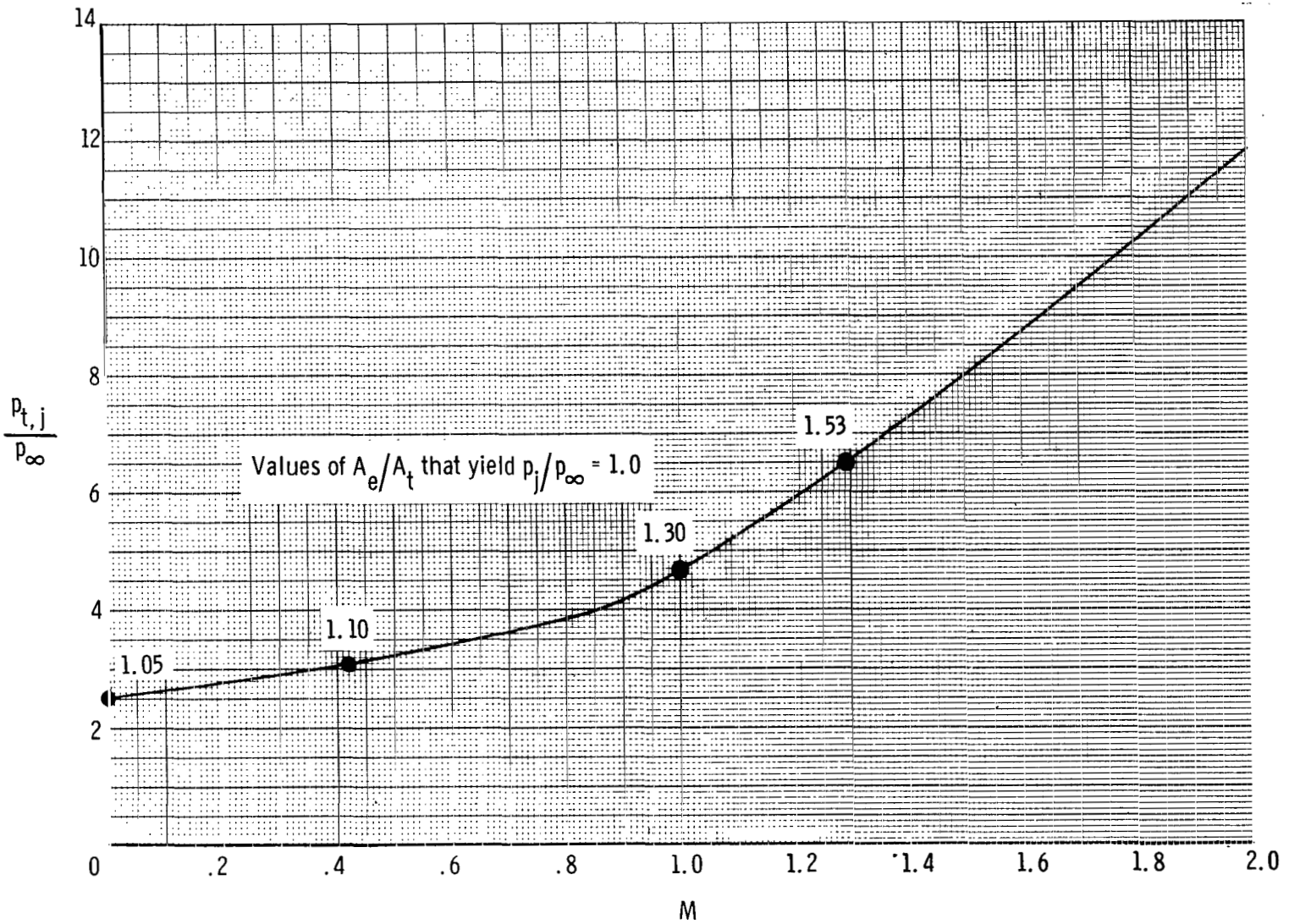

Figure 18.- Typical schedule of advanced engine-operating pressure ratio with flight Mach number.

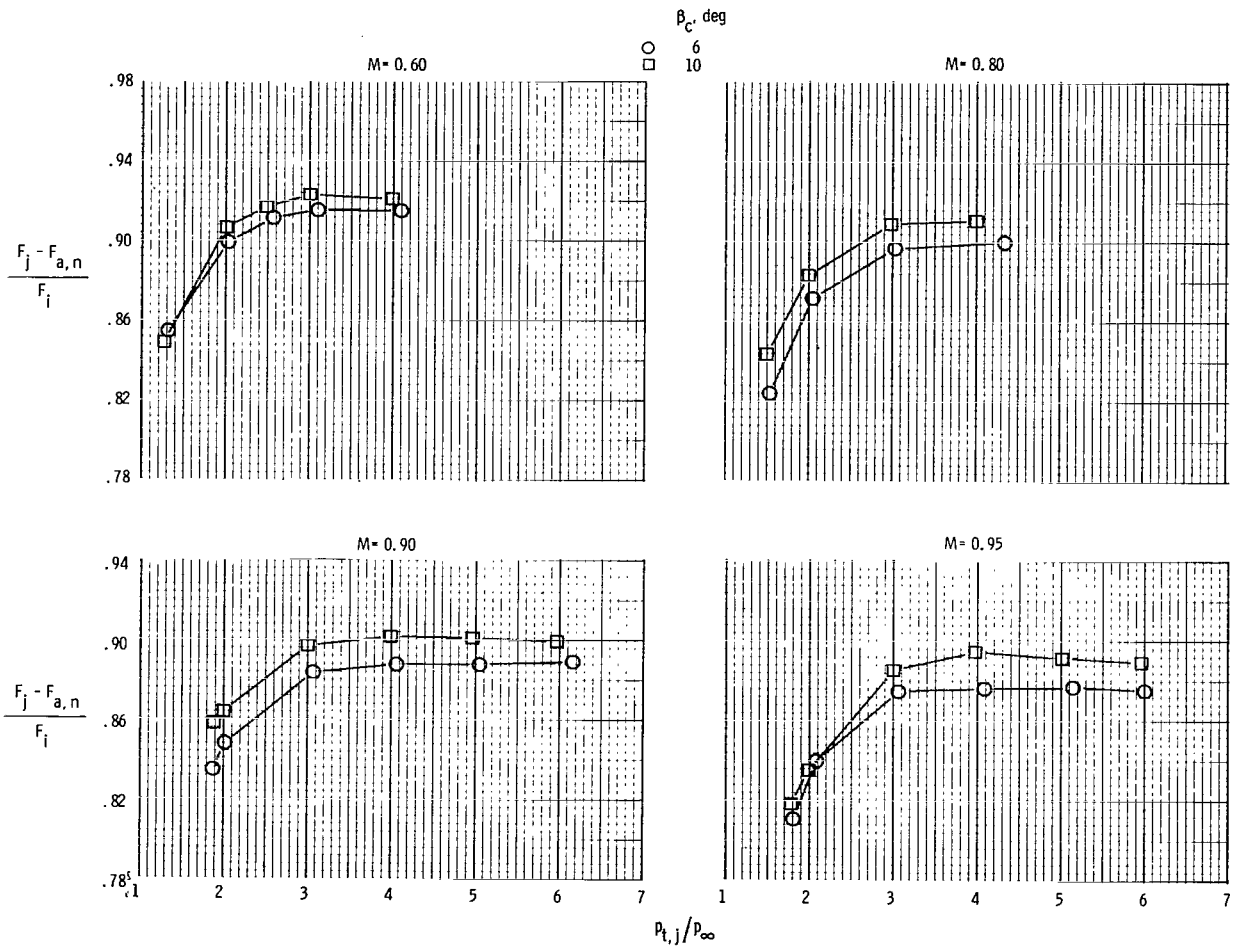

(a) Subsonic free-stream conditions.

Figure 19.- Effect of cowl boattail angle on aeropropulsion thrust ratio for two-dimensional wedge nozzle with A_e/A_t = 1.00. β_w = 10°.

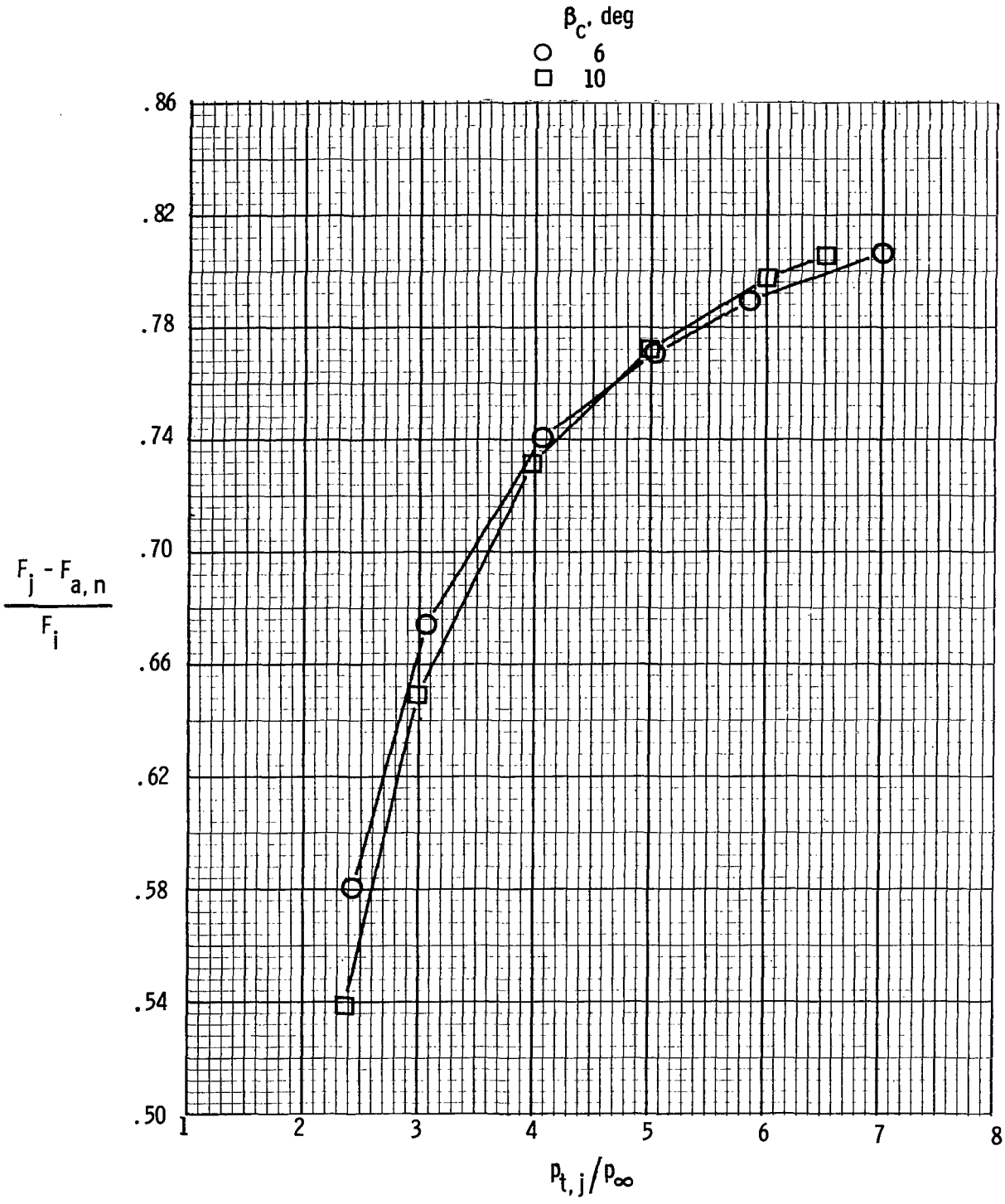

(b) Supersonic free-stream conditions. M = 1.20.

Figure 19.- Concluded.

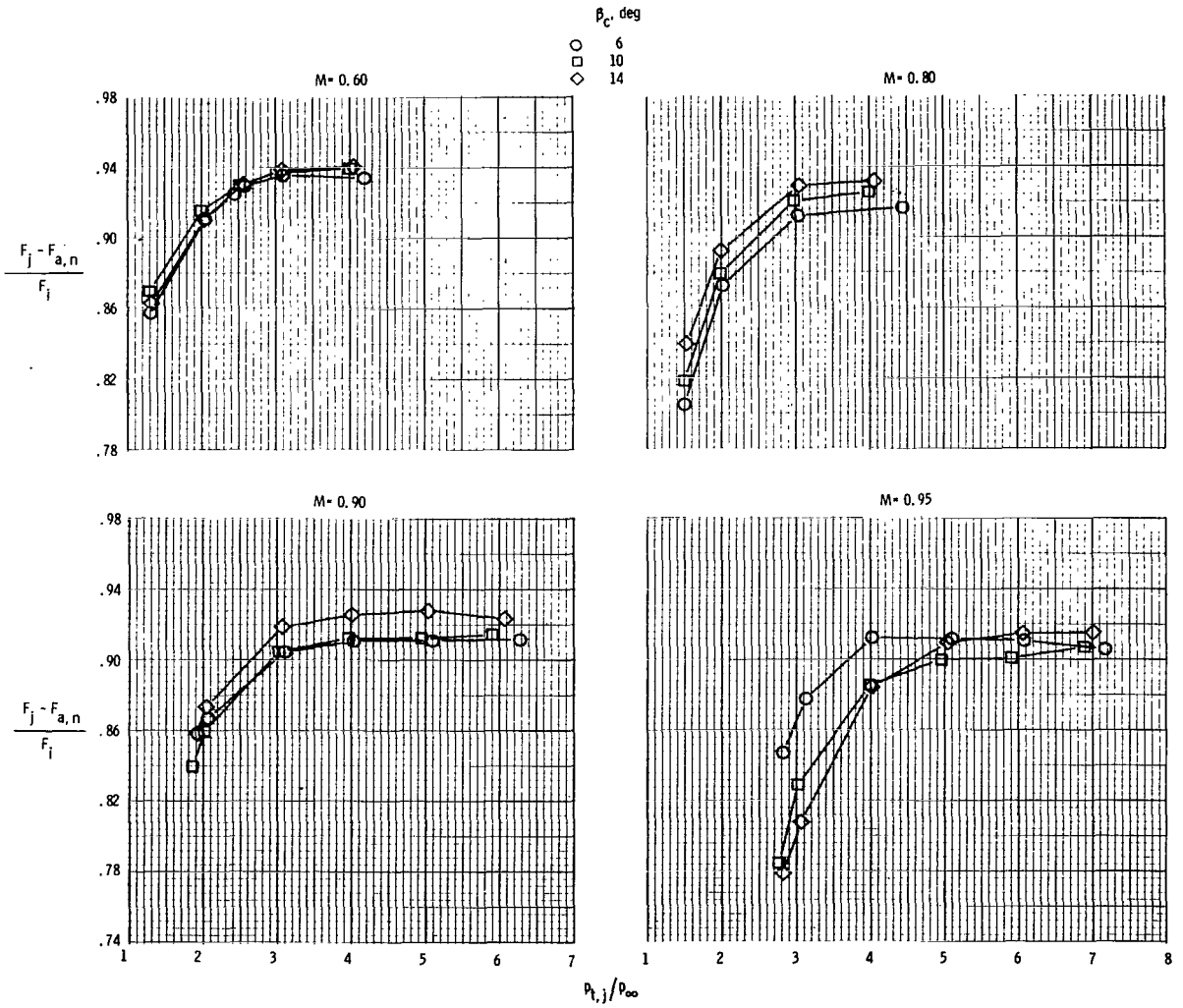

(a) Subsonic free-stream conditions.

Figure 20.- Effect of cowl boattail angle on aeropropulsion thrust ratio for two-dimensional wedge nozzle with $A_e/A_t = 1.05$. $\beta_w = 10^o$.

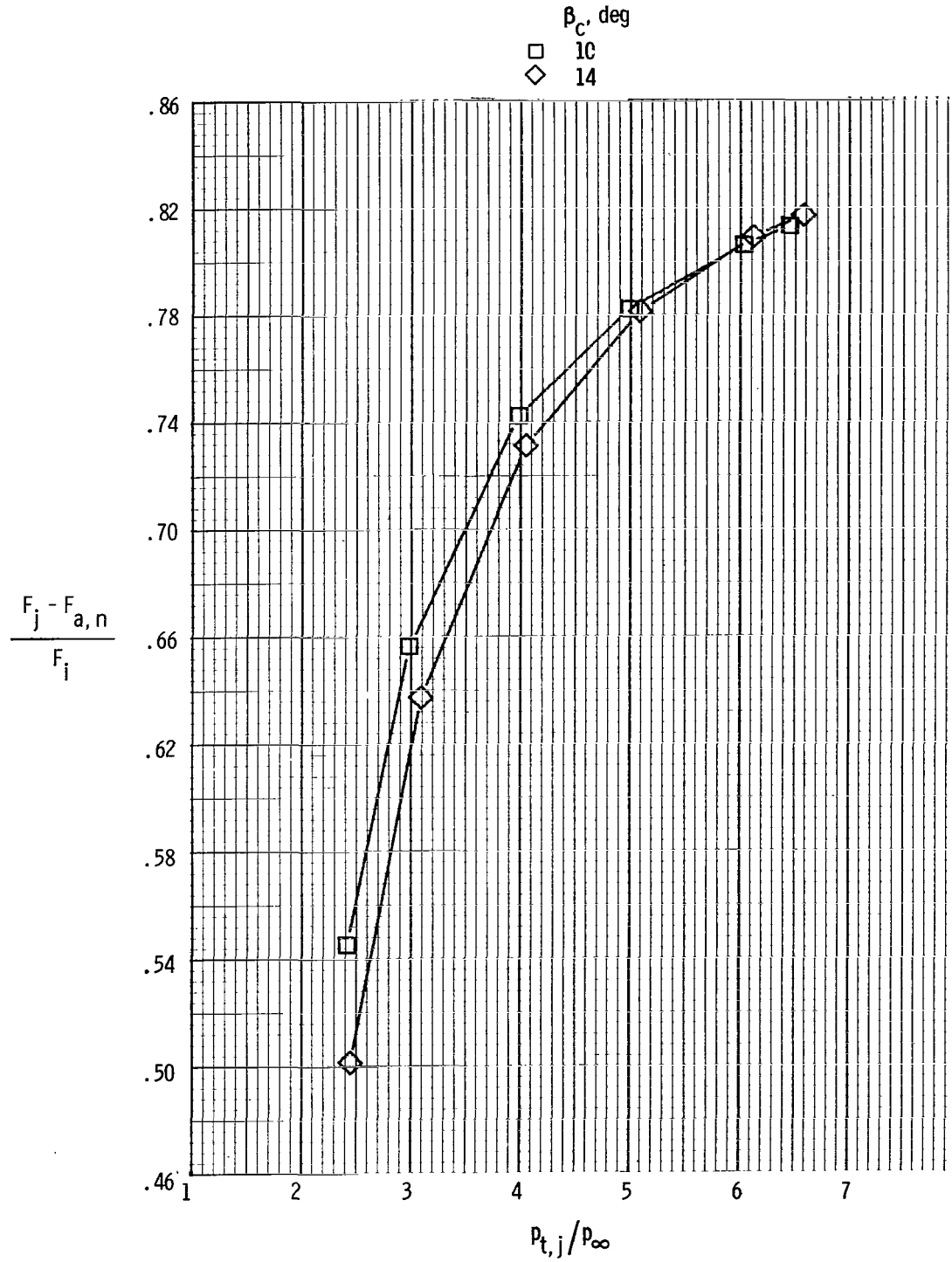

(b) Supersonic free-stream conditions. M = 1.20.

Figure 20.- Concluded.

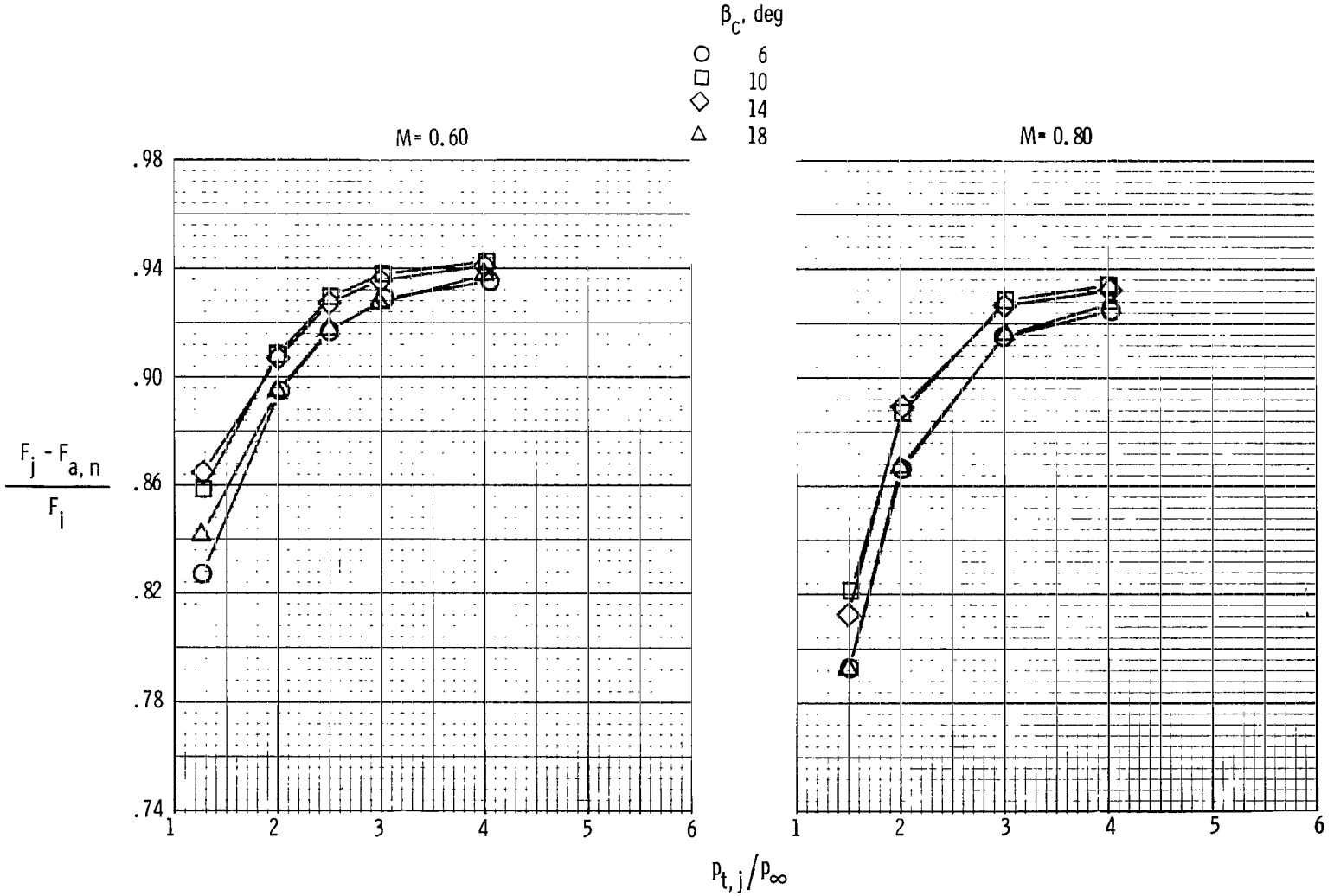

(a) Subsonic free-stream conditions.

Figure 21.- Effect of cowl boattail angle on aeropropulsion thrust ratio for two-dimensional wedge nozzle with $A_e/A_t = 1.10$. $\beta_w = 10^o$.

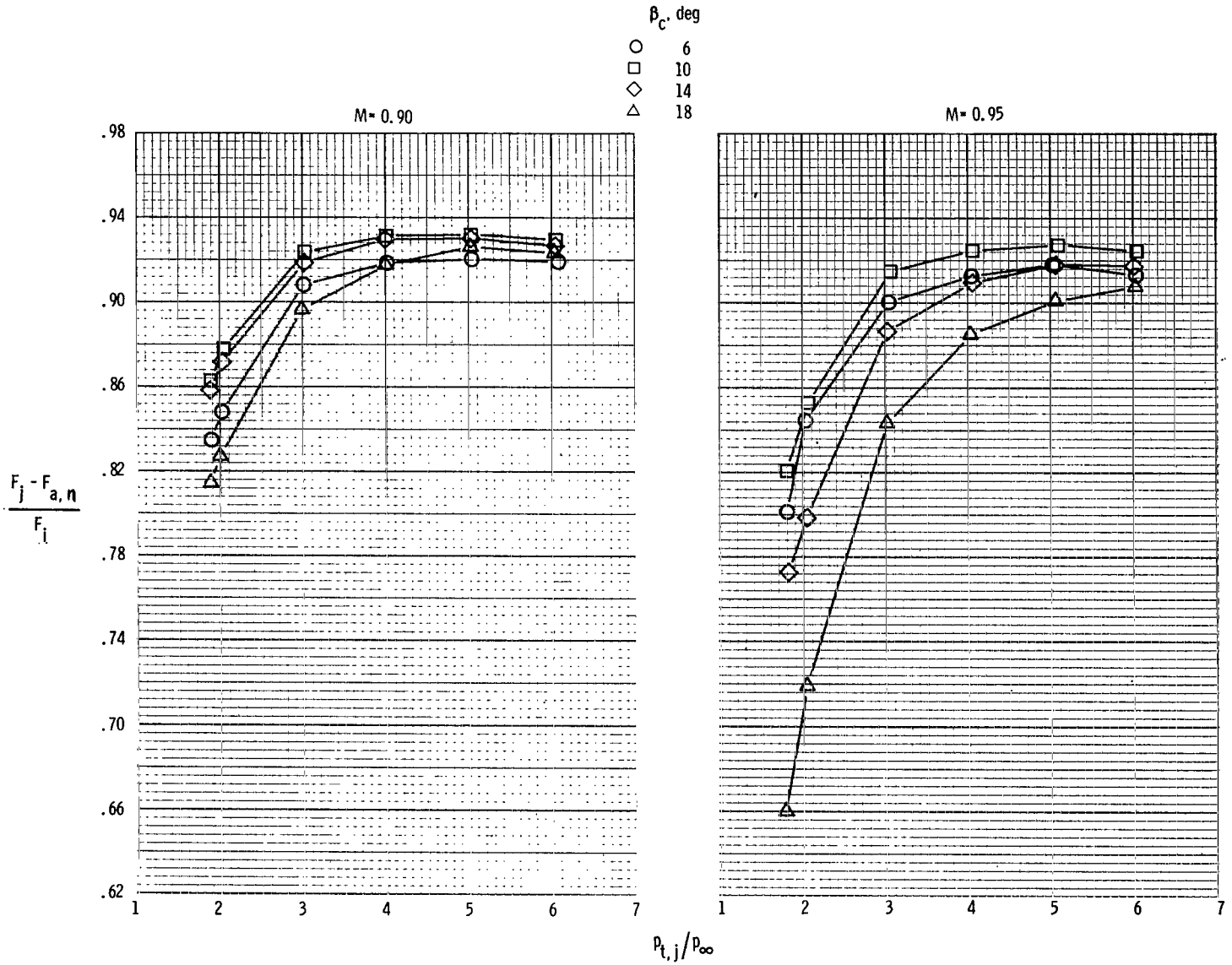

(a) Concluded.

Figure 21.- Continued.

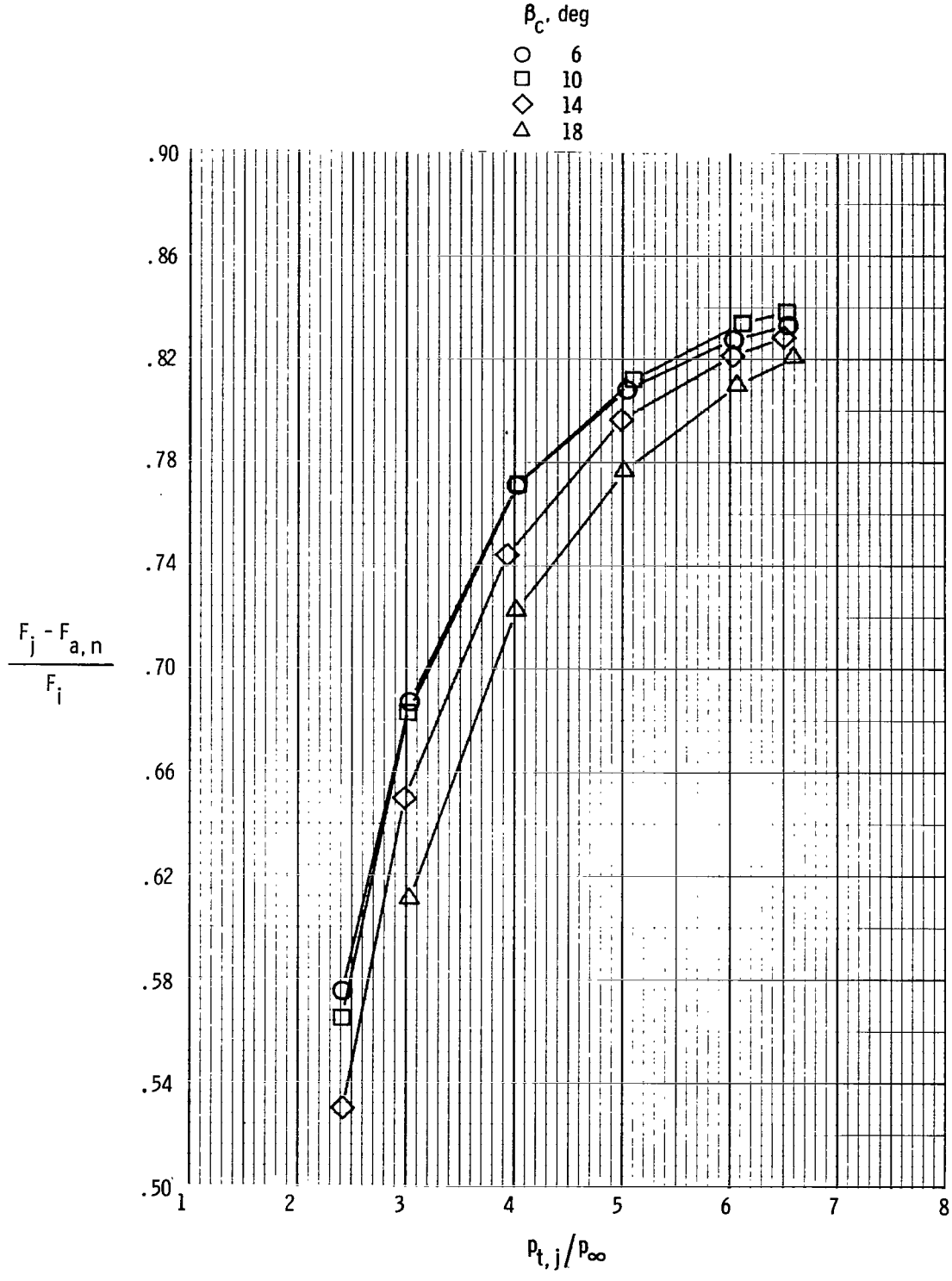

(b) Supersonic free-stream conditions. M = 1.20.

Figure 21.- Concluded.

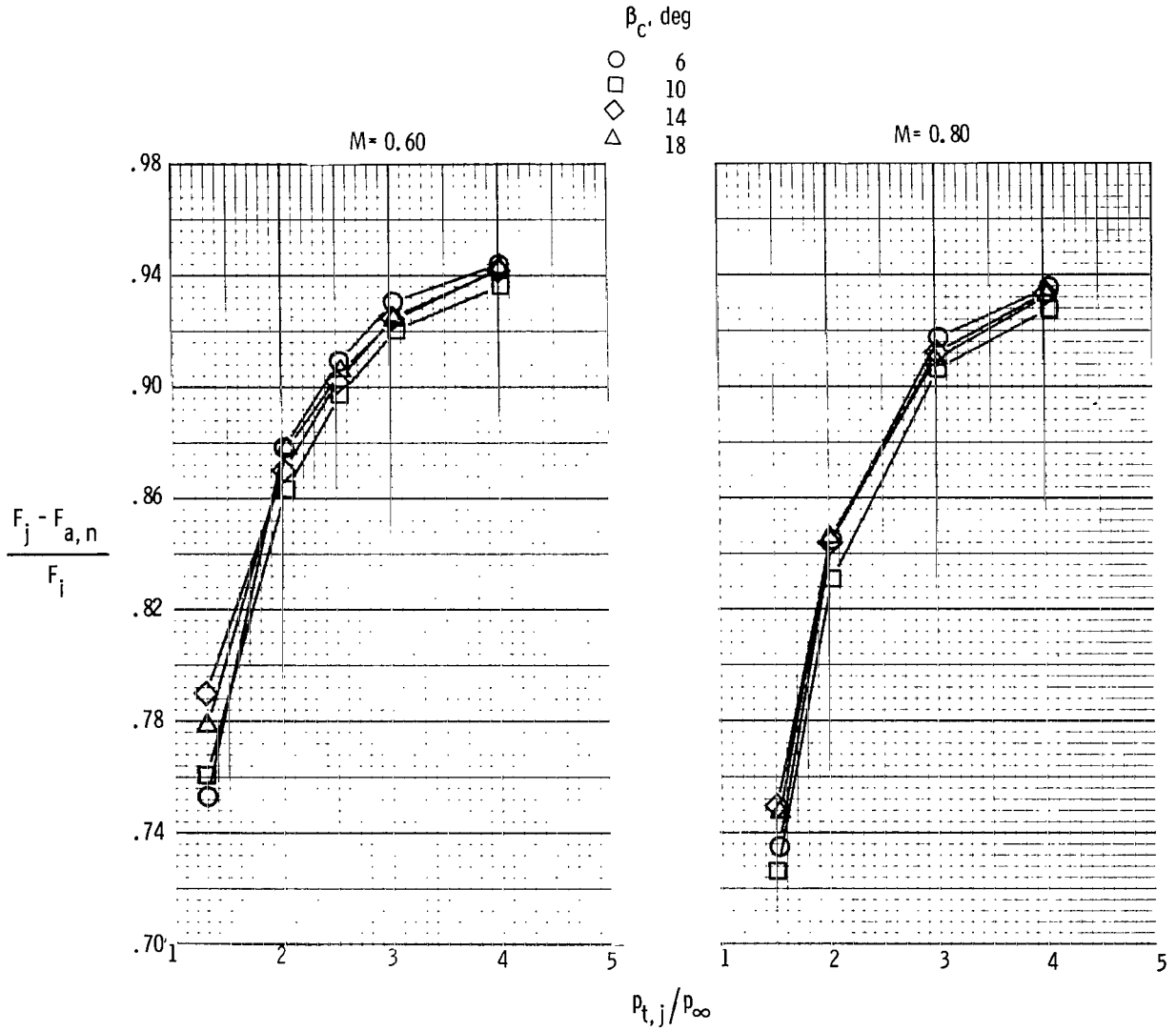

(a) Subsonic free-stream conditions.

Figure 22.- Effect of cowl boattail angle on aeropropulsion thrust ratio for two-dimensional wedge nozzle with $A_e/A_t = 1.30$. $\beta_w = 4.5^o/9^o$.

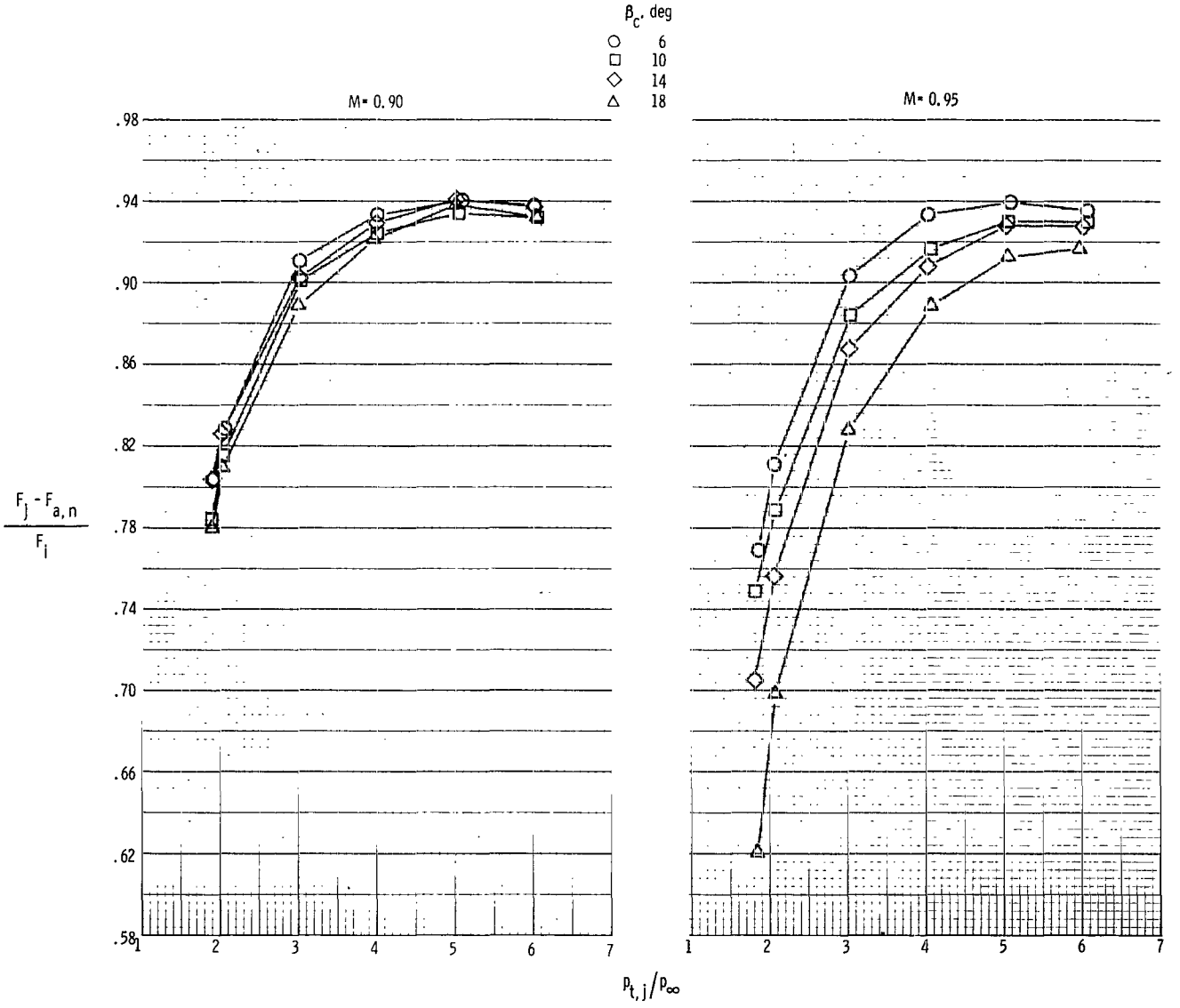

(a) Concluded.

Figure 22.- Continued.

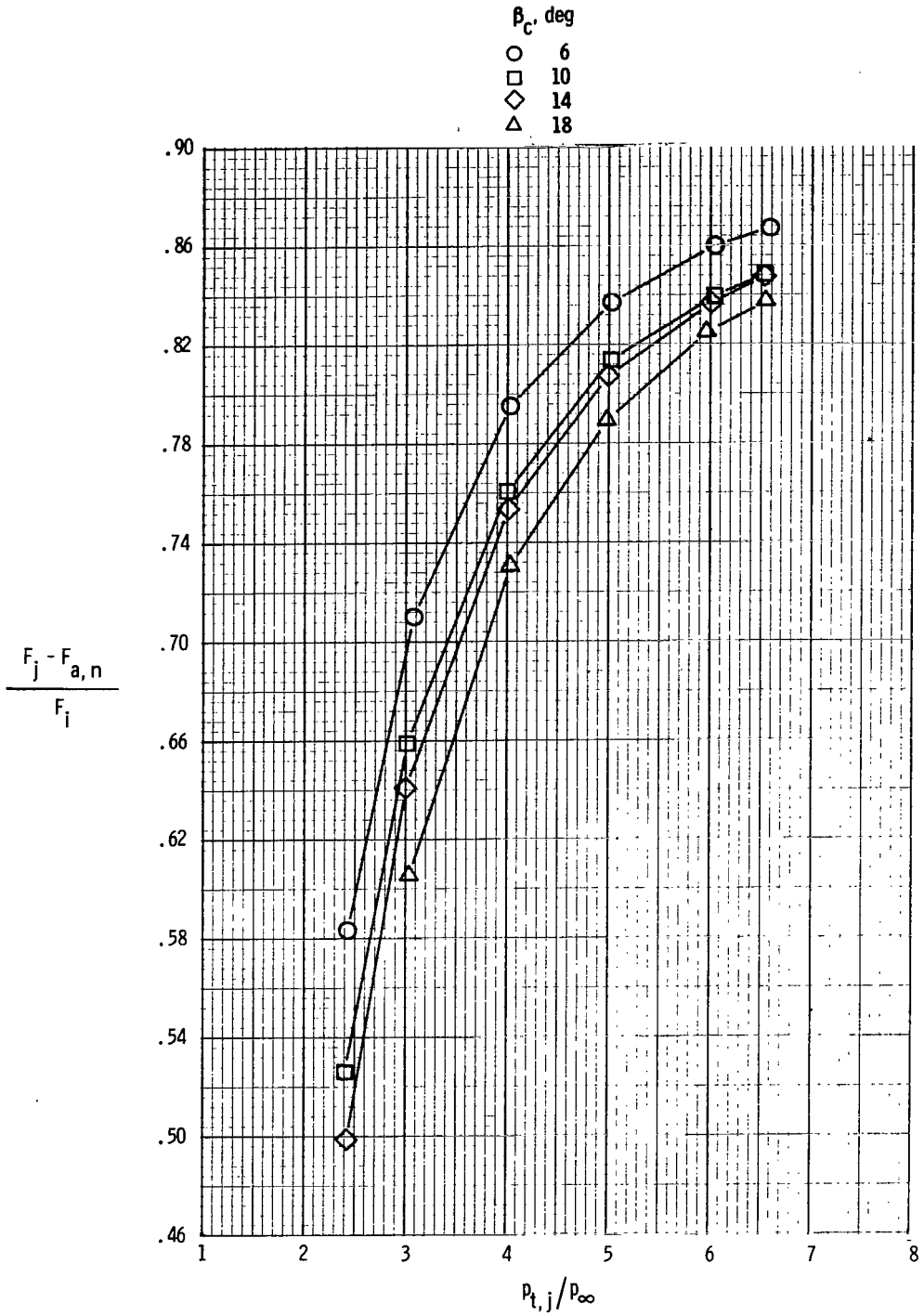

(b) Supersonic free-stream conditions. M = 1.20.

Figure 22.- Concluded.

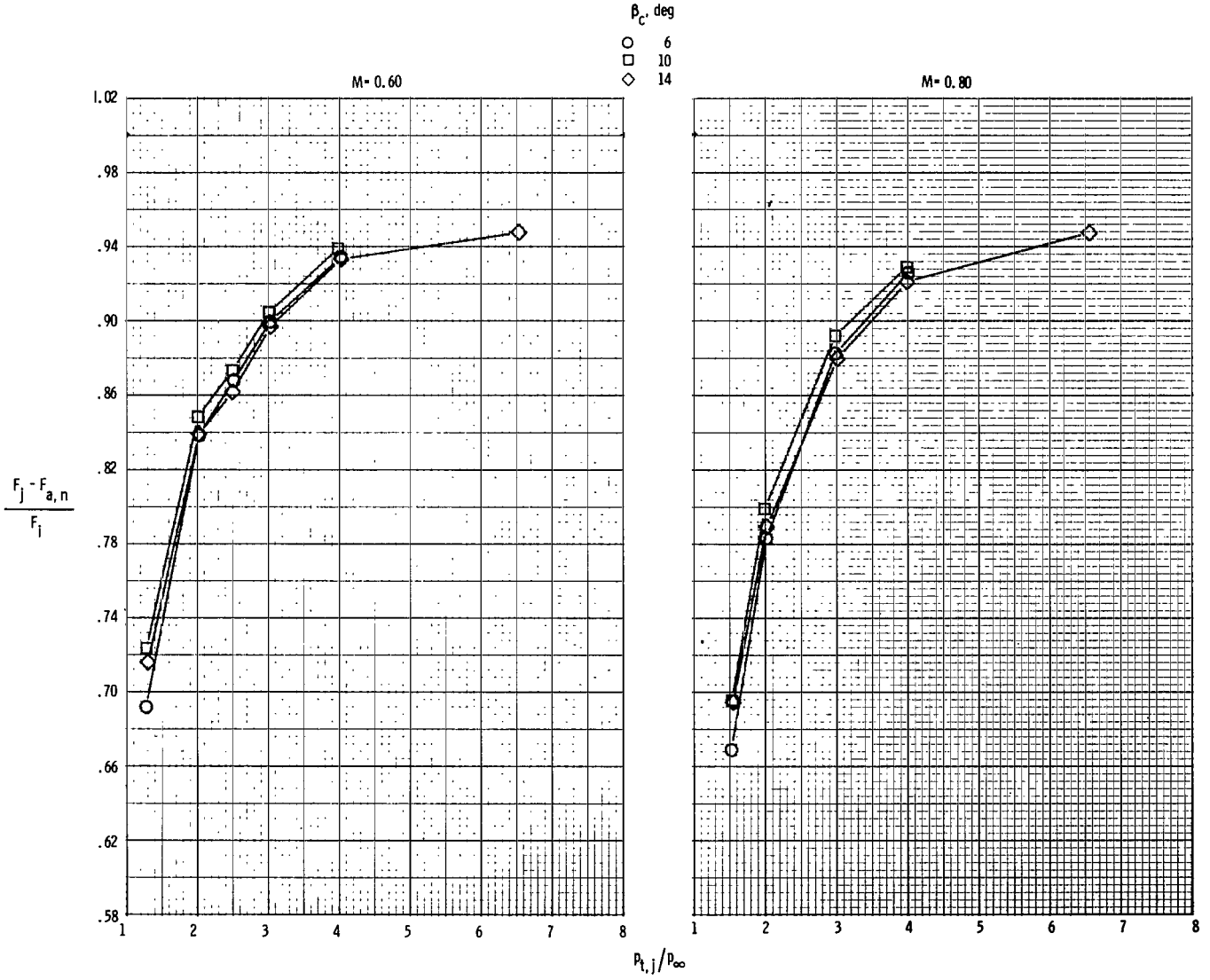

(a) Subsonic free-stream conditions.

Figure 23.- Effect of cowl boattail angle on aeropropulsion thrust ratio for two-dimensional wedge nozzle with $A_e/A_t = 1.53$. $\beta_w = 8^o$.

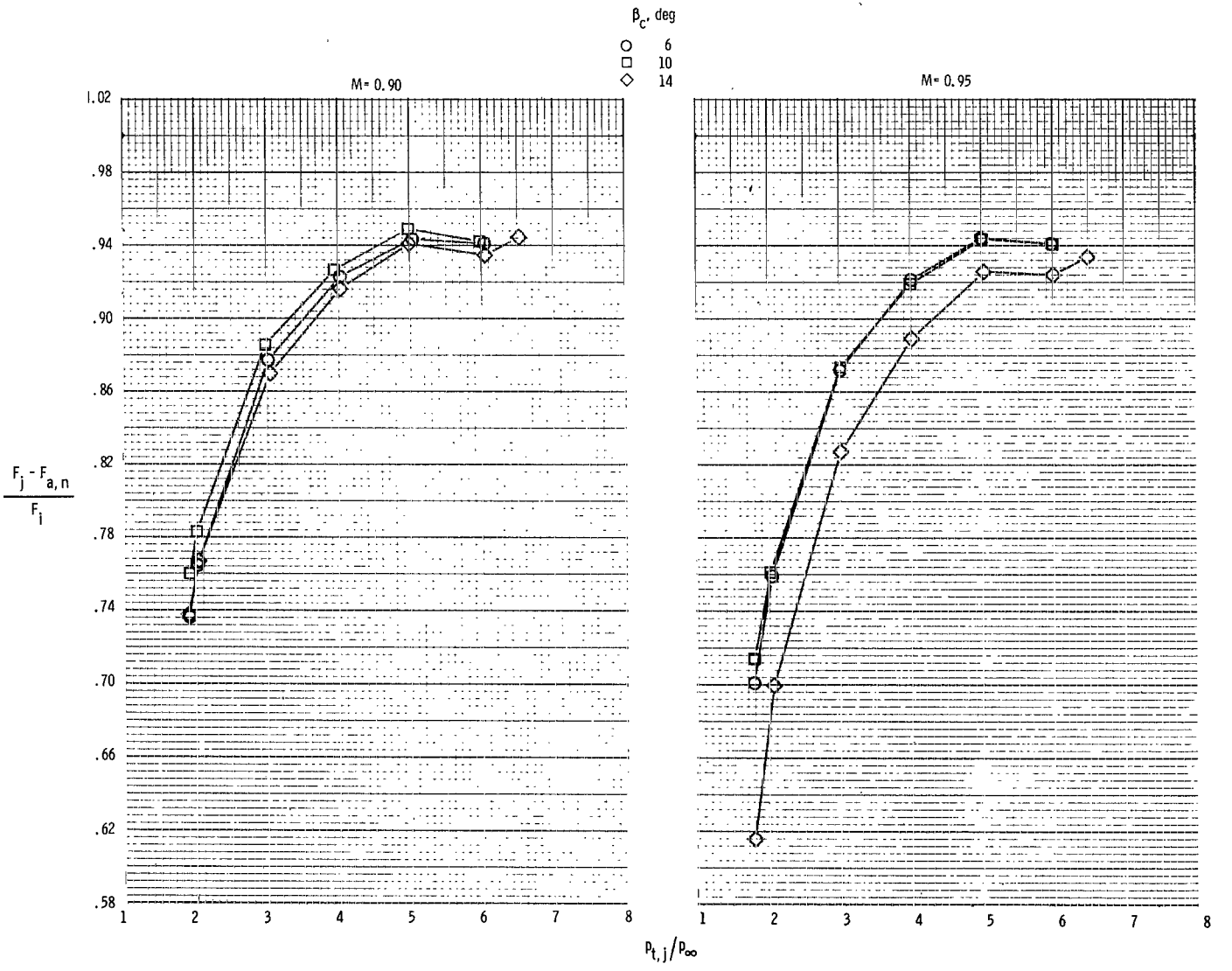

(a) Concluded.

Figure 23.- Continued.

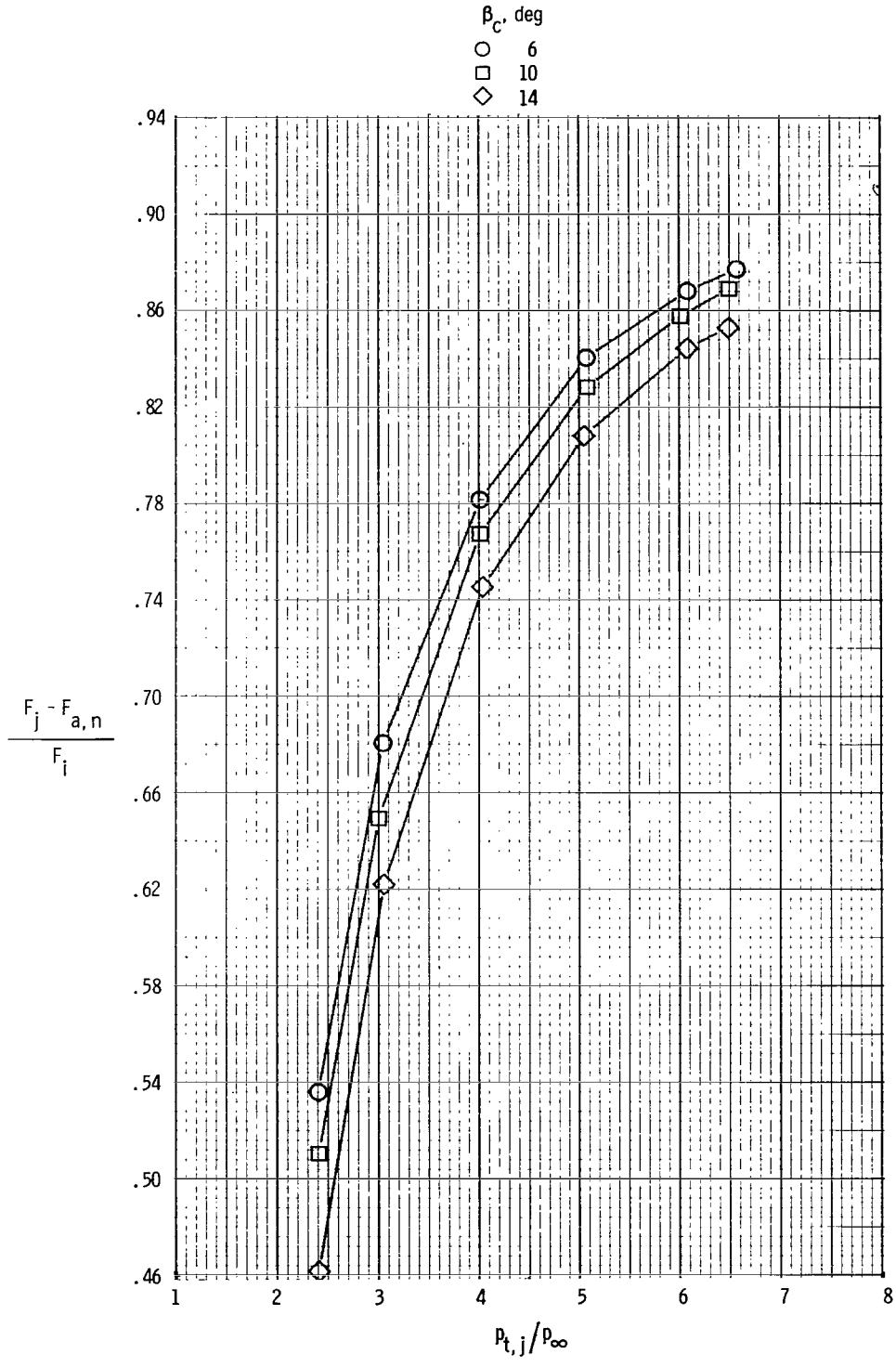

(b) Supersonic free-stream conditions. M = 1.20.

Figure 23.- Concluded.

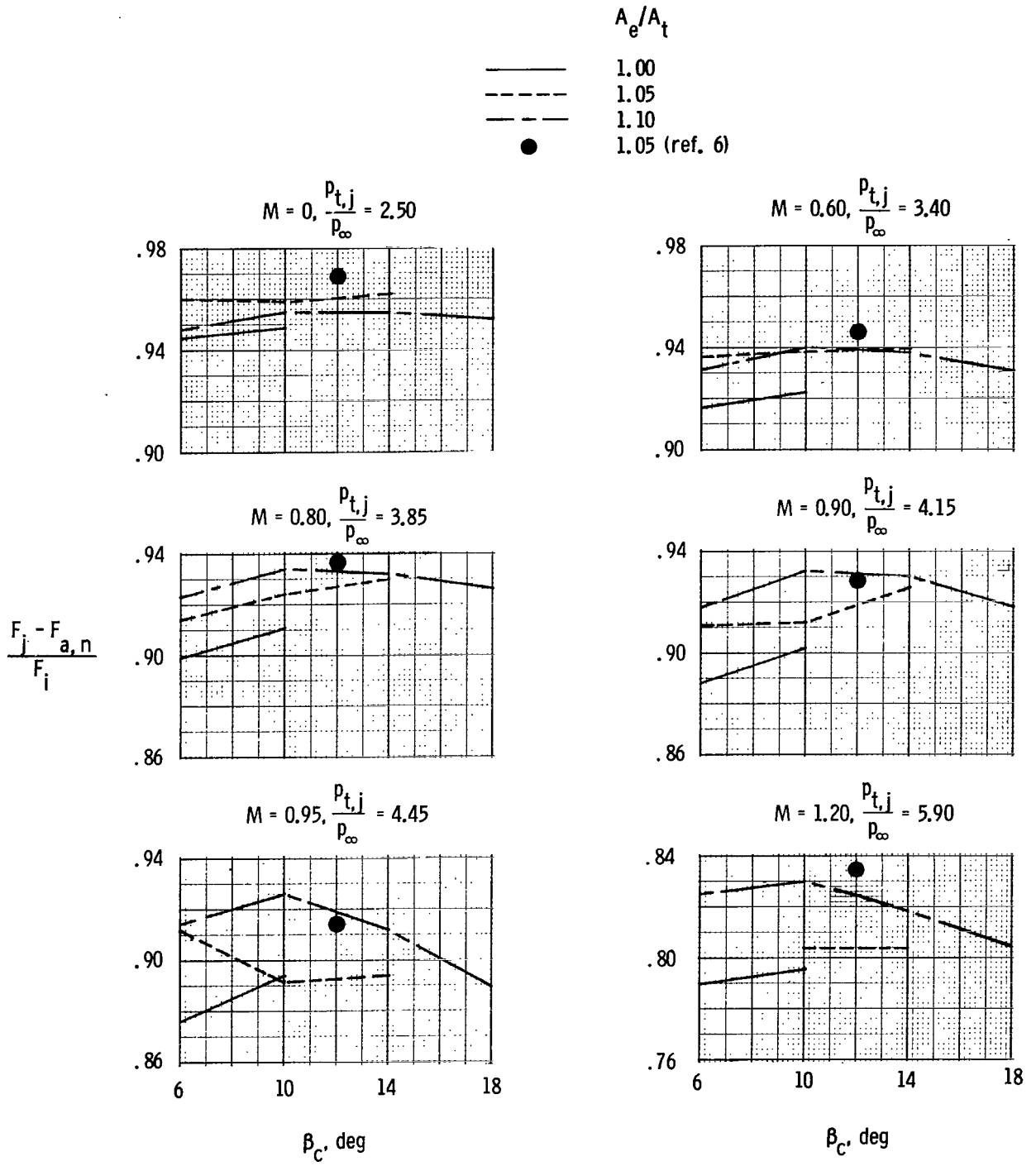

(a) Low internal expansion area ratios. $\beta_w = 10^o$.

Figure 24.- Effect of cowl boattail angle on two-dimensional wedge nozzle performance at several Mach numbers for EPR schedule.

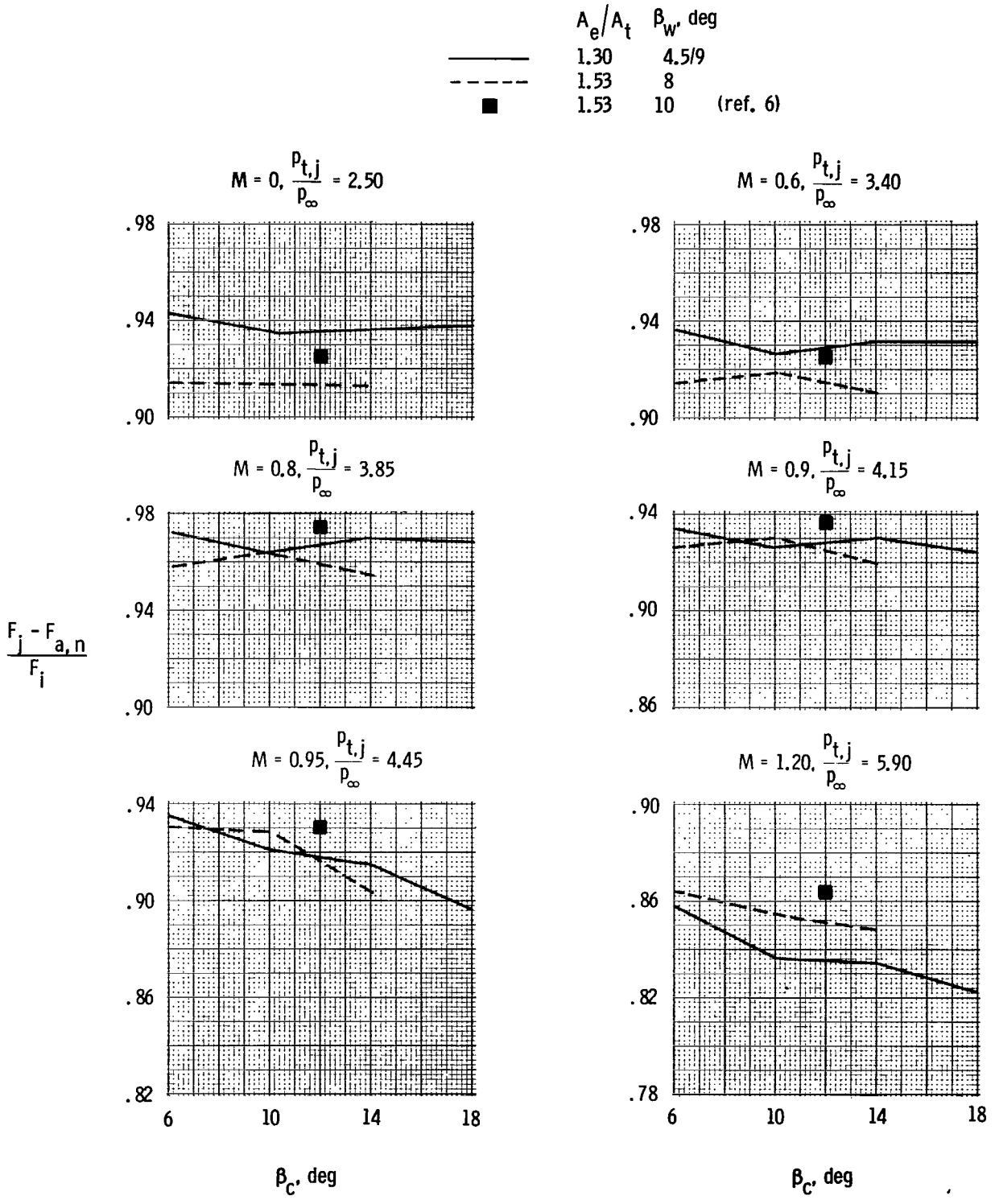

(b) High internal expansion area ratios.

Figure 24.- Concluded.

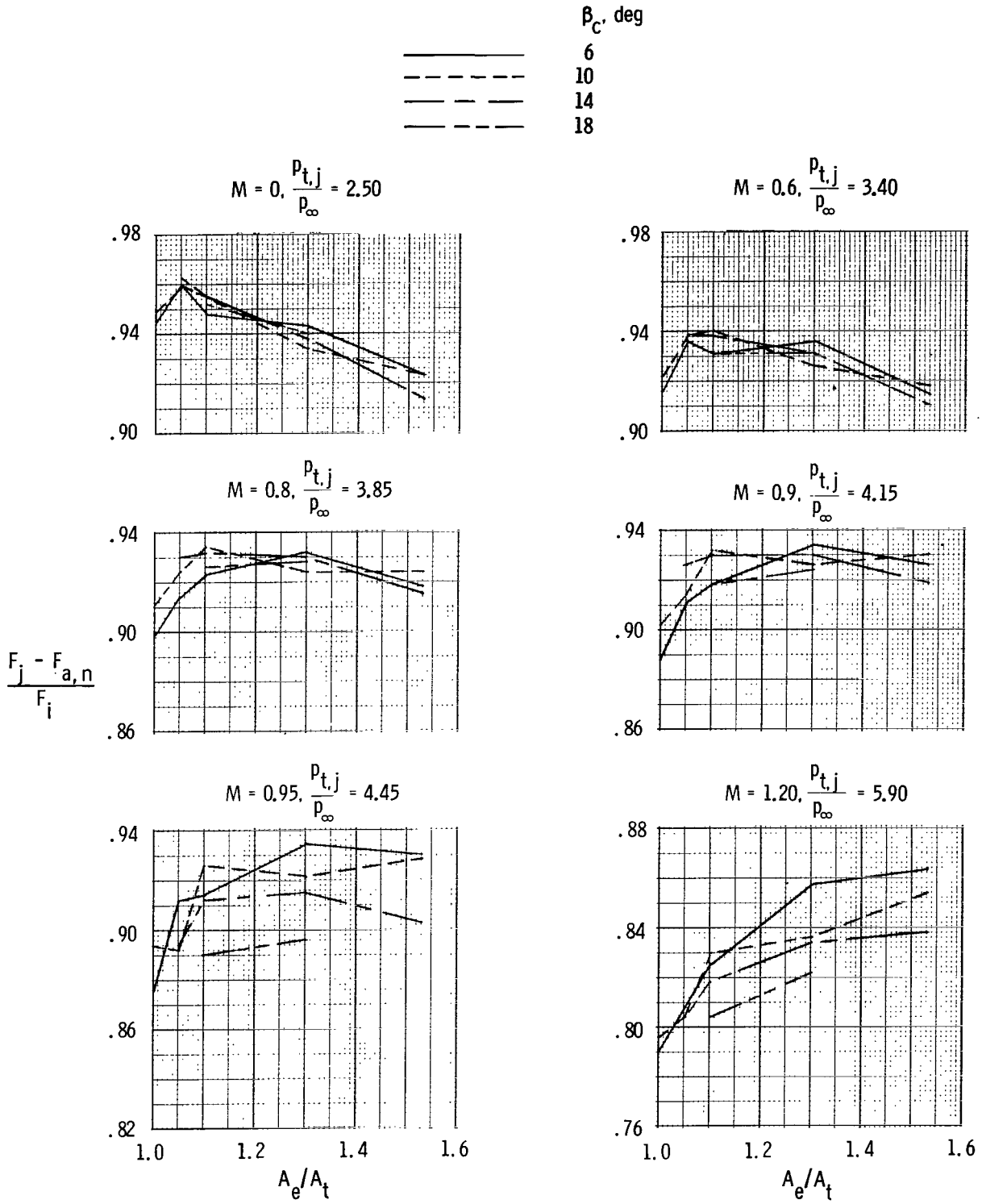

Figure 25.- Effect of internal expansion area ratio on performance of two-dimensional wedge nozzle at EPR schedule for several Mach numbers.

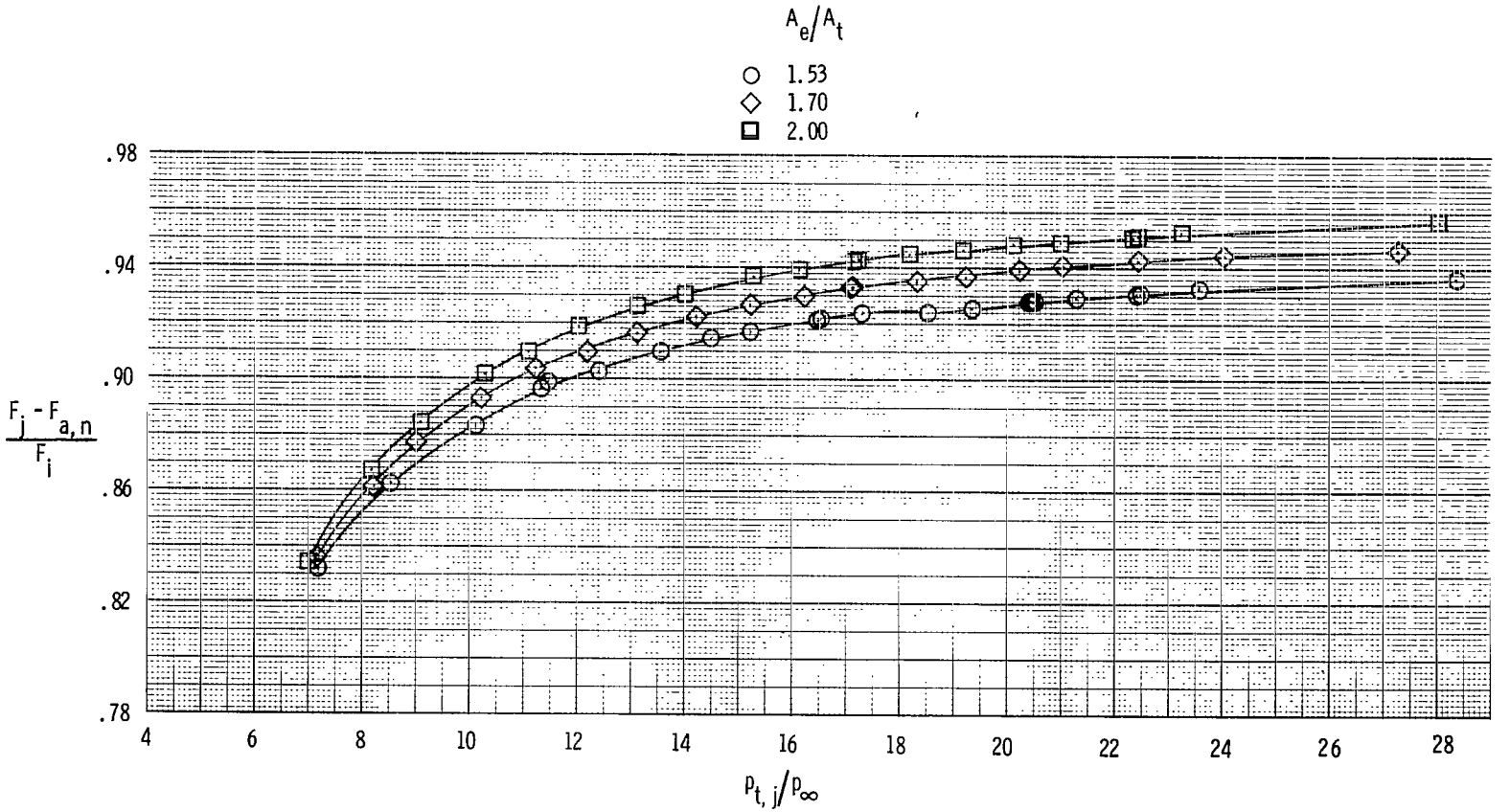

(a) $\beta_c = 6^o$.

Figure 26.- Effect of internal expansion area ratio on two-dimensional nozzle performance at Mach 2.01 for two cowl boattail angles.

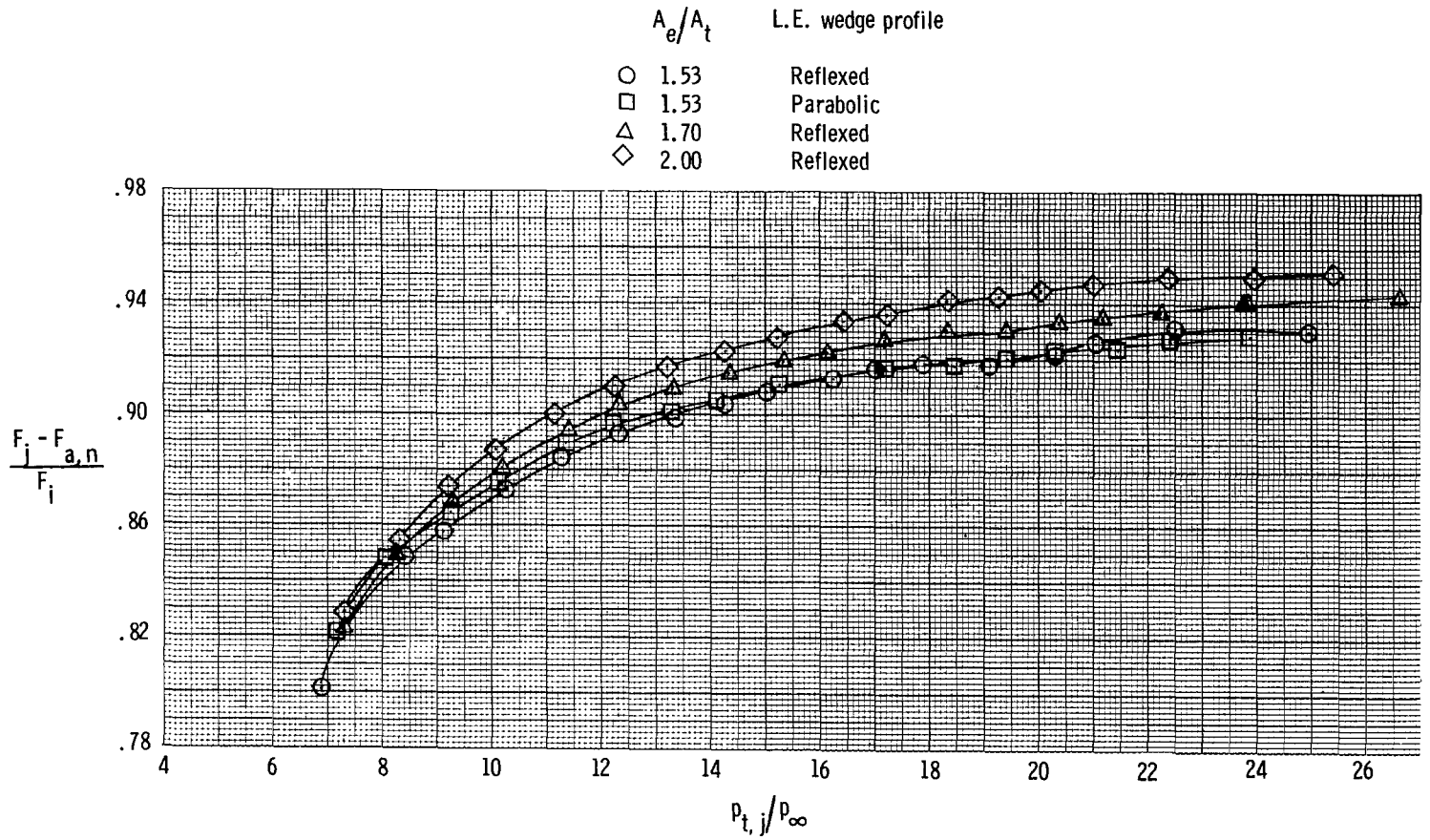

(b) $\beta_c = 10^o$.

Figure 26.- Concluded.

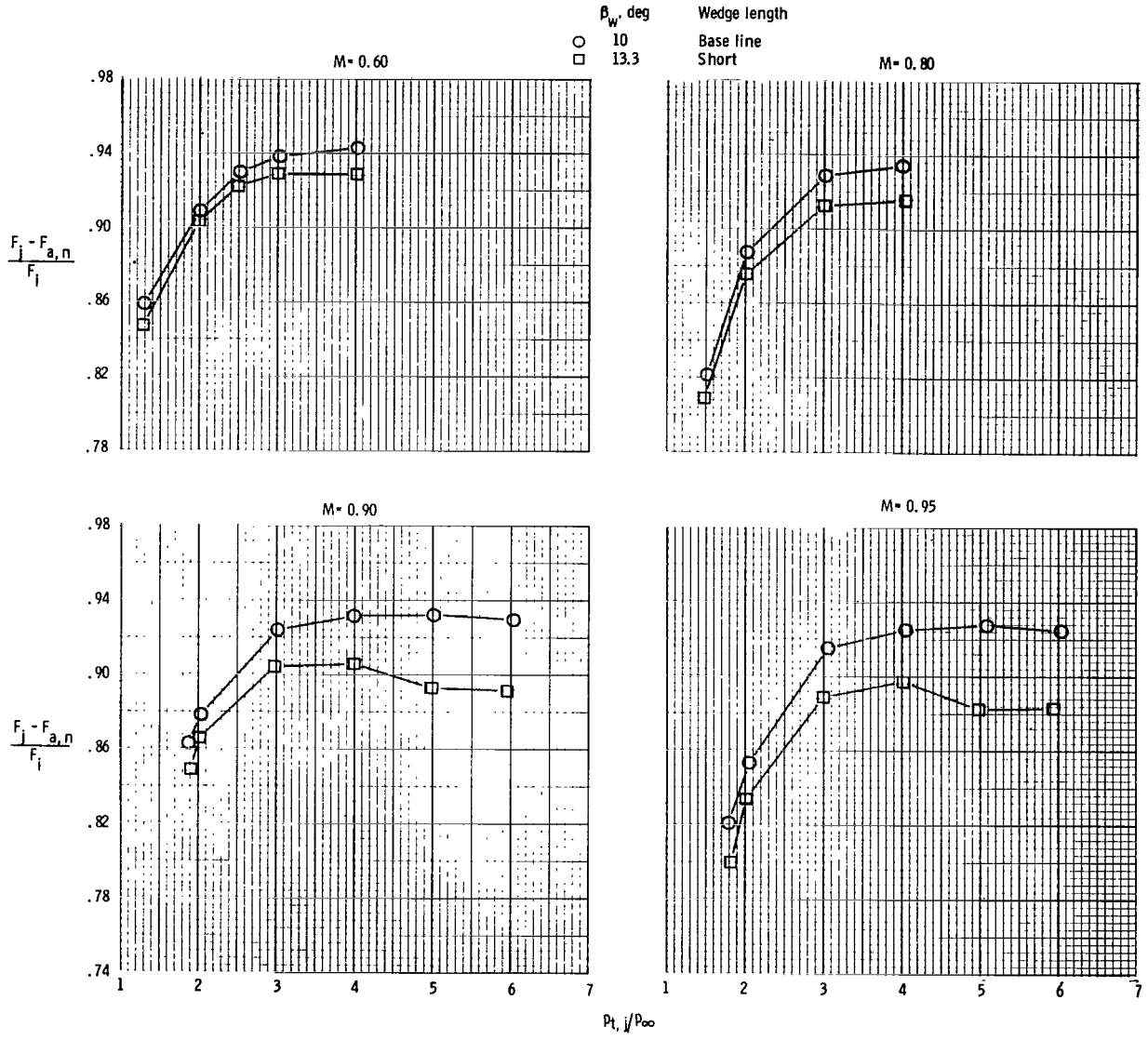

(a) Subsonic free-stream conditions.

Figure 27.- Effect of wedge half-angle on aeropropulsion thrust ratio of two-dimensional wedge nozzle with $A_e/A_t = 1.10$ and $\beta_c = 10^o$.

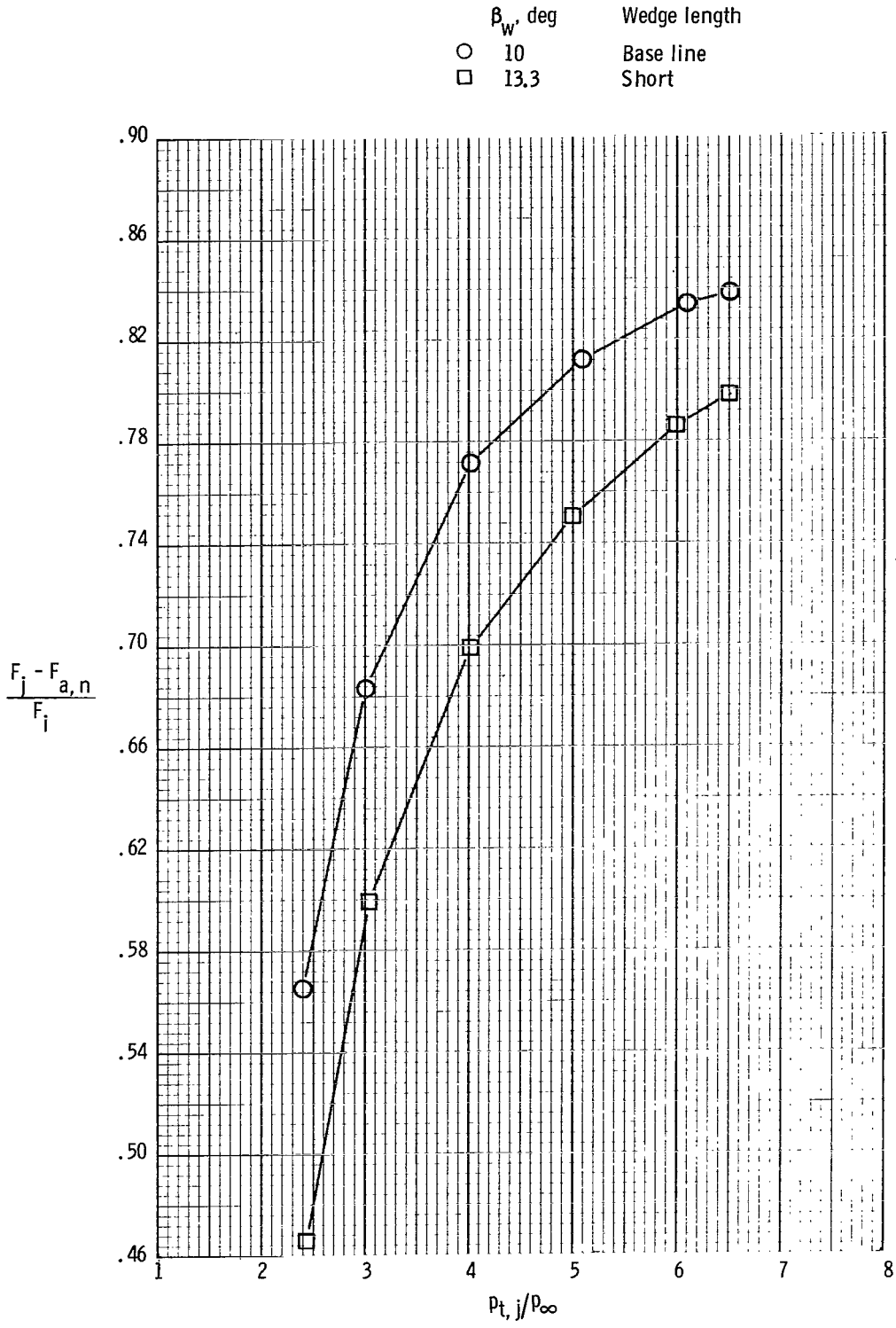

(b) Supersonic free-stream conditions. M = 1.20.

Figure 27.- Concluded.

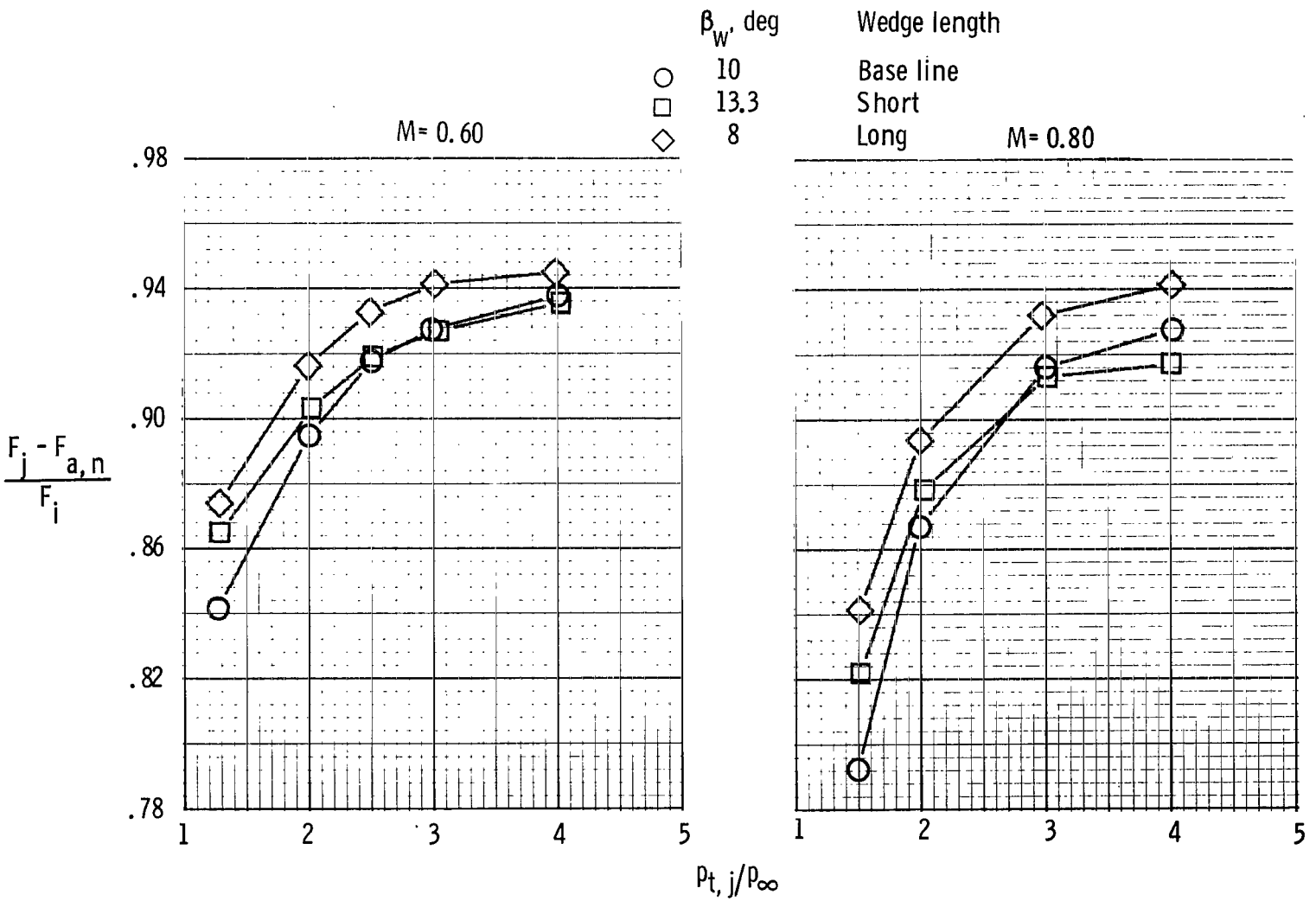

(a) Subsonic free-stream conditions.

Figure 28.- Effect of wedge half-angle on aeropropulsion thrust ratio of two-dimensional wedge nozzle with $A_e/A_t = 1.10$ and $\beta_c = 18^o$.

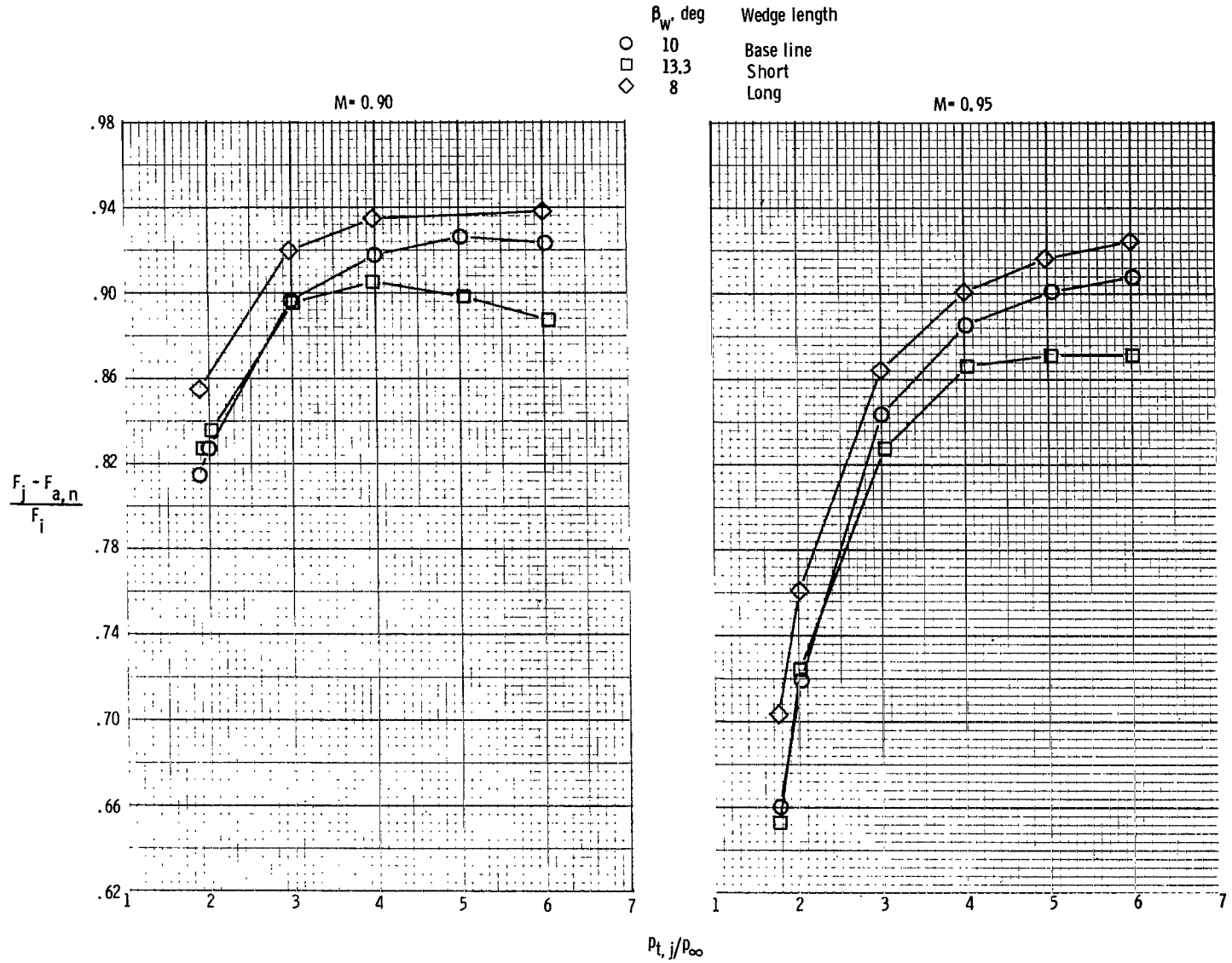

(a) Concluded.

Figure 28.- Continued.

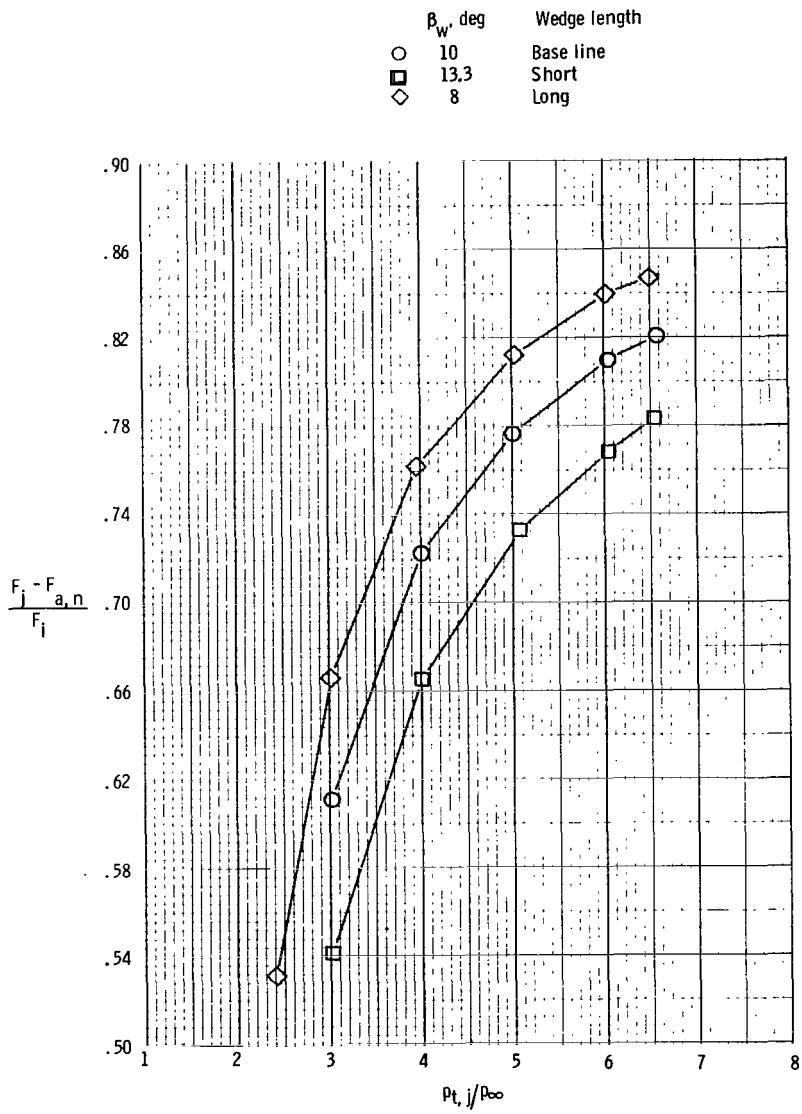

(b) Supersonic free-stream conditions. M = 1.20.

Figure 28.- Concluded.

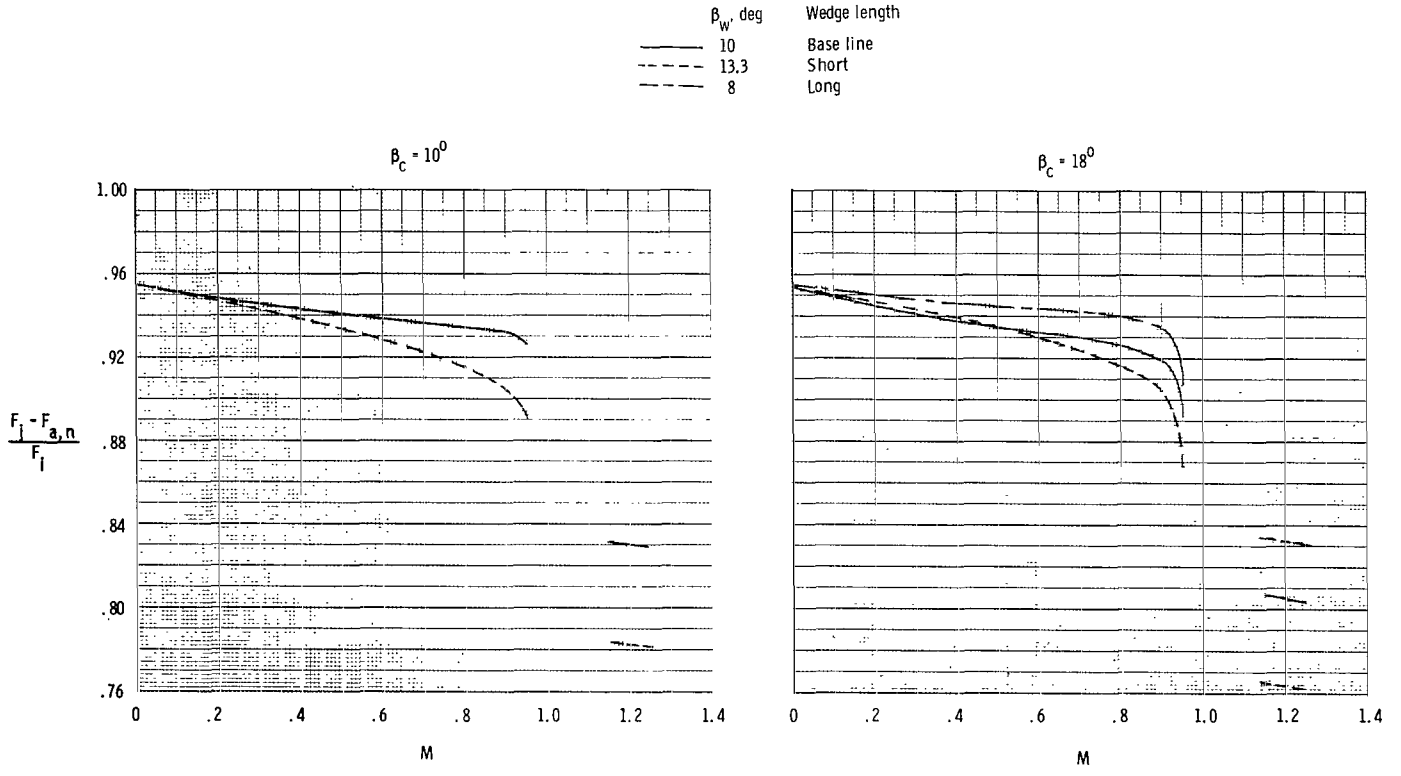

Figure 29.- Effect of wedge half-angle on two-dimensional wedge nozzle performance for two cowl boattail angles at EPR schedule. $A_e/A_t = 1.10$.

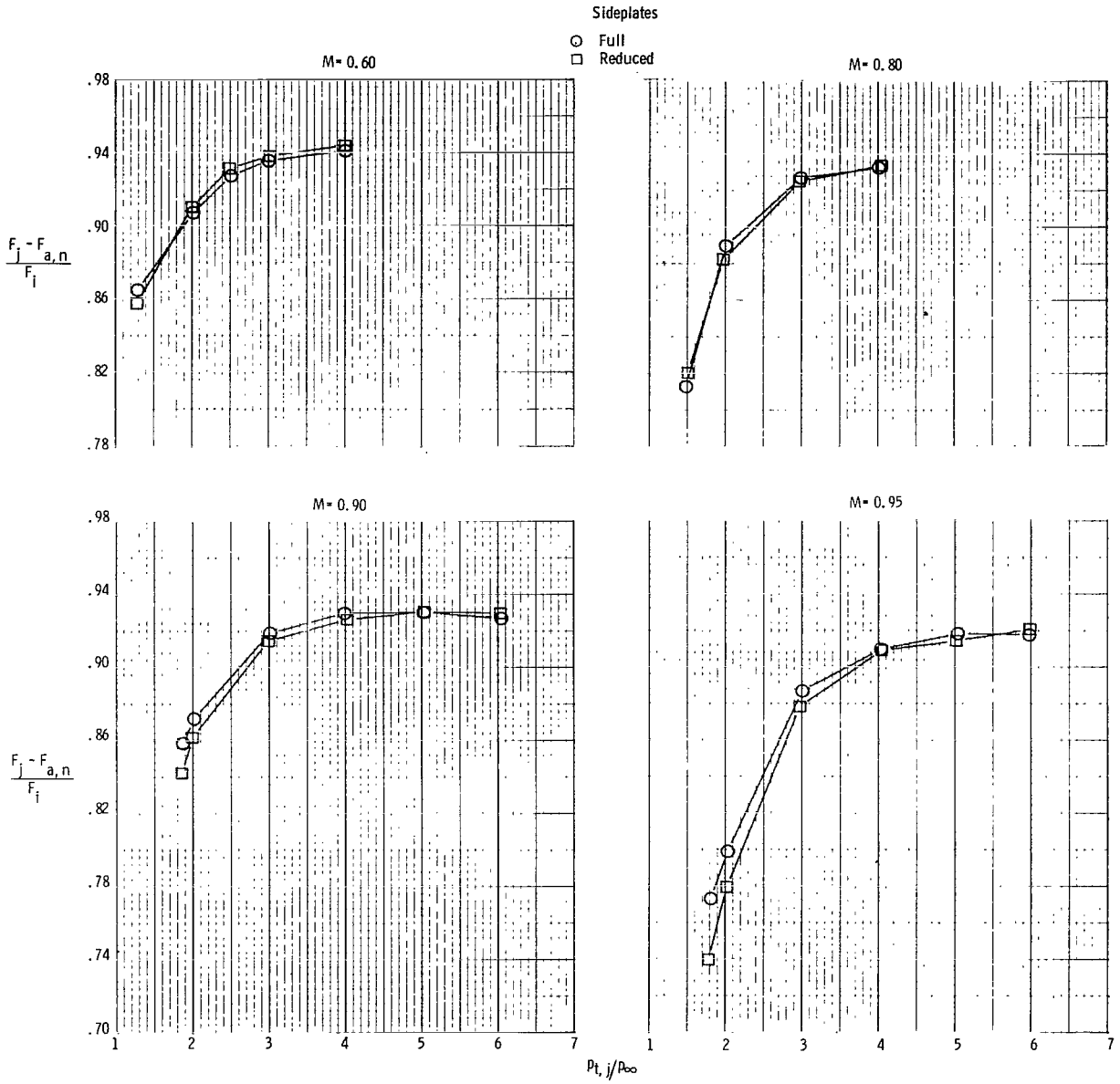

(a) Subsonic free-stream conditions.

Figure 30.- Effect of sideplate reduction on performance of two-dimensional wedge nozzle with $A_e/A_t = 1.10$. $\beta_c = 14^\circ$.

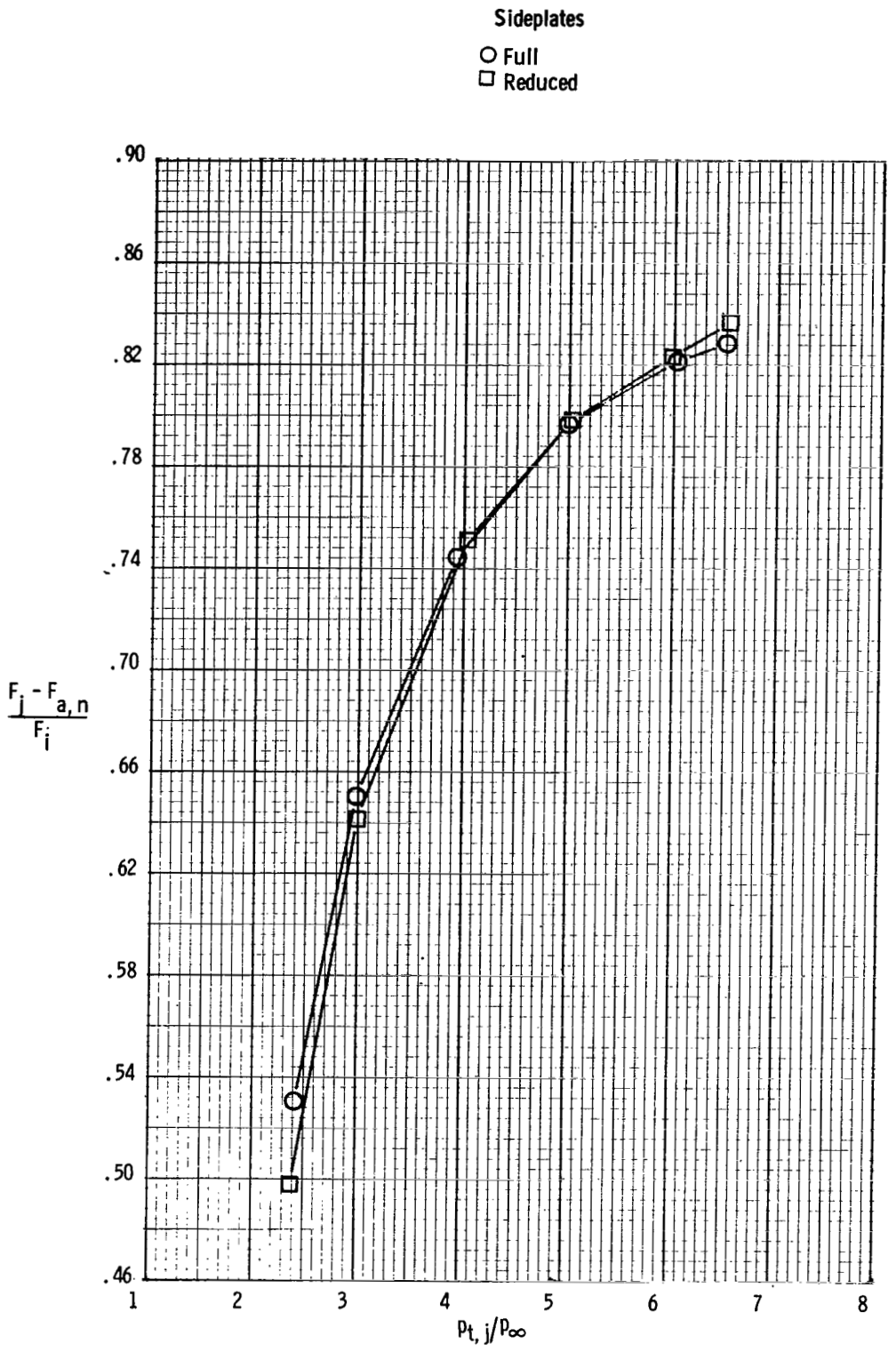

(b) Supersonic free-stream conditions. M = 1.20.

Figure 30.- Concluded.

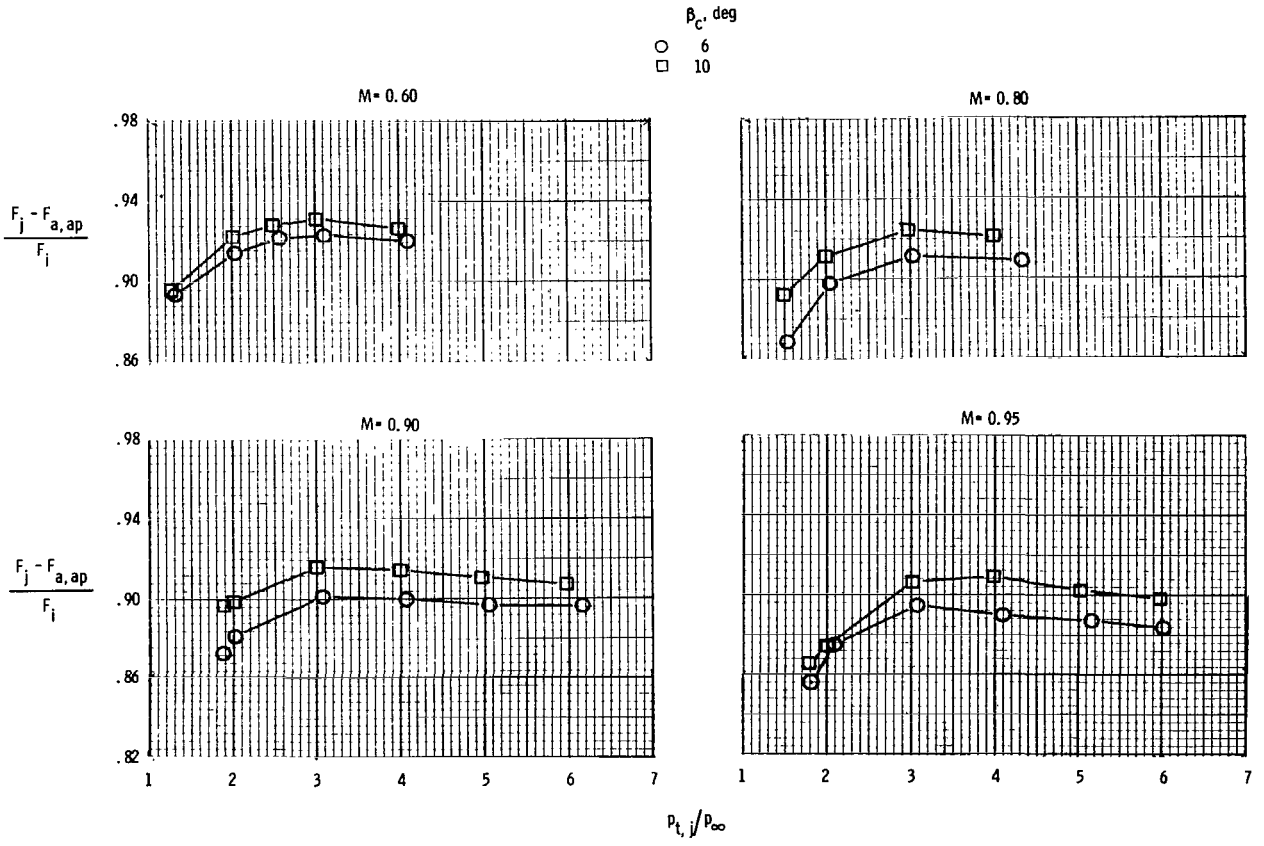

(a) Subsonic free-stream conditions.

Figure 31.- Effect of cowl boattail angle on aeropropulsion performance, neglecting skin friction drag, of two-dimensional wedge nozzle with $A_e/A_t = 1.00$. $\beta_w = 10^o$.

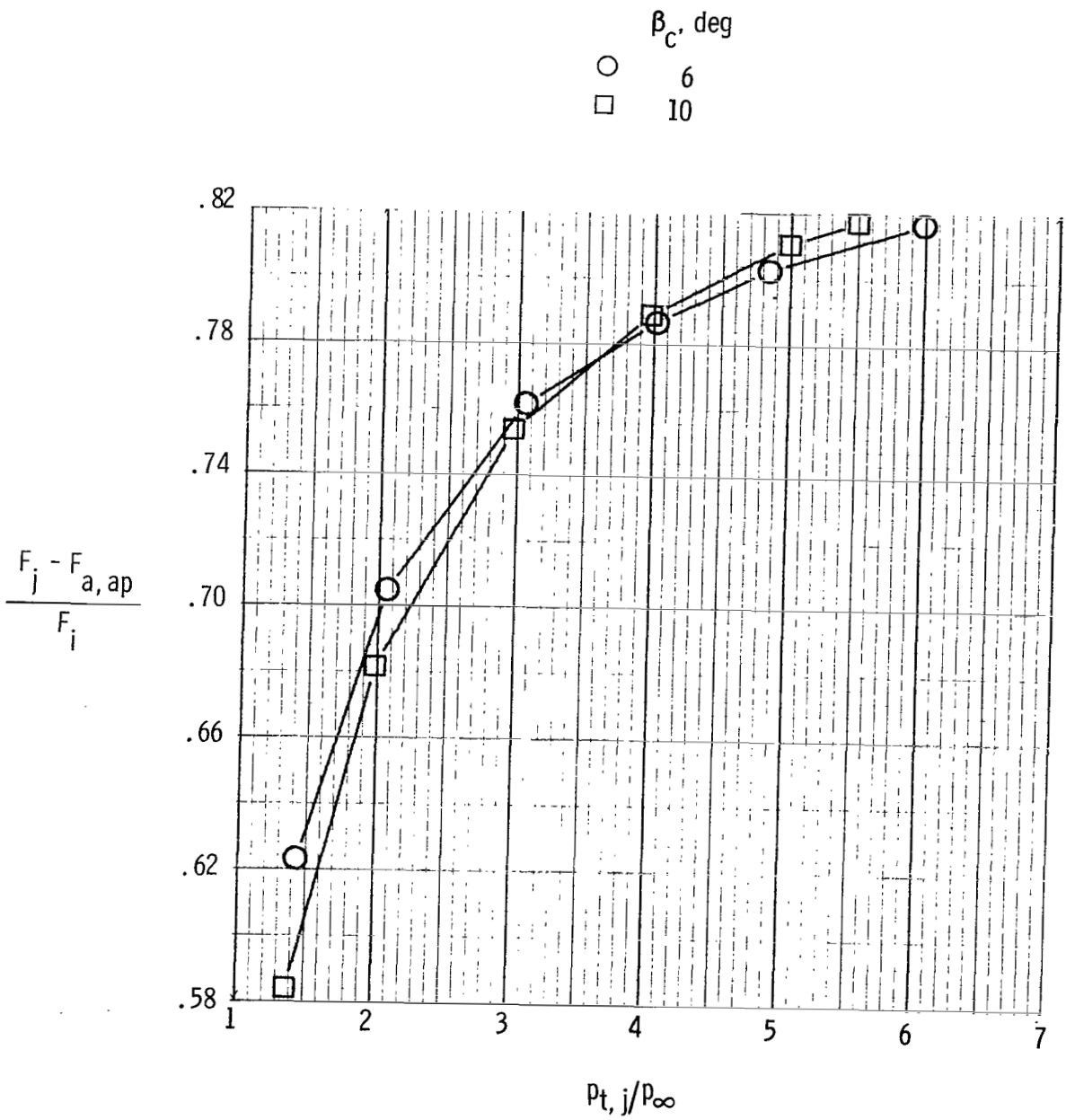

(b) Supersonic free-stream conditions. M = 1.20.

Figure 31.- Concluded.

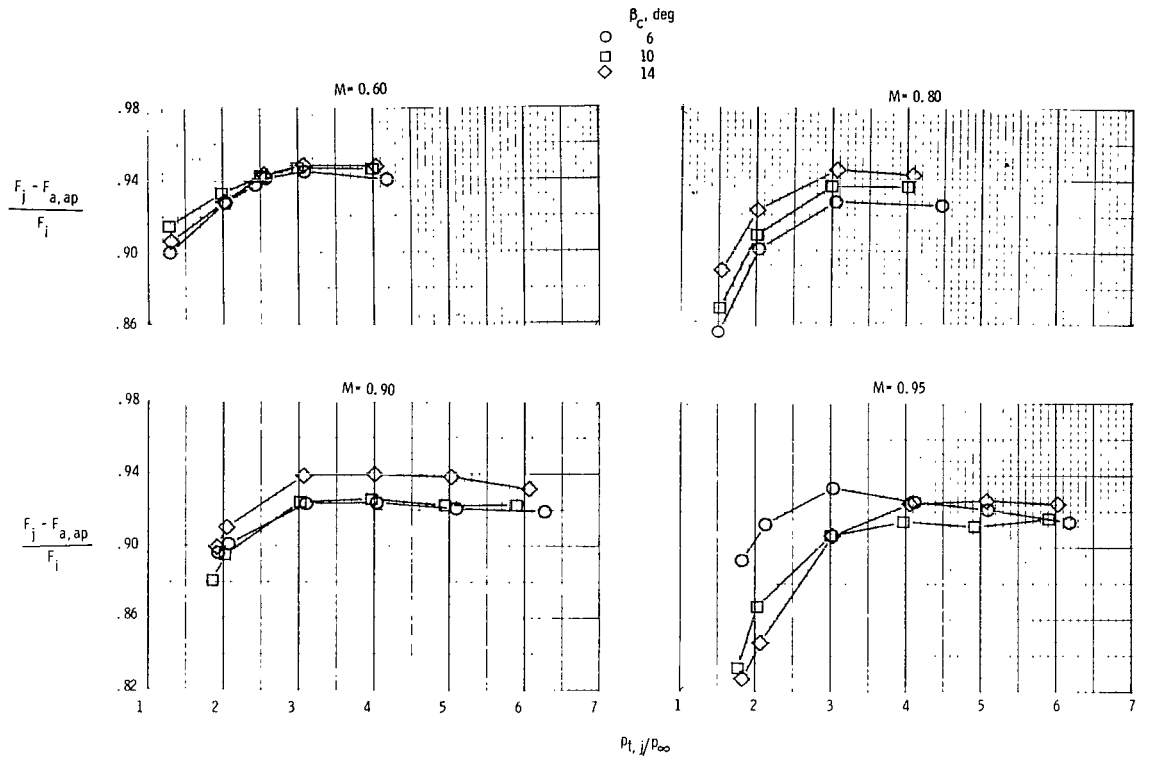

(a) Subsonic free-stream conditions.

Figure 32.- Effect of cowl boattail angle on aeropropulsion performance, neglecting skin friction drag, of two-dimensional wedge nozzle with $A_e/A_t = 1.05$. $\beta_w = 10^o$.

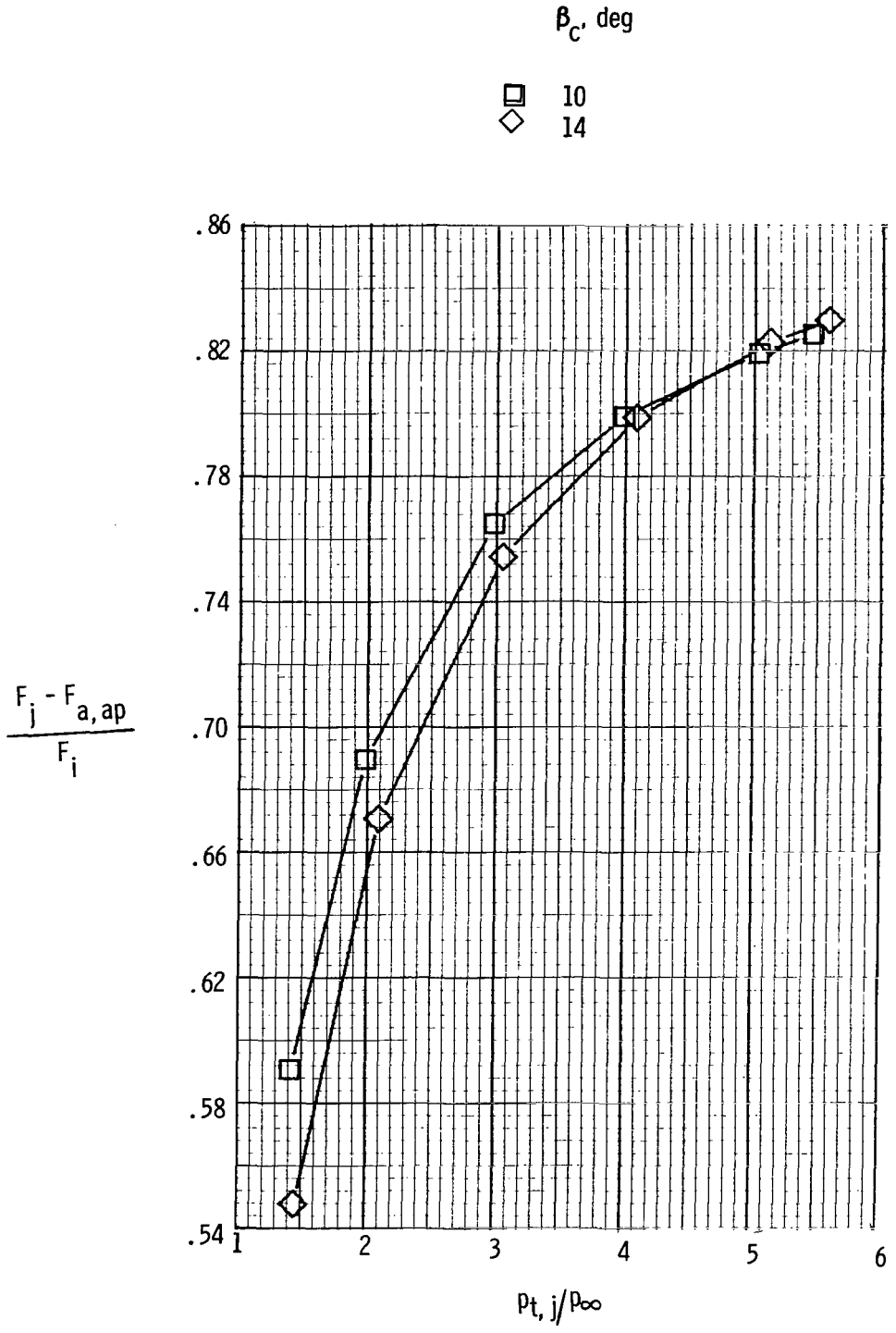

(b) Supersonic free-stream conditions. M = 1.20.

Figure 32.- Concluded.

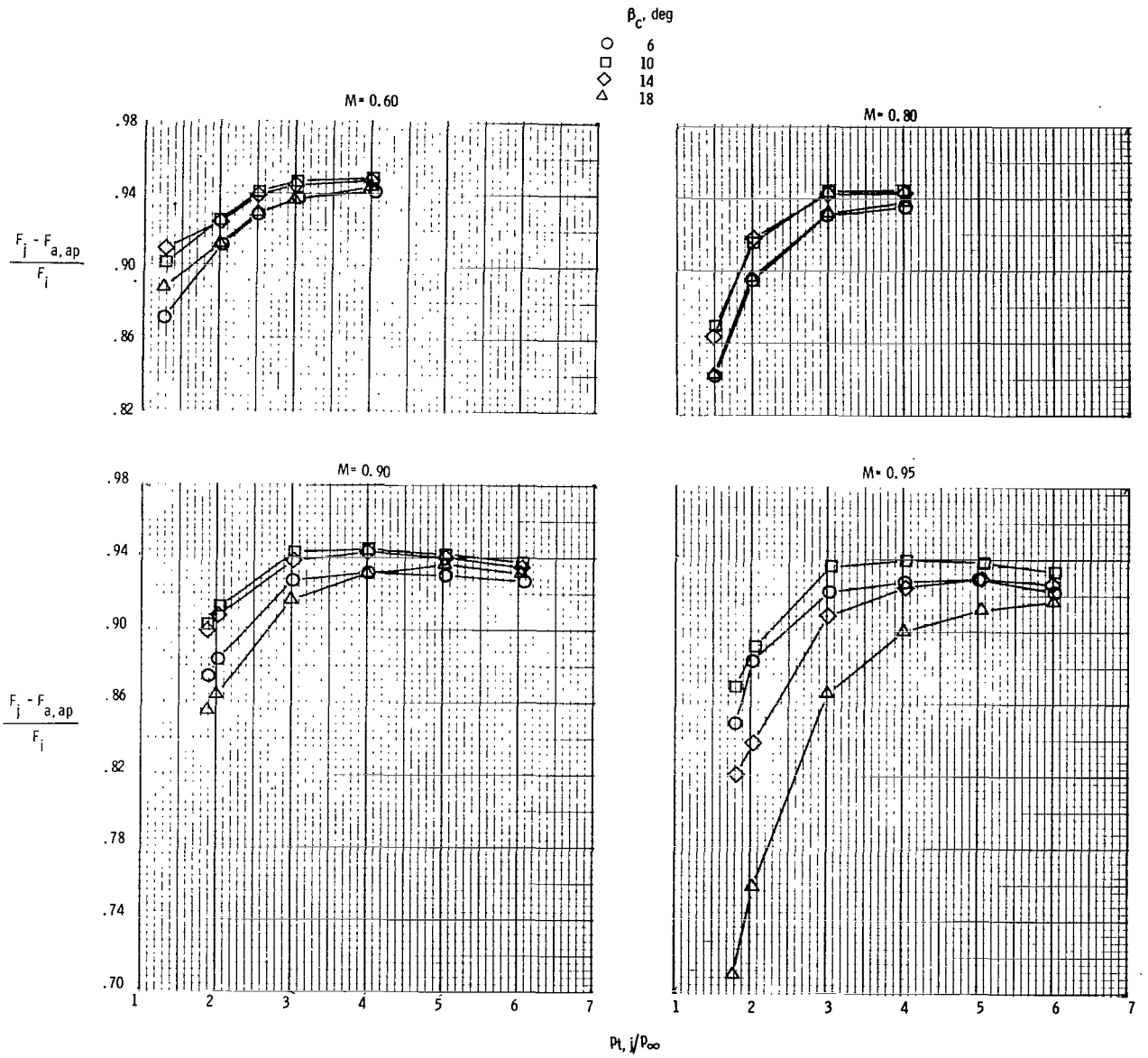

(a) Subsonic free-stream conditions.

Figure 33.- Effect of cowl boattail angle on aeropropulsion performance, neglecting skin friction drag, of two-dimensional wedge nozzle with $A_e/A_t = 1.10$. $\beta_w = 10^o$.

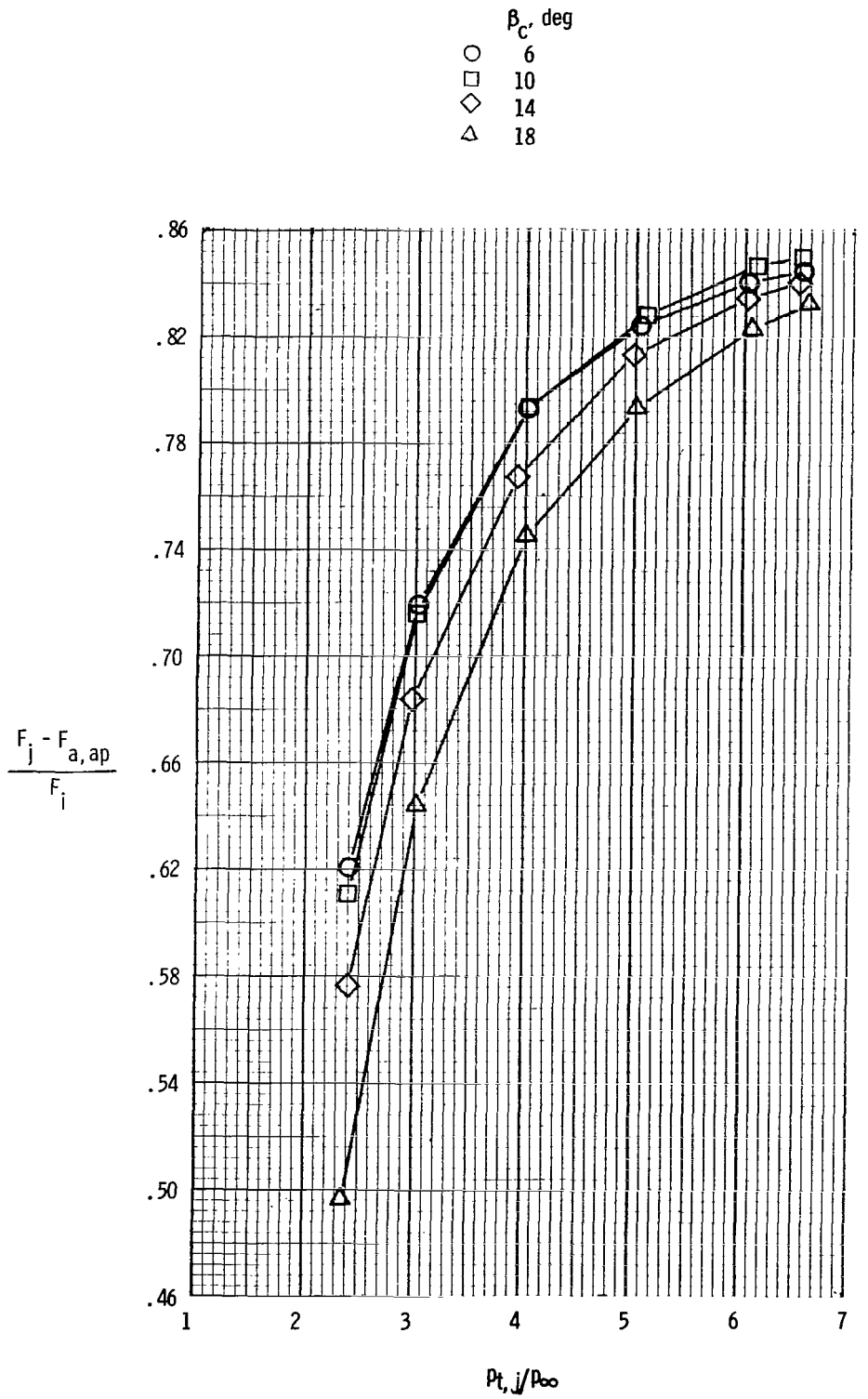

(b) Supersonic free-stream conditions. M = 1.20.

Figure 33.- Concluded.

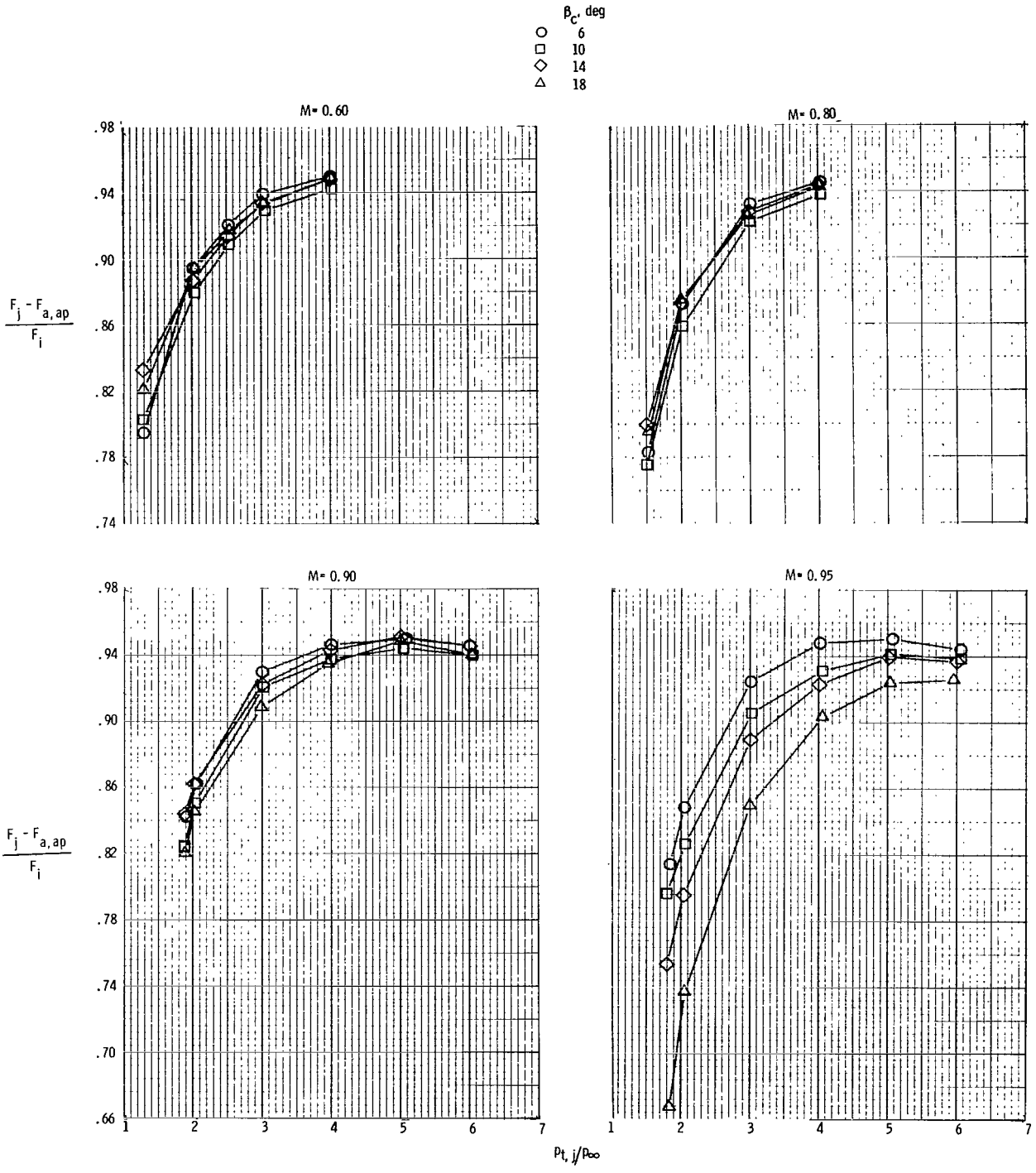

(a) Subsonic free-stream conditions.

Figure 34.- Effect of cowl boattail angle on aeropropulsion performance, neglecting skin friction drag, of two-dimensional wedge nozzle with $A_e/A_t = 1.30$. $\beta_w = 4.5^o/9^o$.

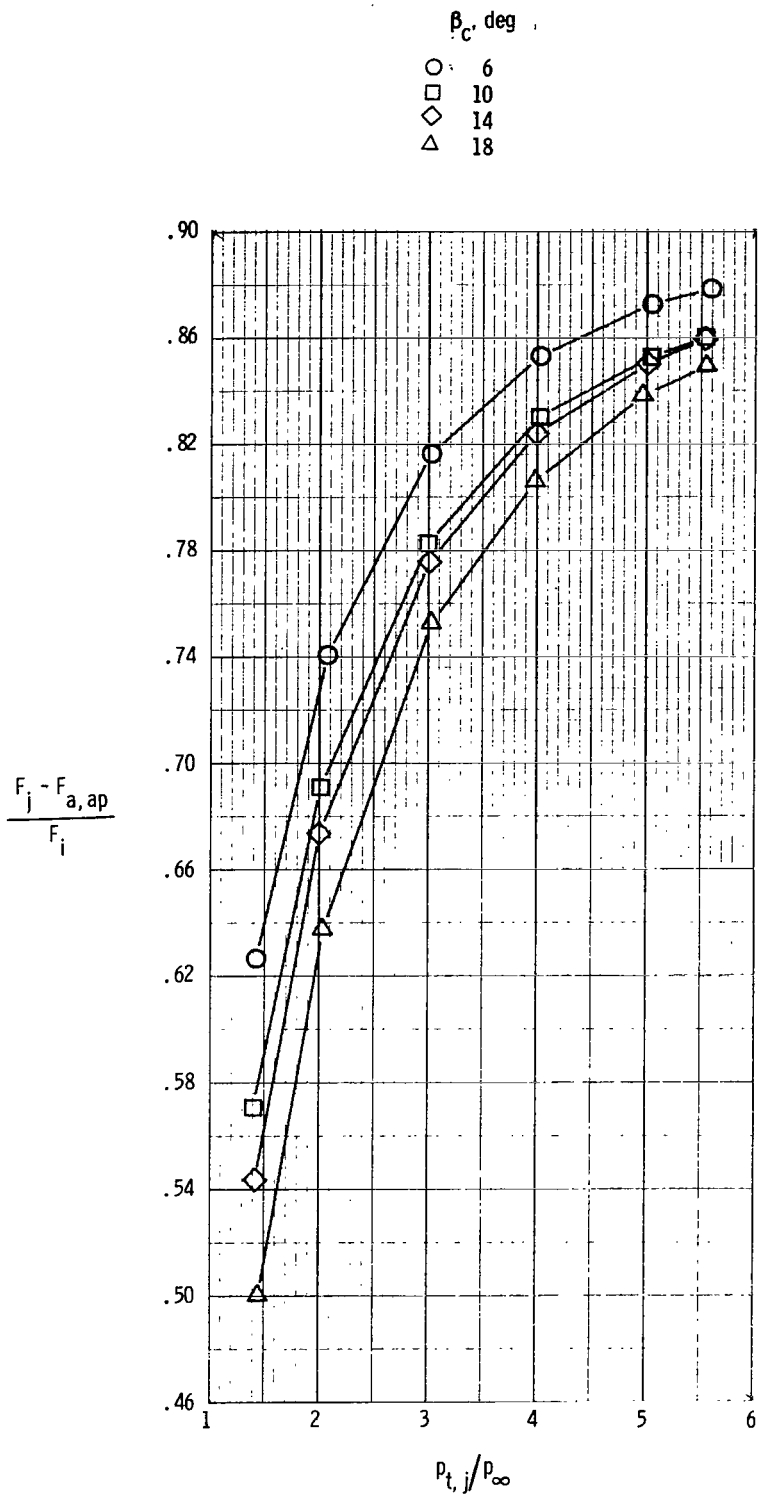

(b) Supersonic free-stream conditions. M = 1.20.

Figure 34.- Concluded.

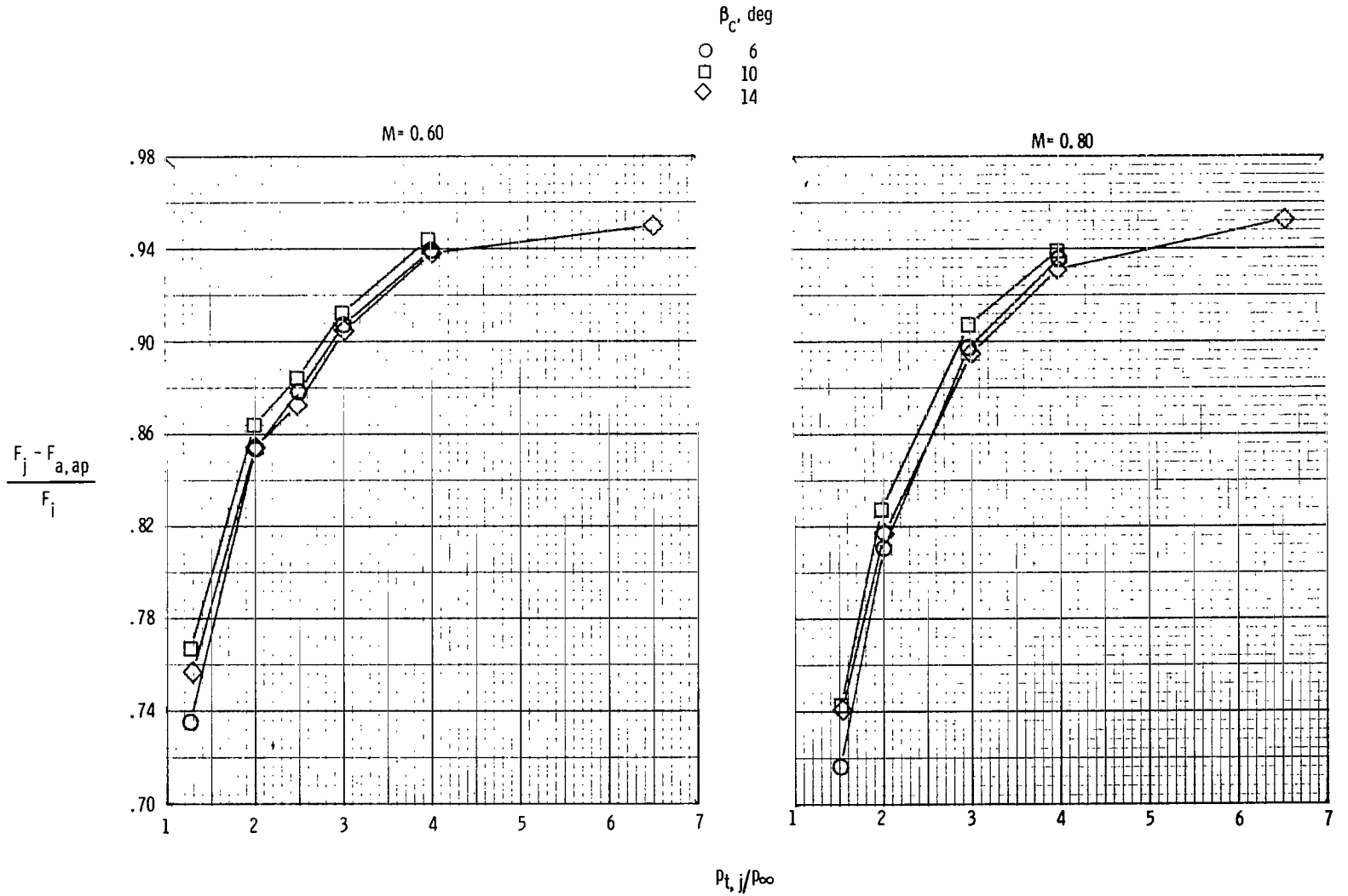

(a) Subsonic free-stream conditions.

Figure 35.- Effect of cowl boattail angle on aeropropulsion performance, neglecting skin friction drag, of two-dimensional wedge nozzle with $A_e/A_t = 1.53$. $\beta_w = 8^o$.

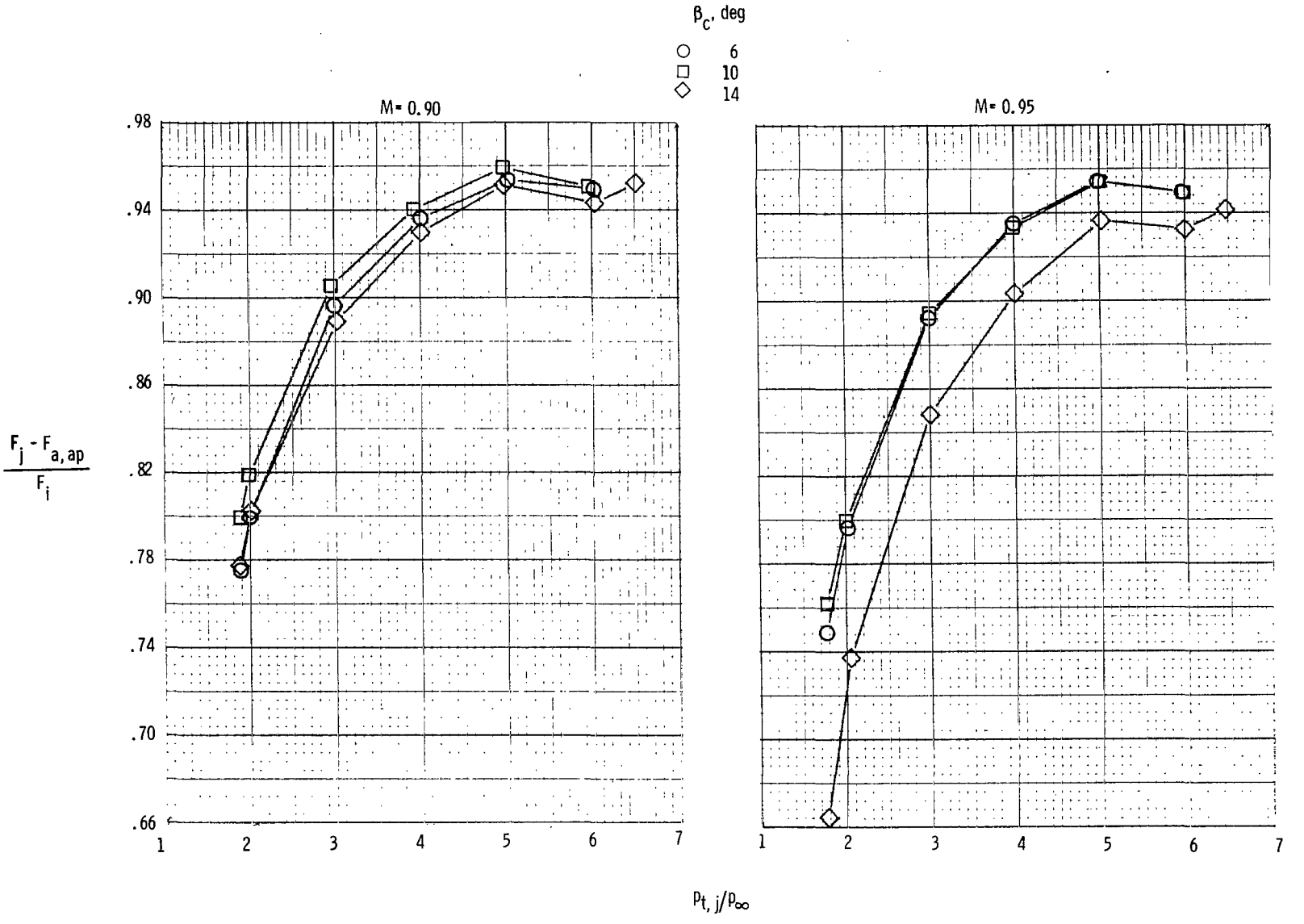

(a) Concluded.

Figure 35.- Continued.

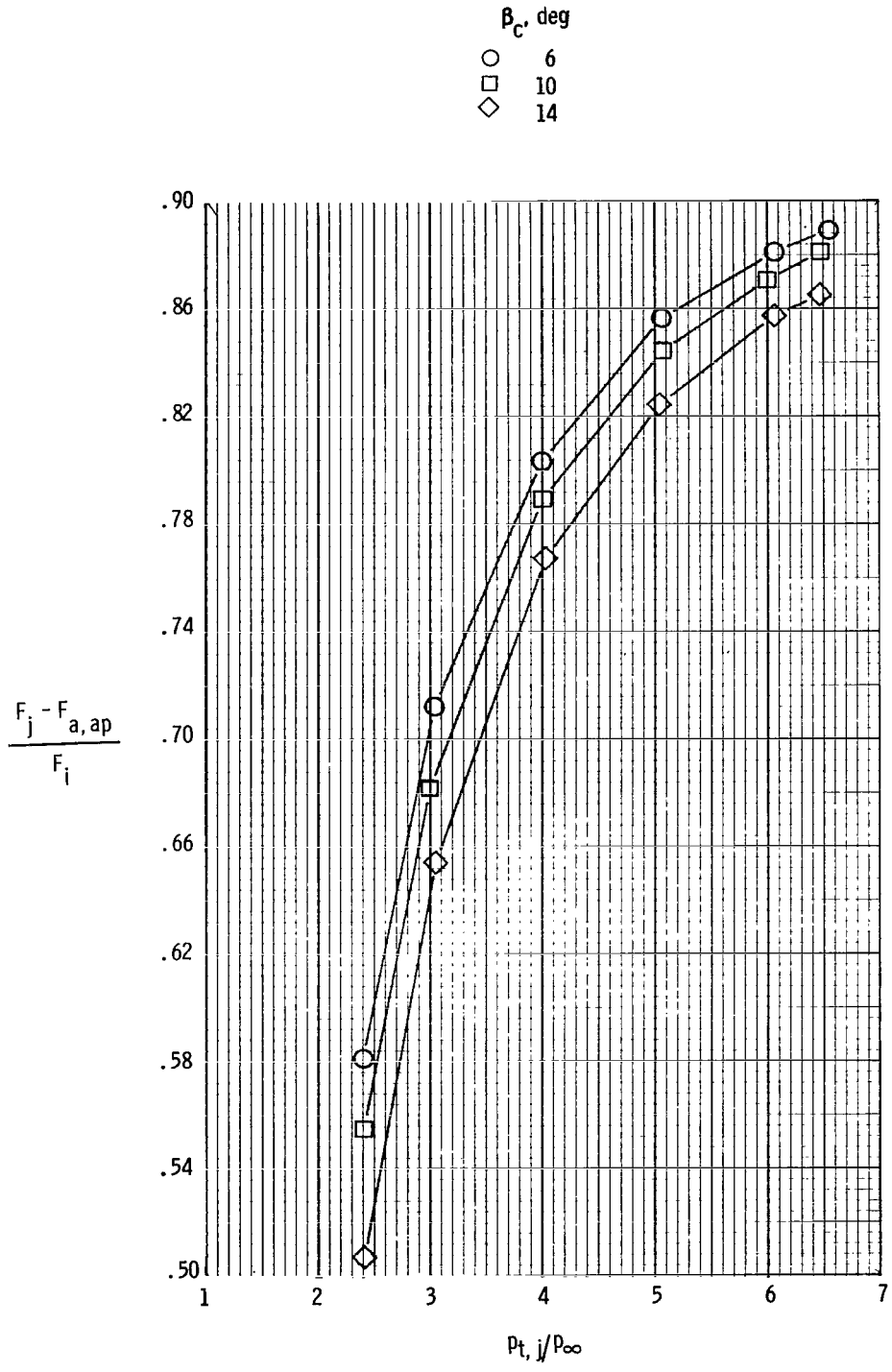

(b) Supersonic free-stream conditions. M = 1.20.

Figure 35.- Concluded.

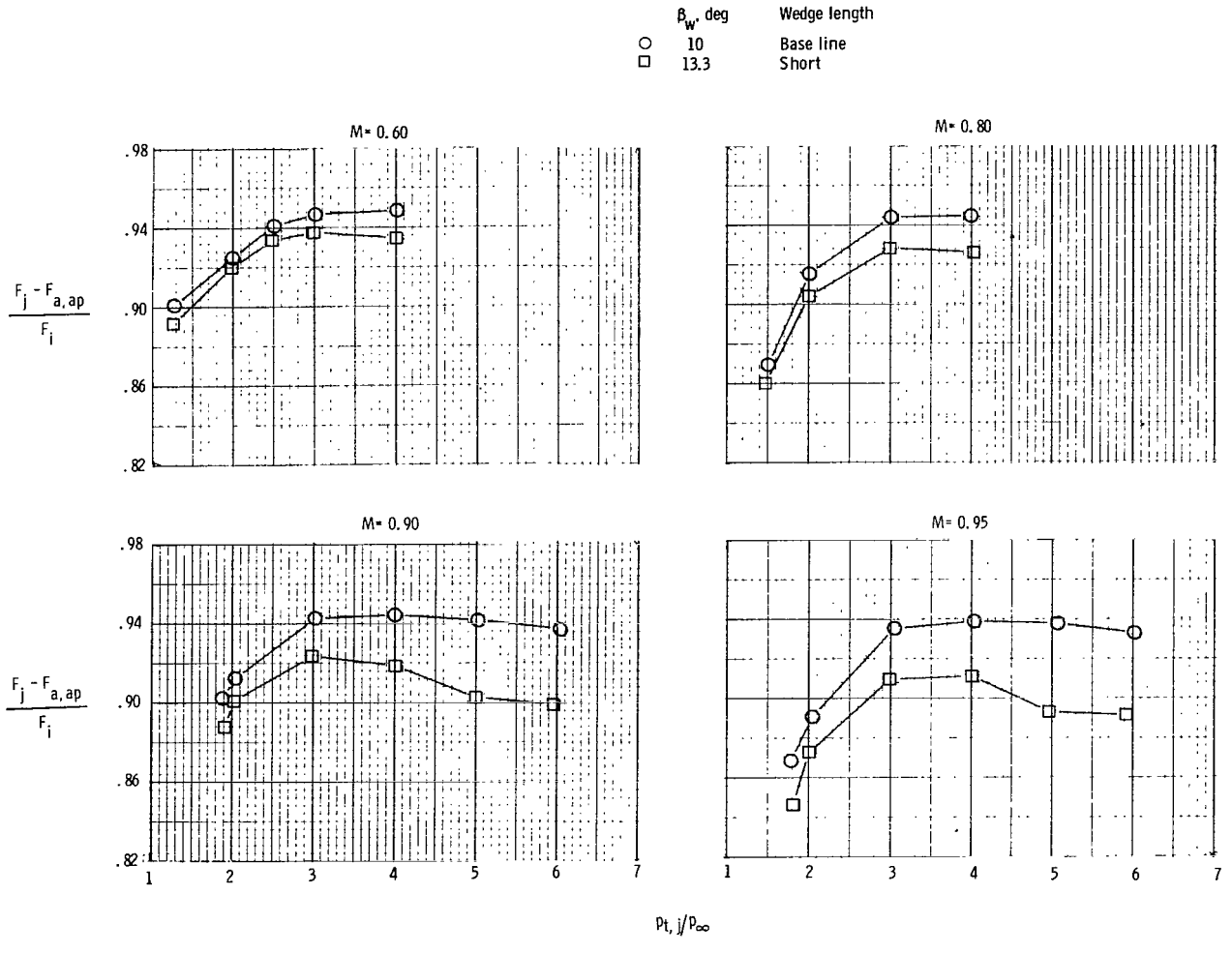

(a) Subsonic free-stream conditions.

Figure 36.- Effect of wedge half-angle on aeropropulsion performance, neglecting skin friction drag, of two-dimensional wedge nozzle with $A_e/A_t = 1.10$. $\beta_c = 10^o$.

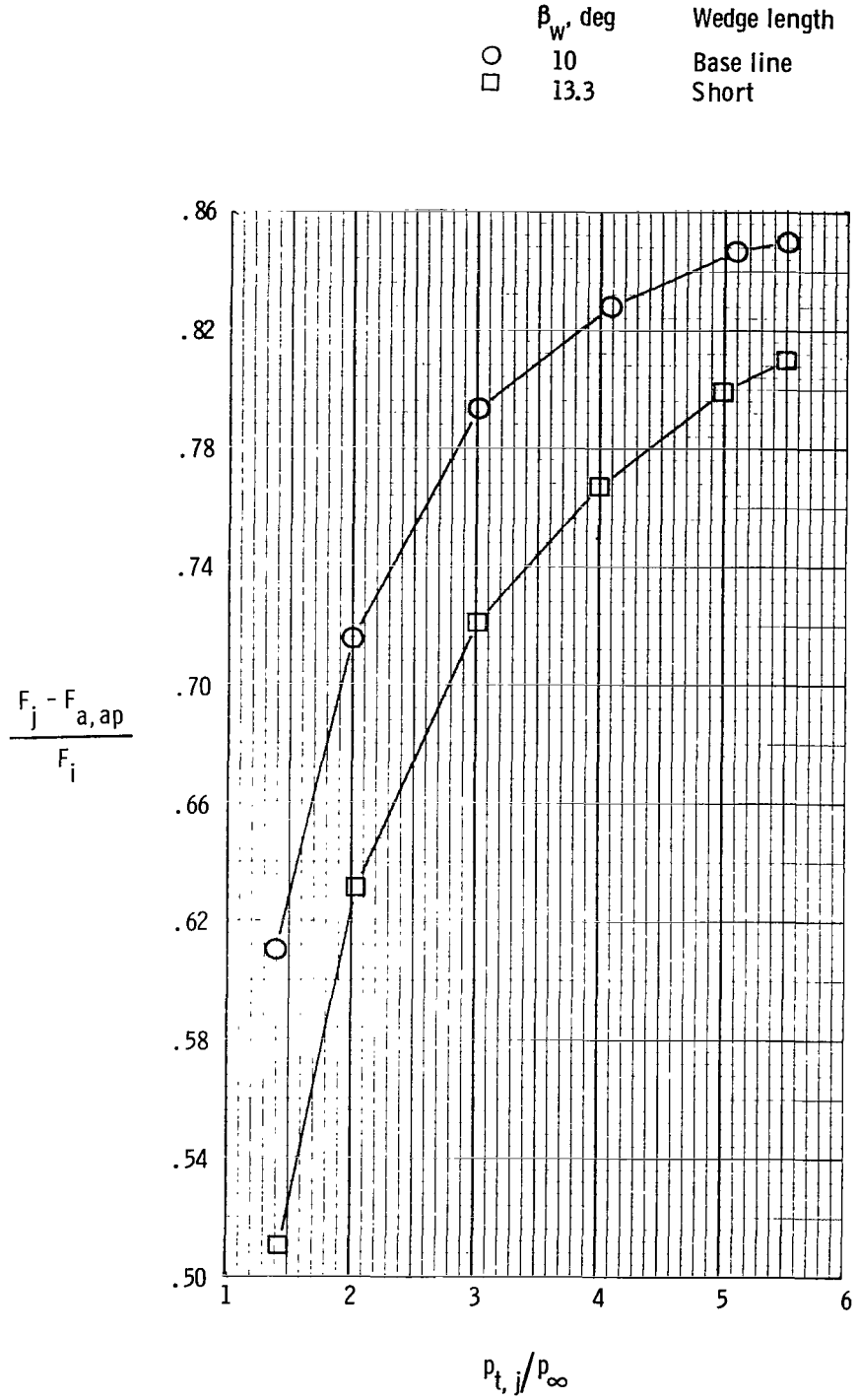

(b) Supersonic free-stream conditions. M = 1.20.

Figure 36.- Concluded.

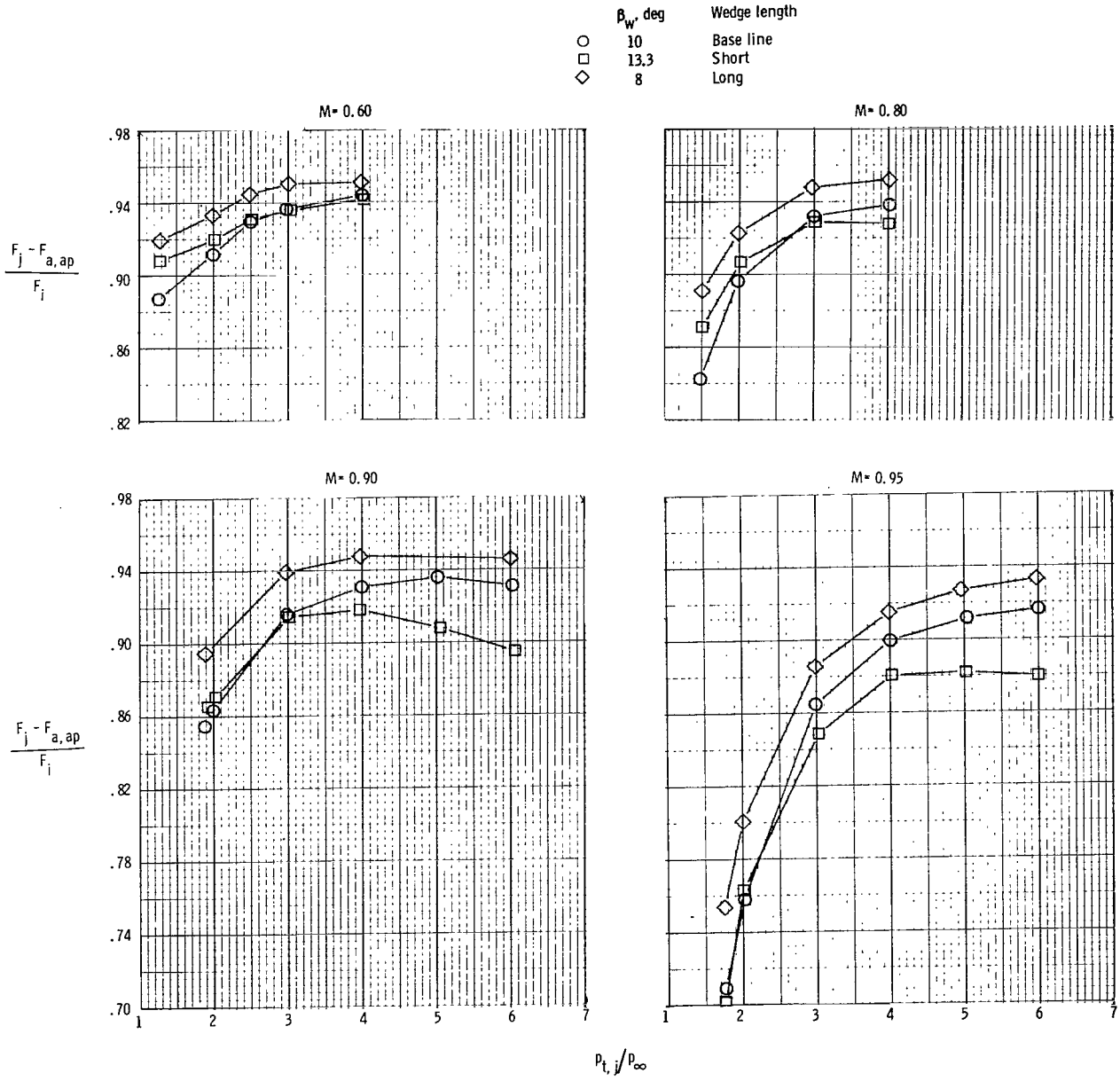

(a) Subsonic free-stream conditions.

Figure 37.- Effect of wedge half-angle on aeropropulsion performance, neglecting skin friction drag, of two-dimensional wedge nozzle with $A_e/A_t = 1.10$. $\beta_c = 18^o$.

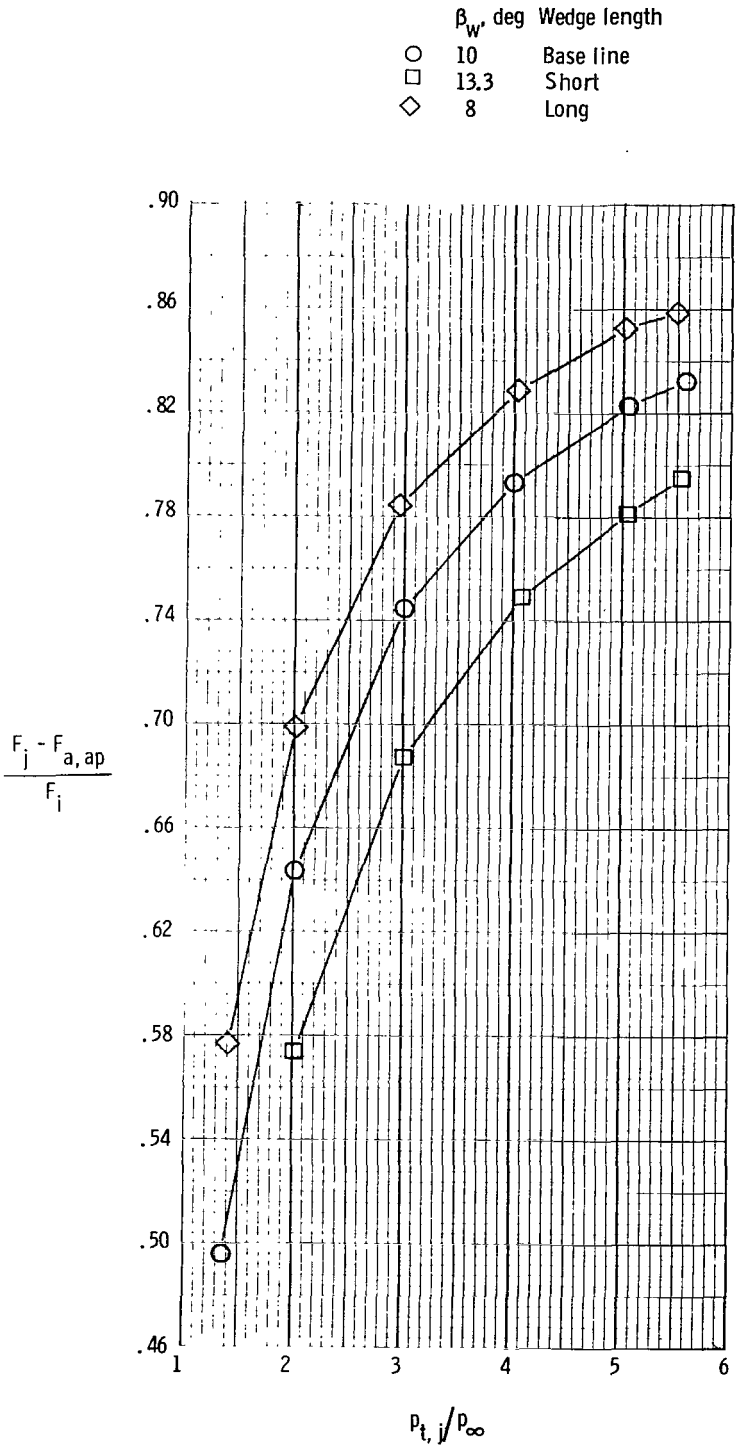

(b) Supersonic free-stream conditions. M = 1.20.

Figure 37.- Concluded.

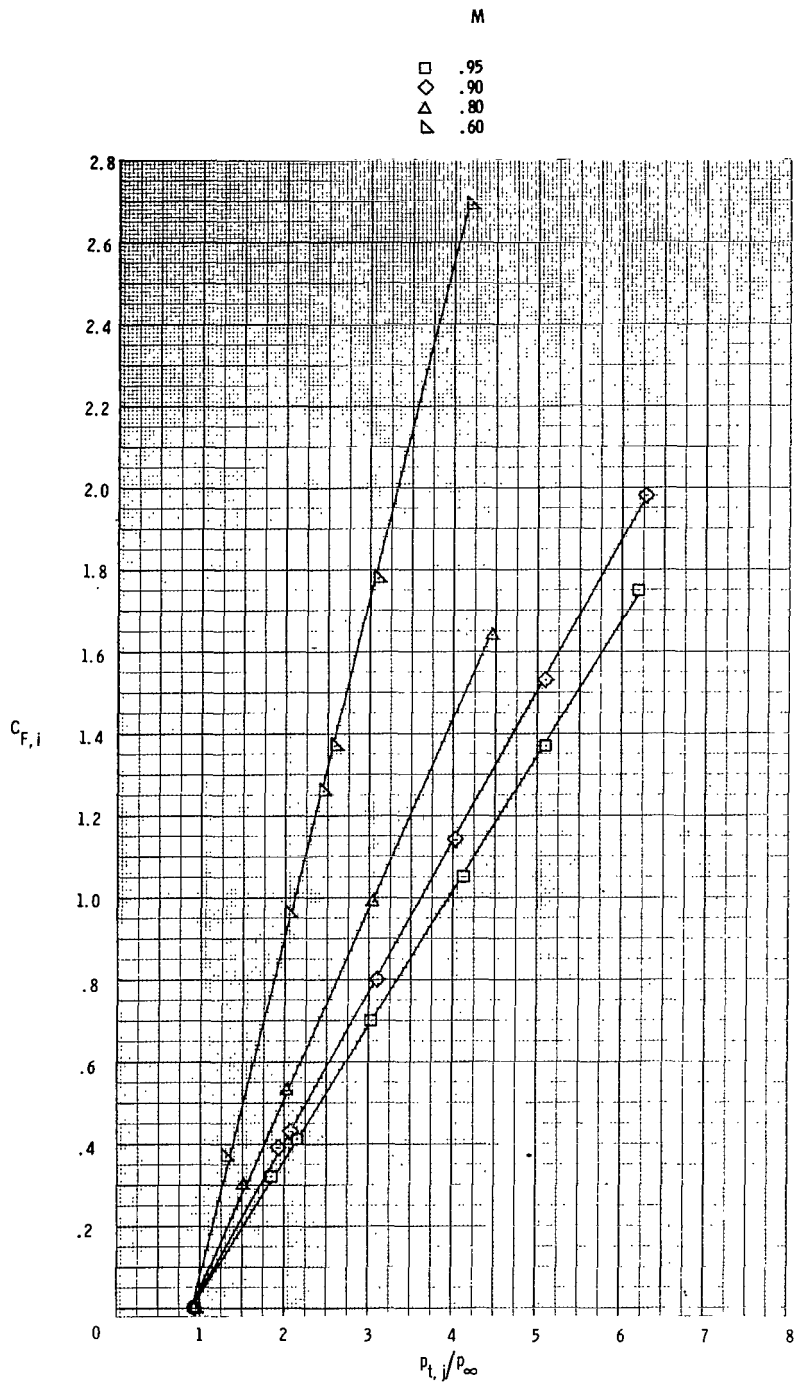

(a) $\beta_c = 6^o$; $A_e/A_t = 1.05$; $\beta_w = 10^o$.

Figure 38.- Variation of aerodynamic ideal thrust coefficient with nozzle pressure ratio for most configurations at all test Mach numbers.

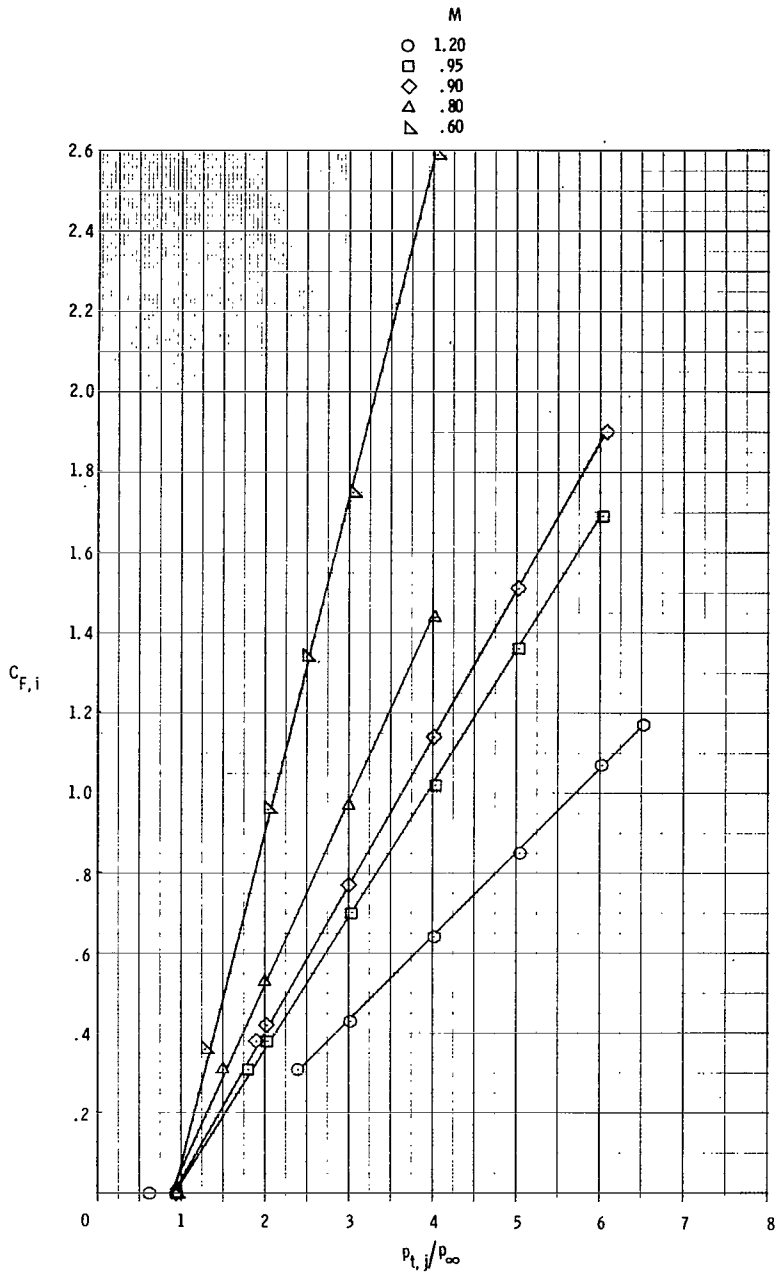

(b) $\beta_c = 6^o$; $A_e/A_t = 1.10$; $\beta_w = 10^o$.

Figure 38.- Continued.

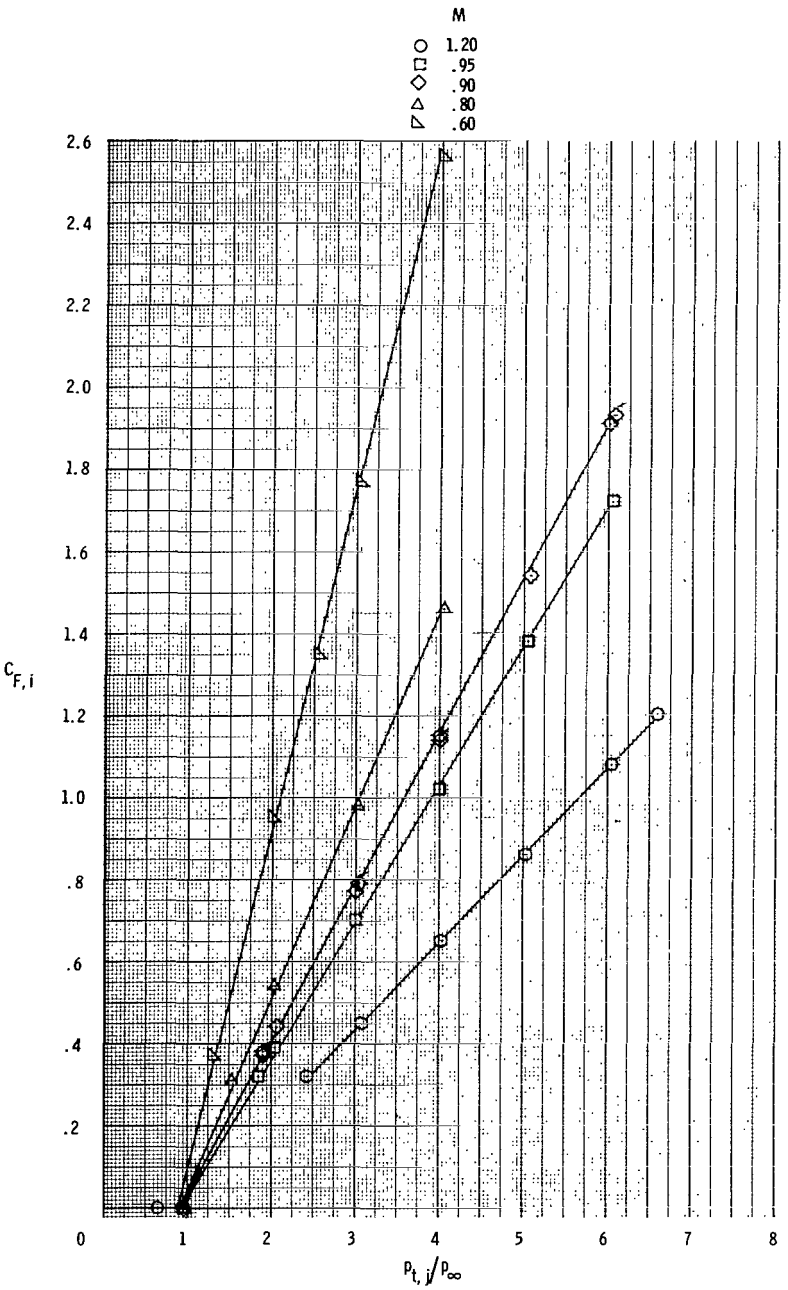

(c) $\beta_c = 6^o$; $A_e/A_t = 1.30$; $\beta_w = 4.5^o/9^o$.

Figure 38.- Continued.

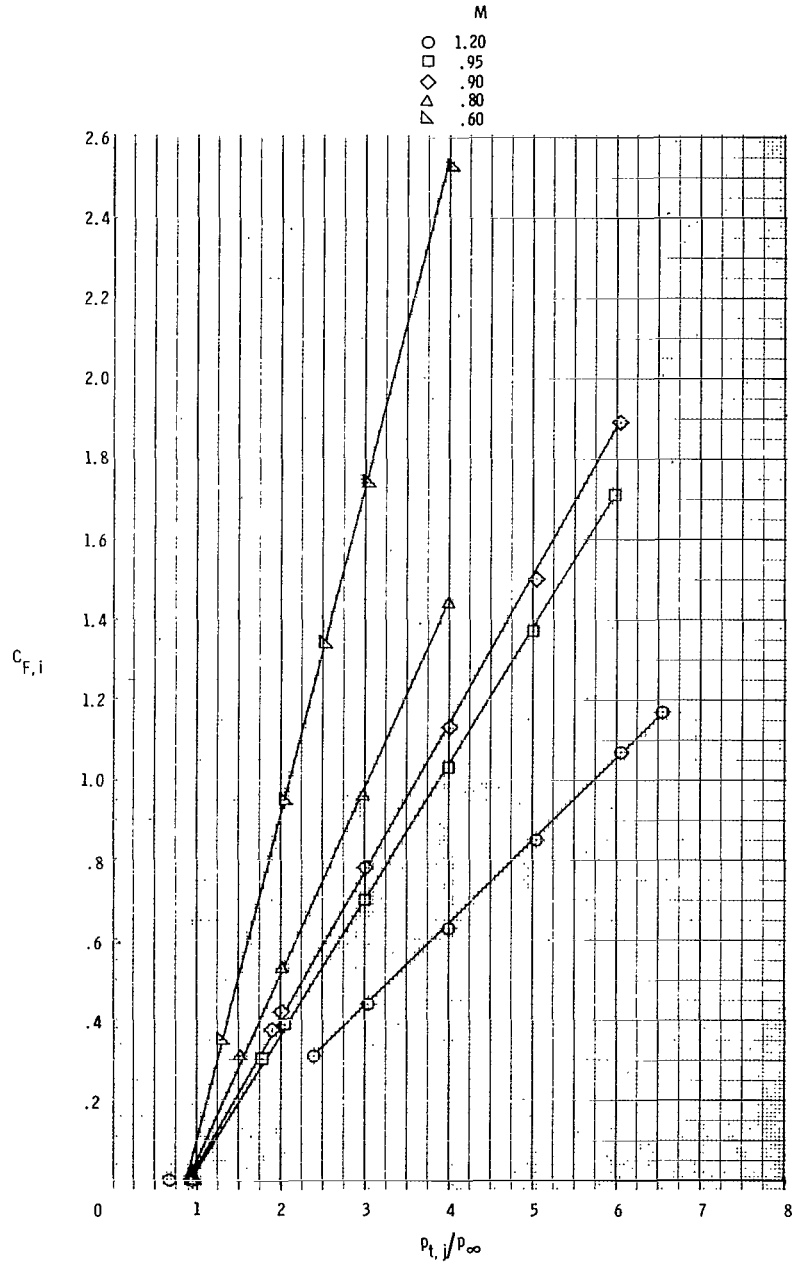

(d) $\beta_c = 6^o$; $A_e/A_t = 1.53$; $\beta_w = 8^o$.

Figure 38.- Continued.

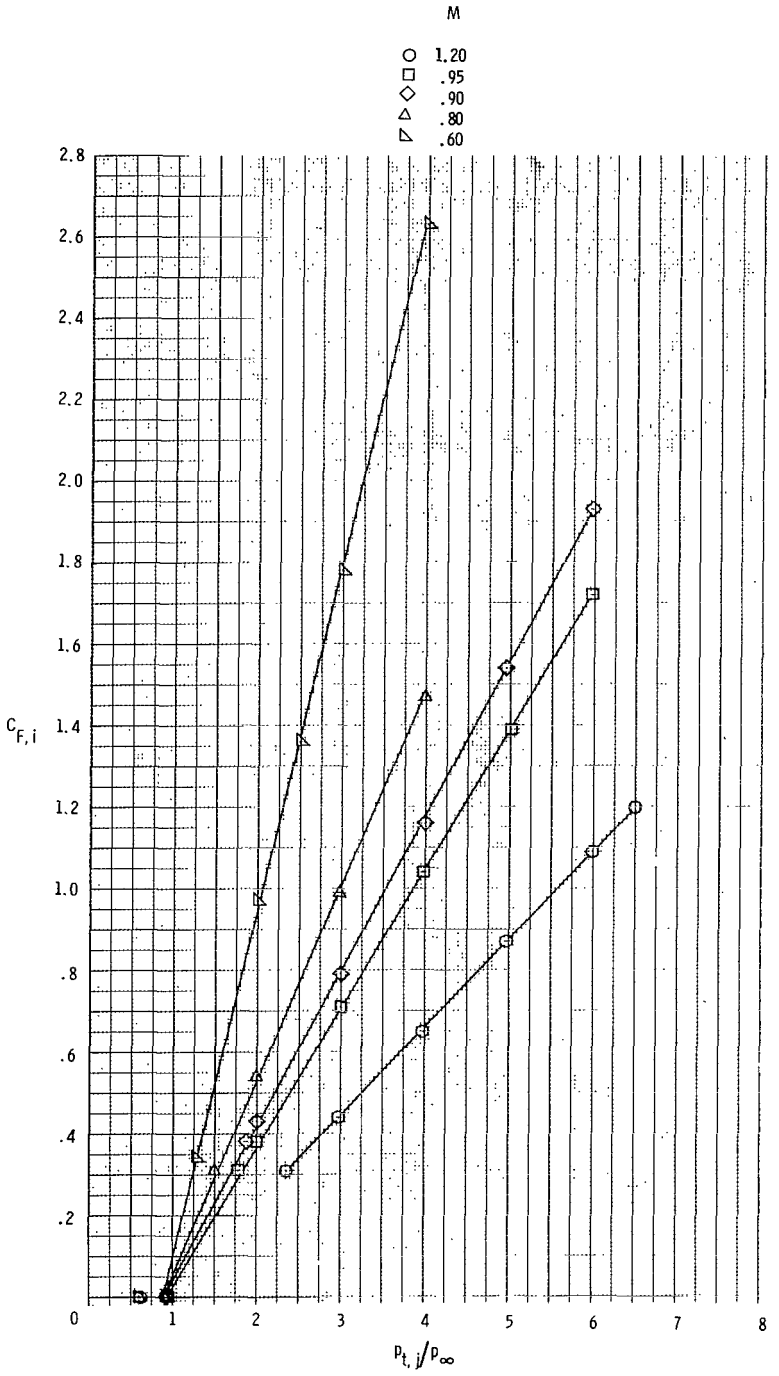

(e) $\beta_c = 10^o$; $A_e/A_t = 1.00$; $\beta_w = 10^o$..

Figure 38.- Continued.

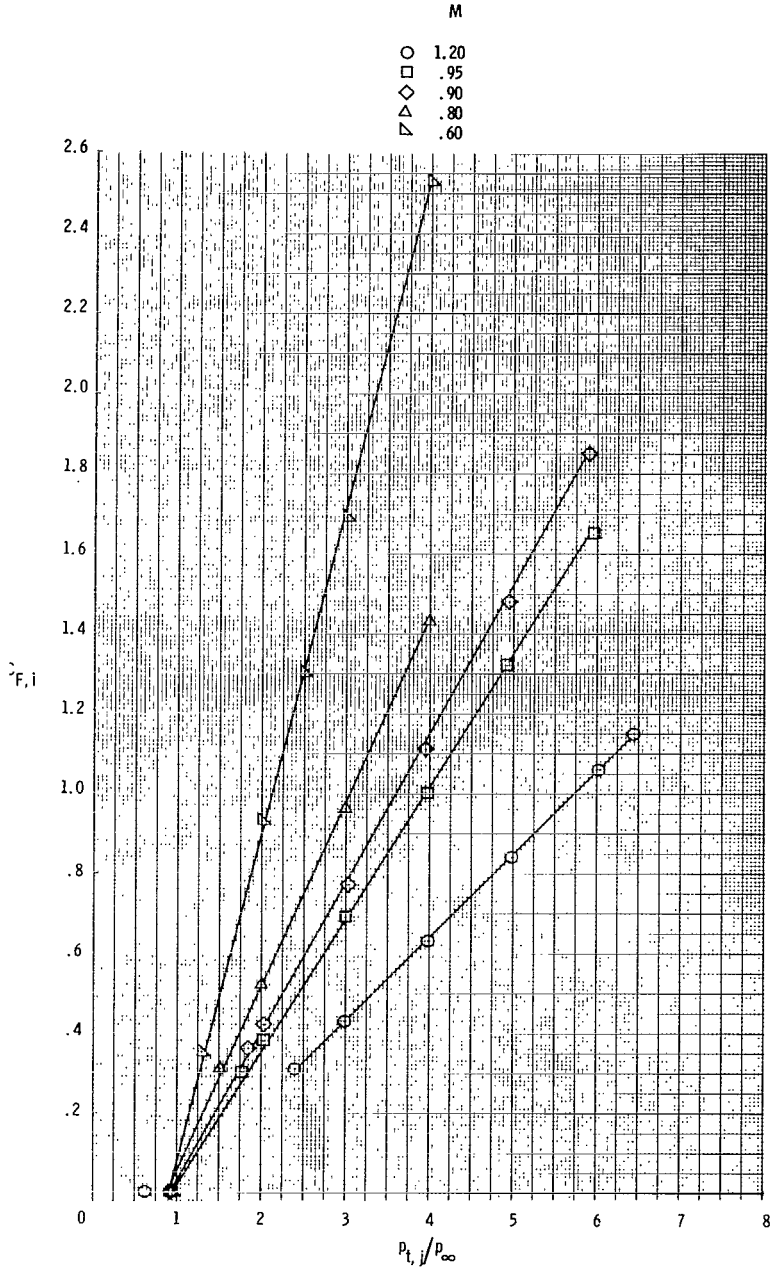

(f) $\beta_c = 10^o$; $A_e/A_t = 1.05$; $\beta_w = 10^o$.

Figure 38.- Continued.

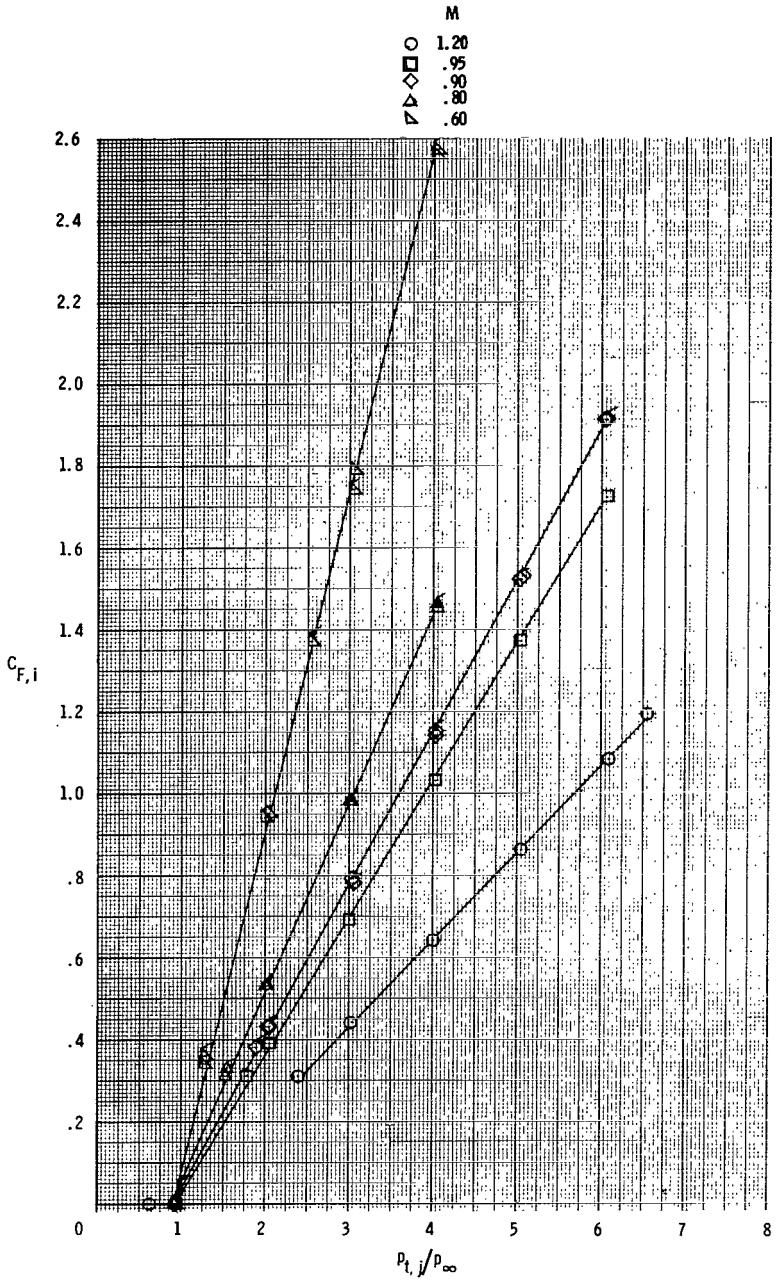

(g) $\beta_c = 10^o$; $A_e/A_t = 1.10$; base-line wedge; $\beta_w = 10^o$.

Figure 38.- Continued.

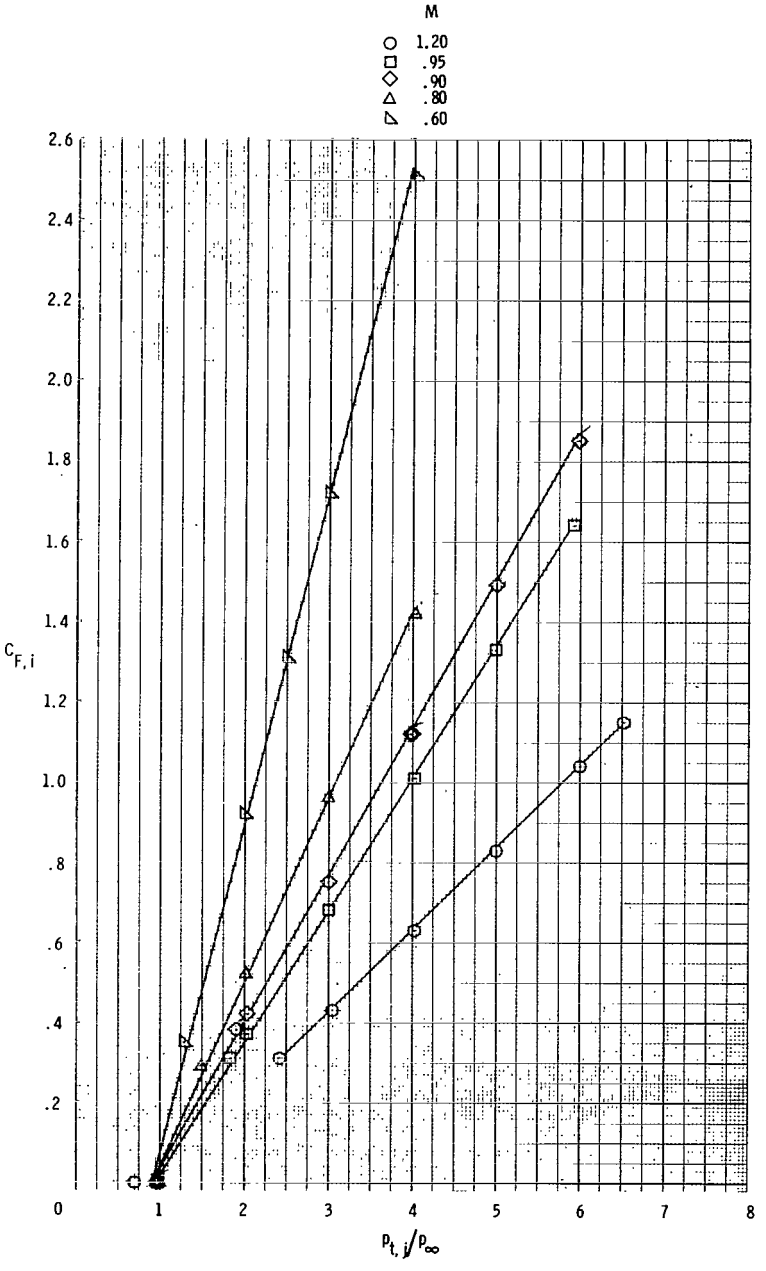

(h) $\beta_c = 10^o$; $A_e/A_t = 1.10$; short wedge; $\beta_w = 13.3^o$.

Figure 38.- Continued.

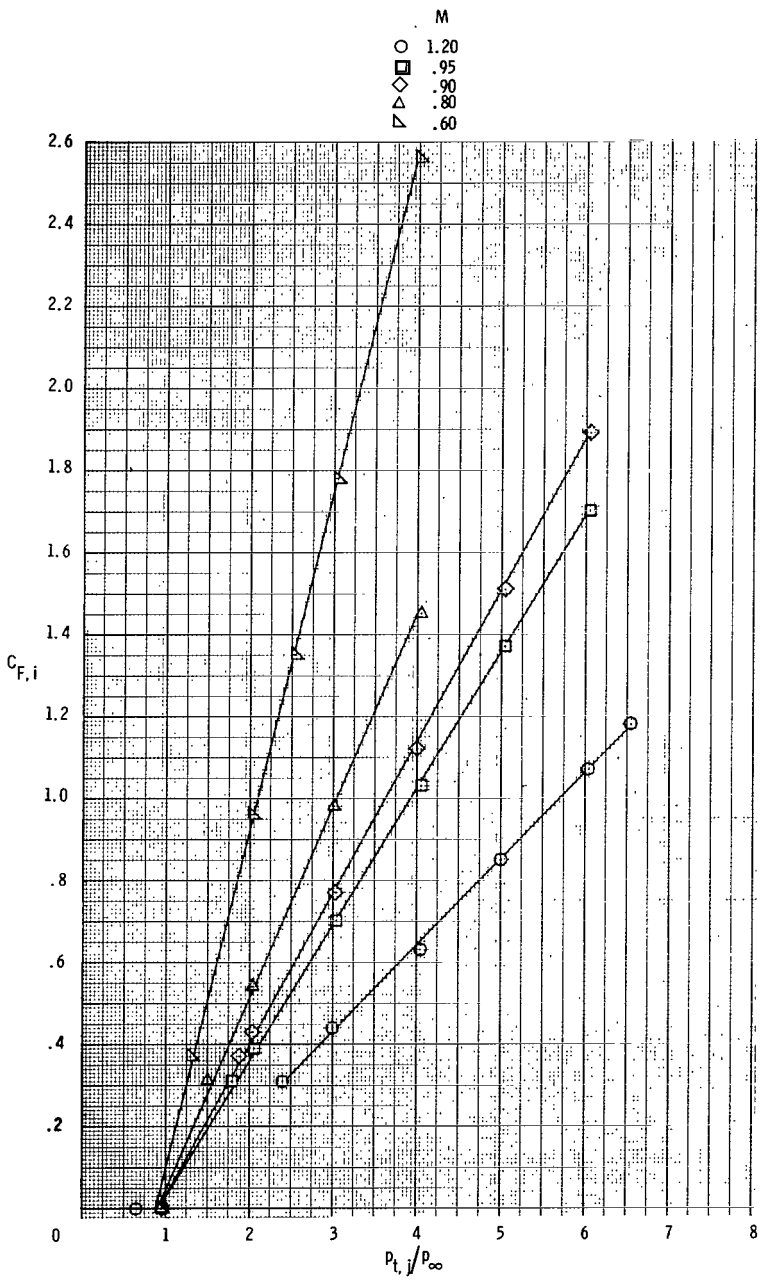

(i) $\beta_c = 10^o$; $A_e/A_t = 1.30$; $\beta_w = 4.5^o/9^o$.

Figure 38.- Continued.

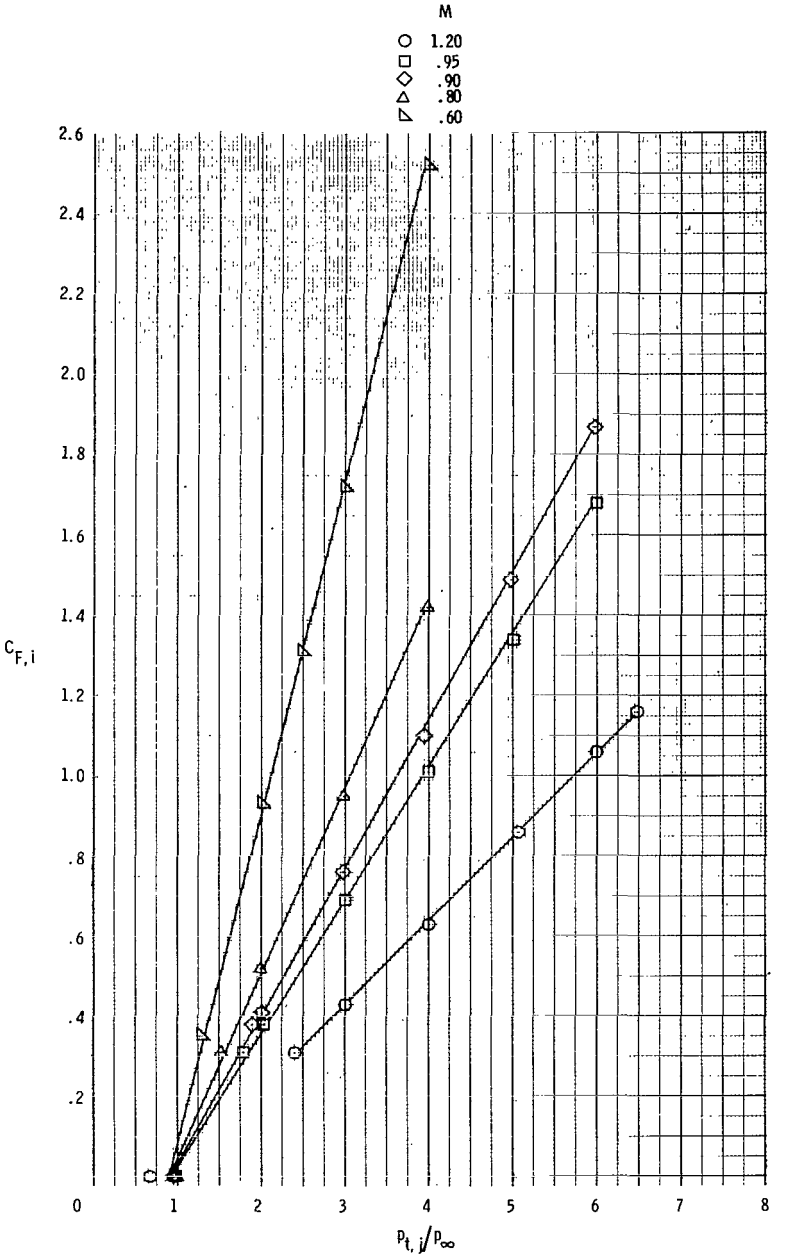

(j) $\beta_c = 10^o$; $A_e/A_t = 1.53$; $\beta_w = 8^o$.

Figure 38.- Continued.

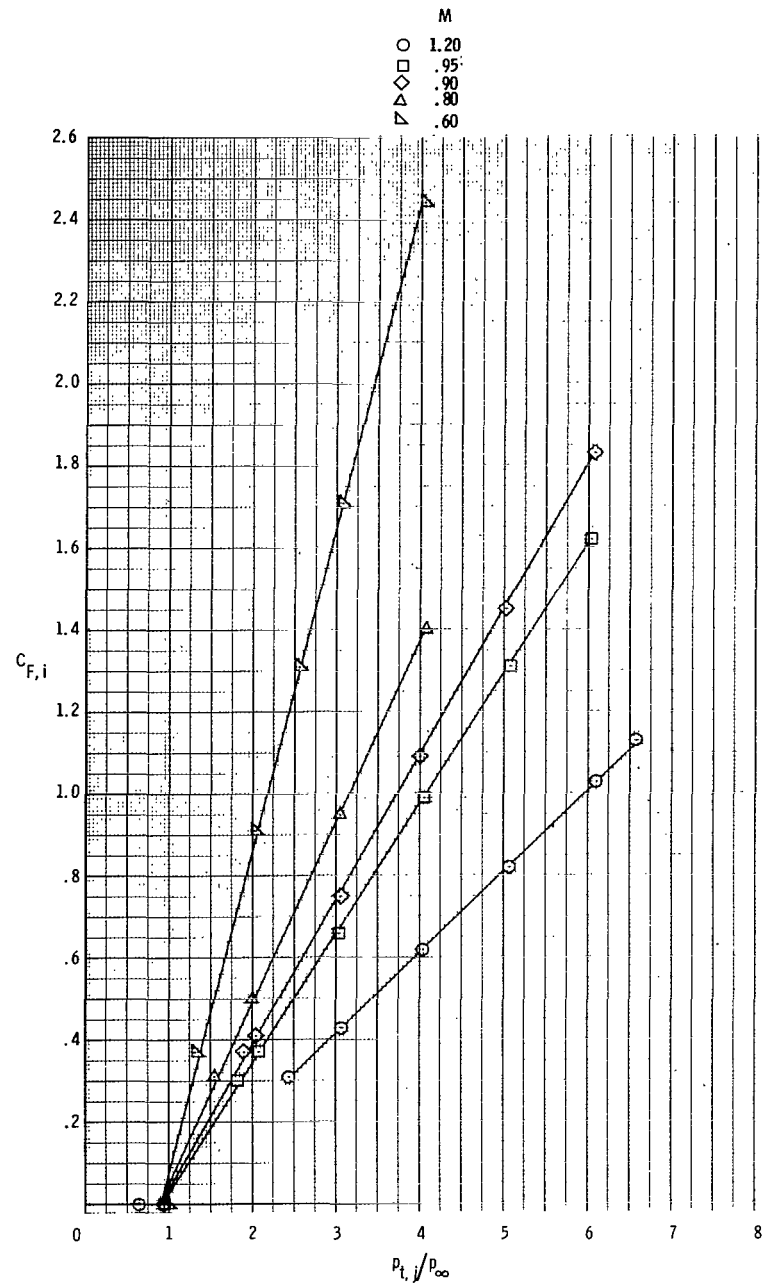

(k) $\beta_c = 14^o$; $A_e/A_t = 1.05$; $\beta_w = 10^o$.

Figure 38.- Continued.

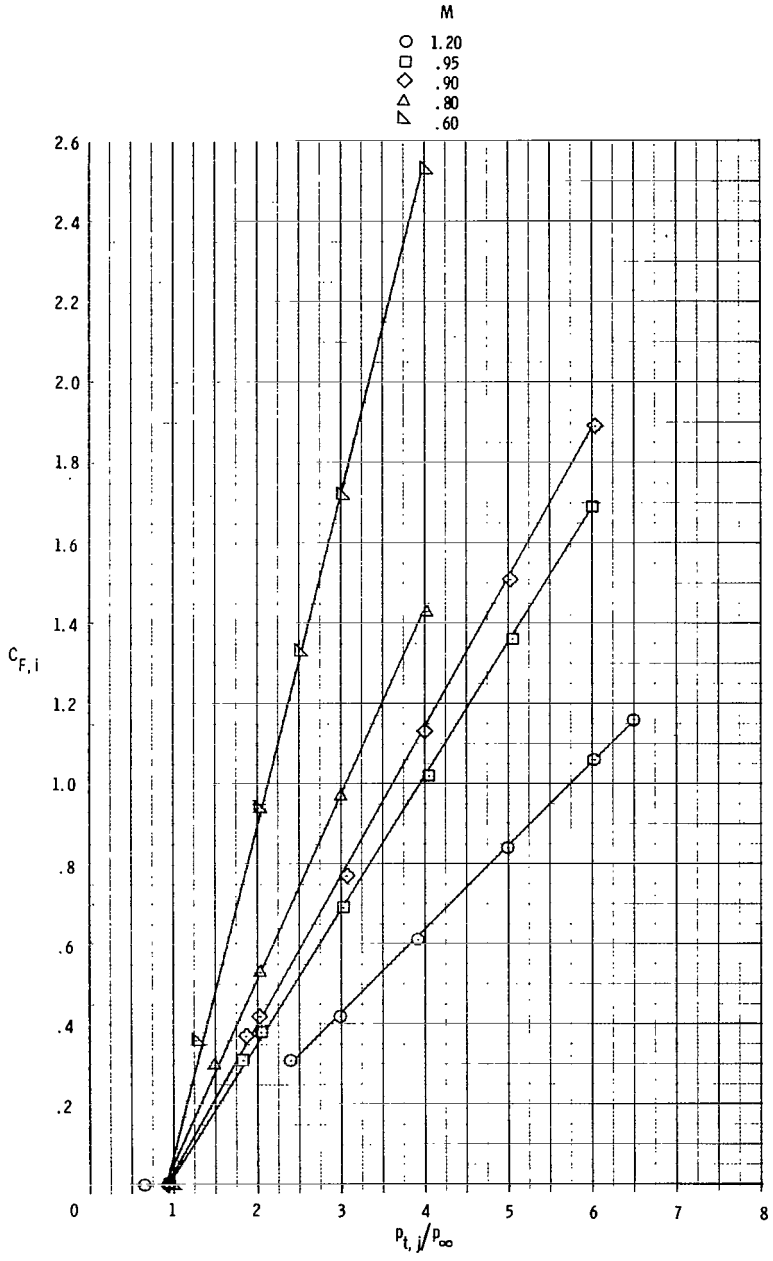

(l) $\beta_c = 14^o$; $A_e/A_t = 1.10$; no sideplate reduction; $\beta_w = 10^o$.

Figure 38.- Continued.

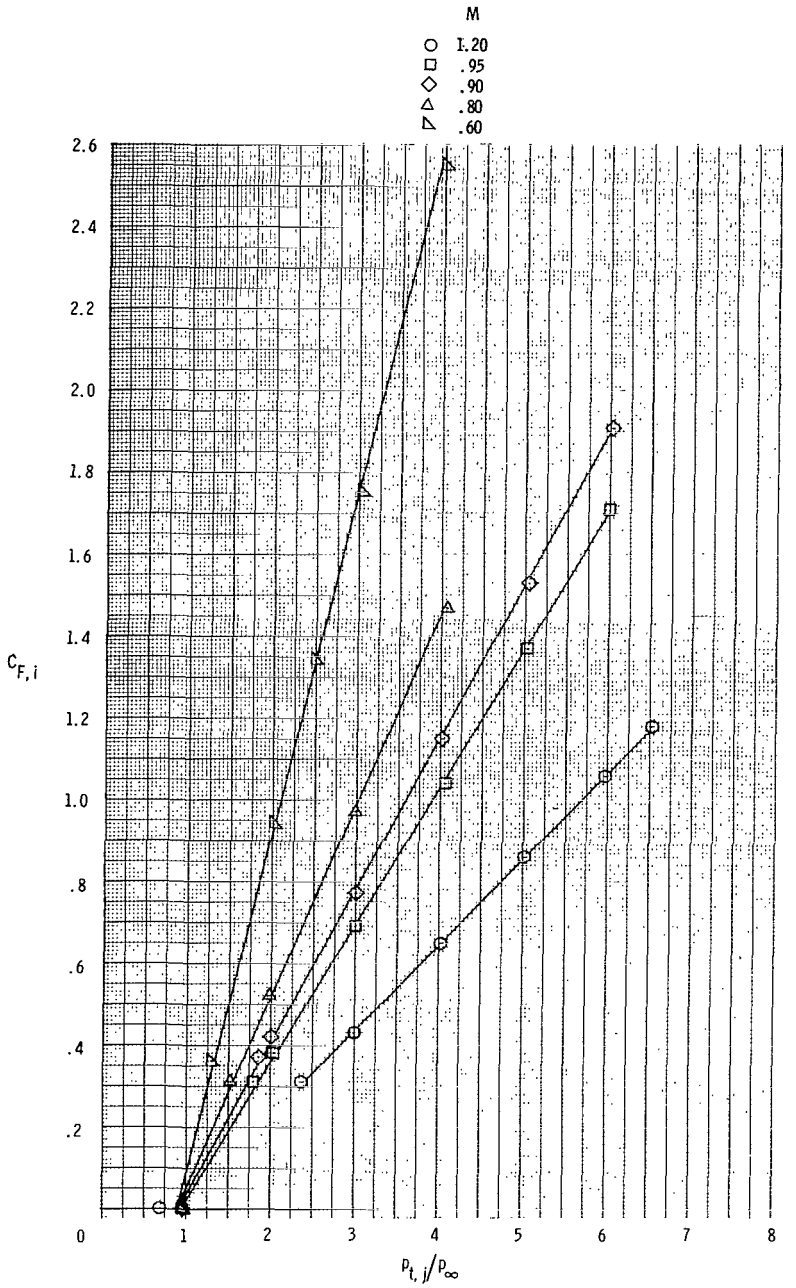

(m) $\beta_c = 14^o$; $A_e/A_t = 1.10$; sideplates reduced; $\beta_w = 10^o$.

Figure 38.- Continued.

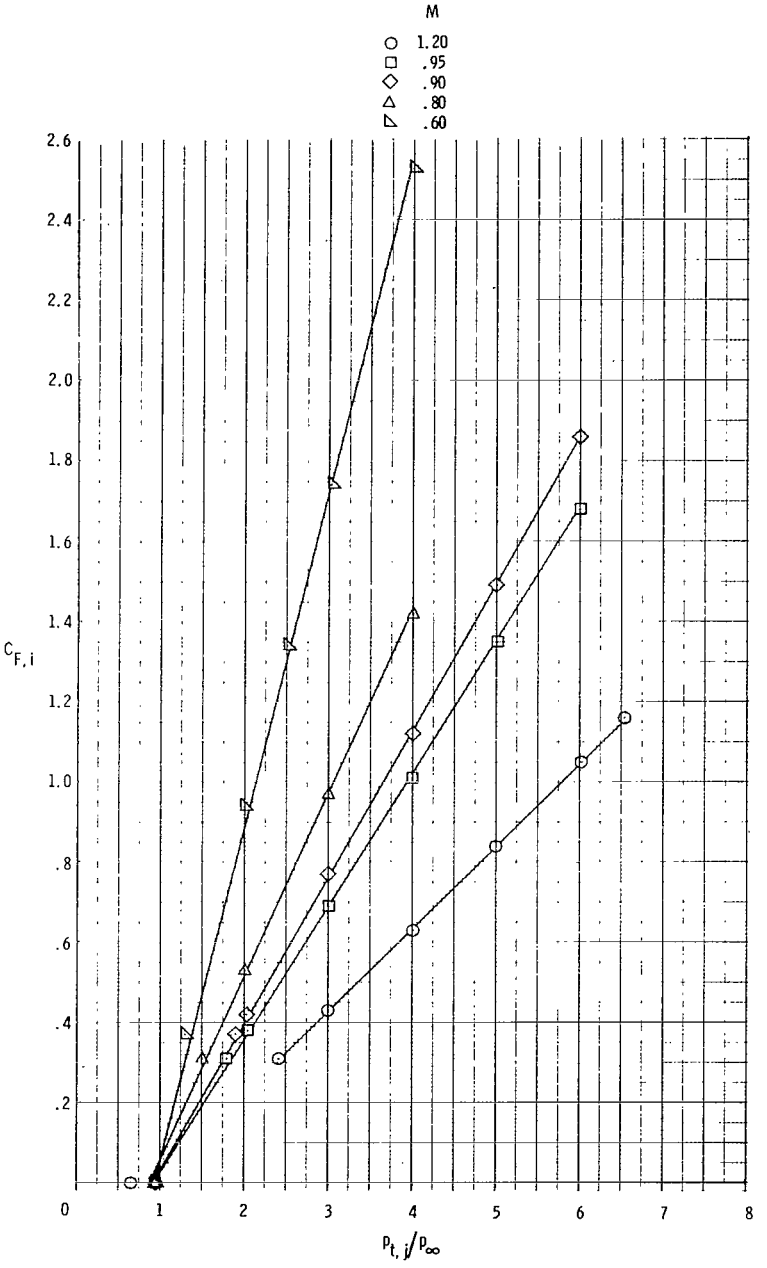

(n) $\beta_c = 14^o$; $A_e/A_t = 1.30$; $\beta_w = 4.5^o/9^o$.

Figure 38.- Continued.

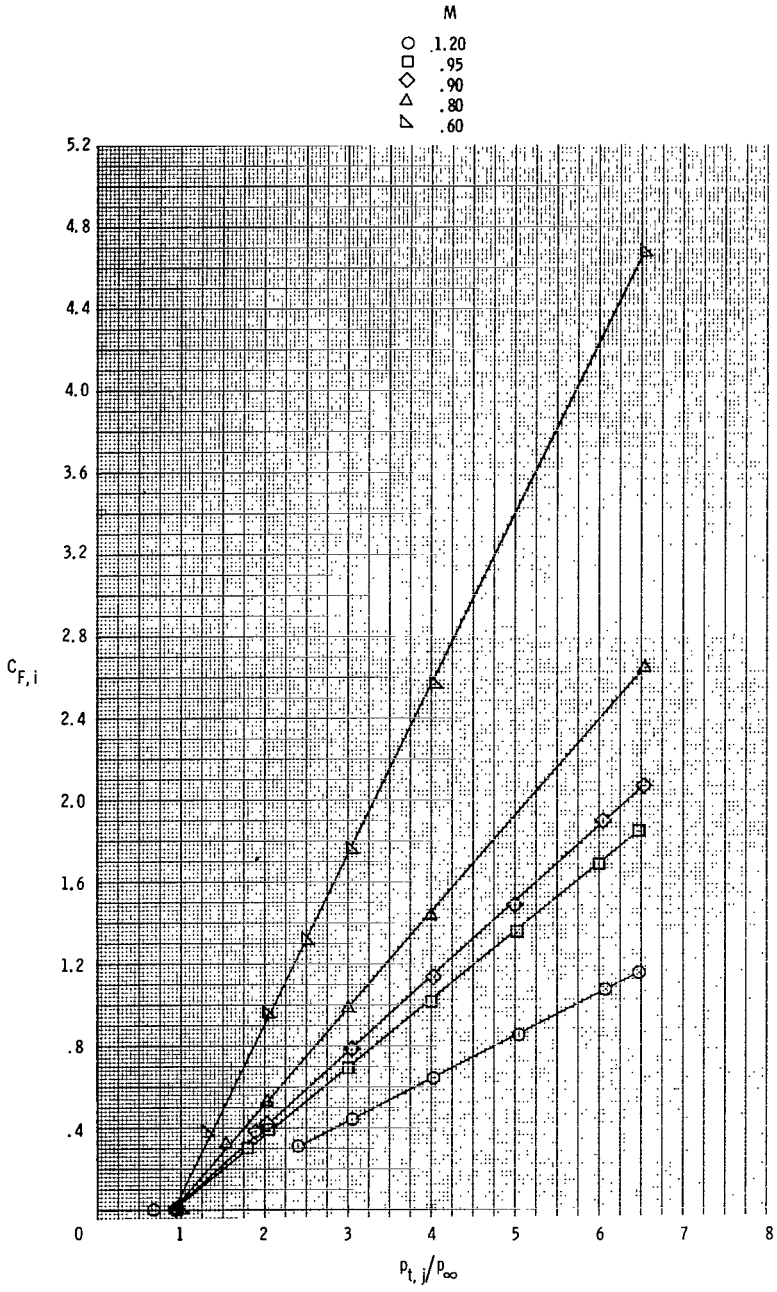

(o) $\beta_c = 14^o$; $A_e/A_t = 1.53$; $\beta_w = 8^o$.

Figure 38.- Continued.

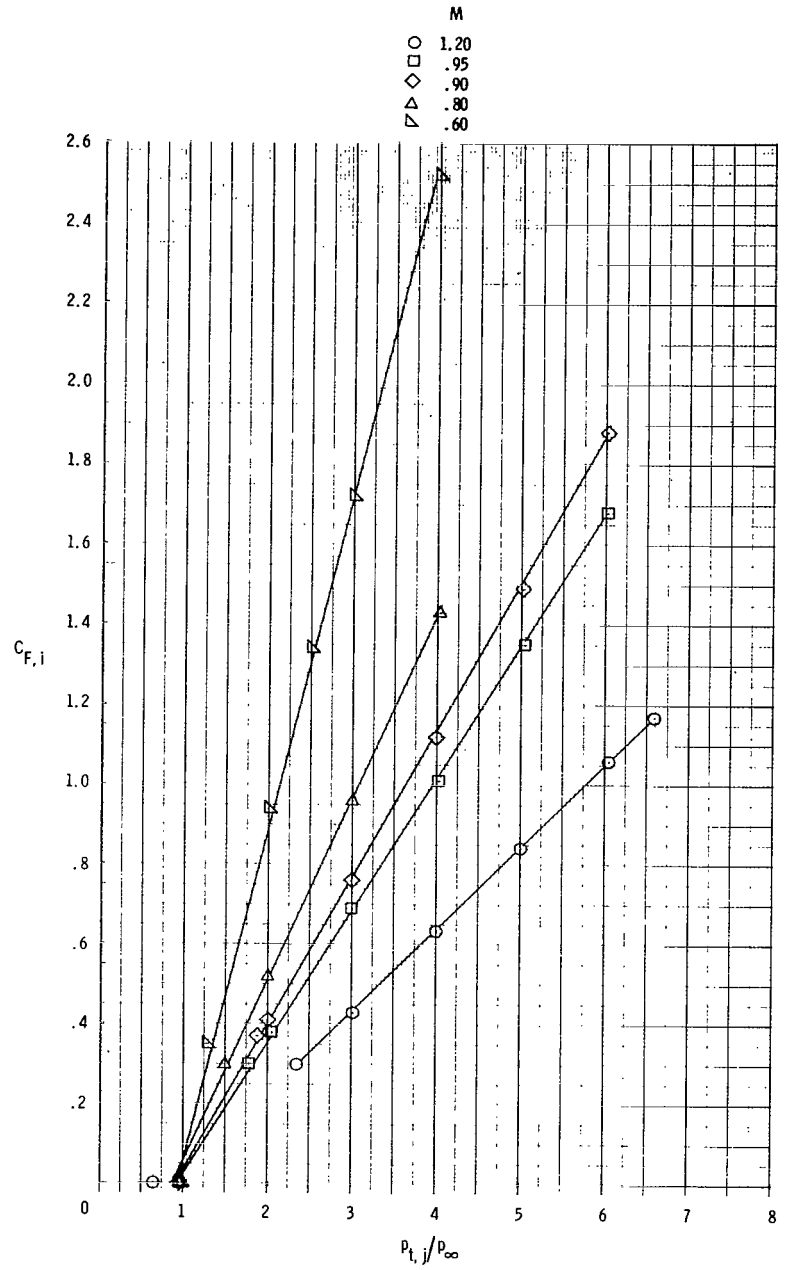

(p) $\beta_c = 18^o$; $A_e/A_t = 1.10$; base-line wedge; $\beta_w = 10^o$.

Figure 38.- Continued.

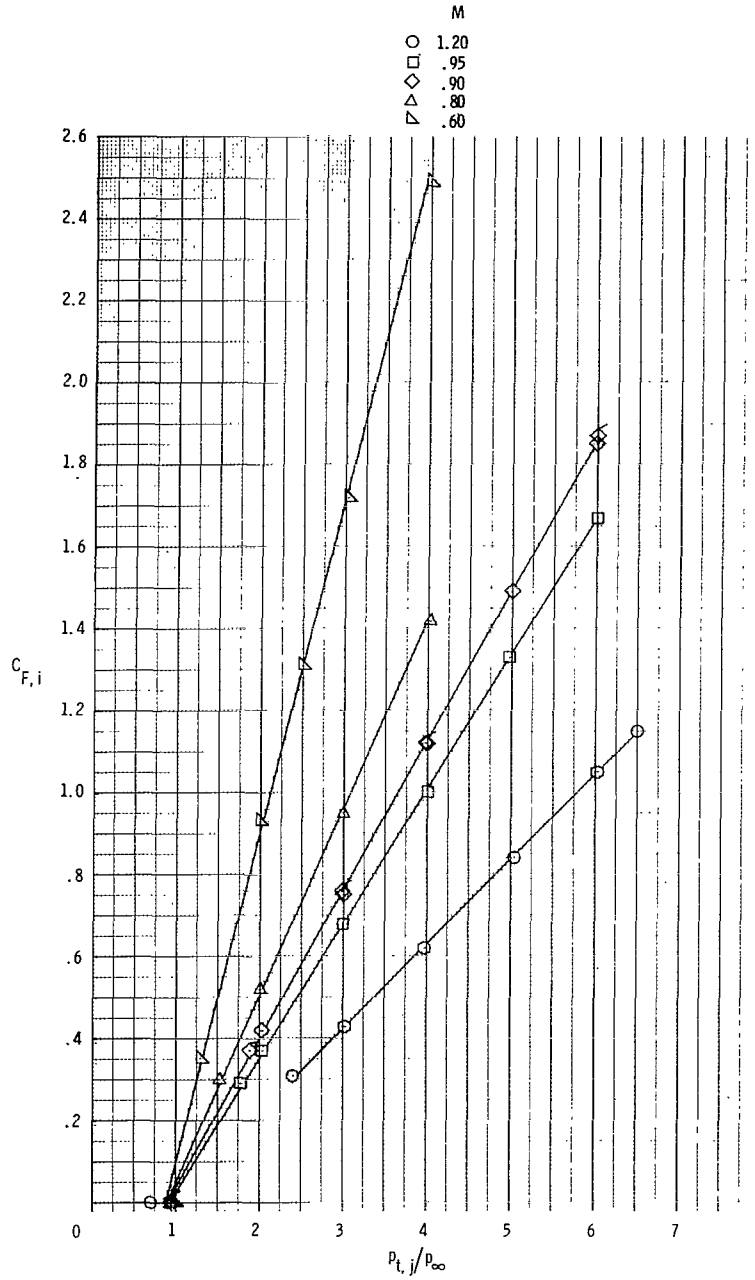

(q) $\beta_c = 18^o$; $A_e/A_t = 1.10$; long wedge; $\beta_w = 8^o$.

Figure 38.- Continued.

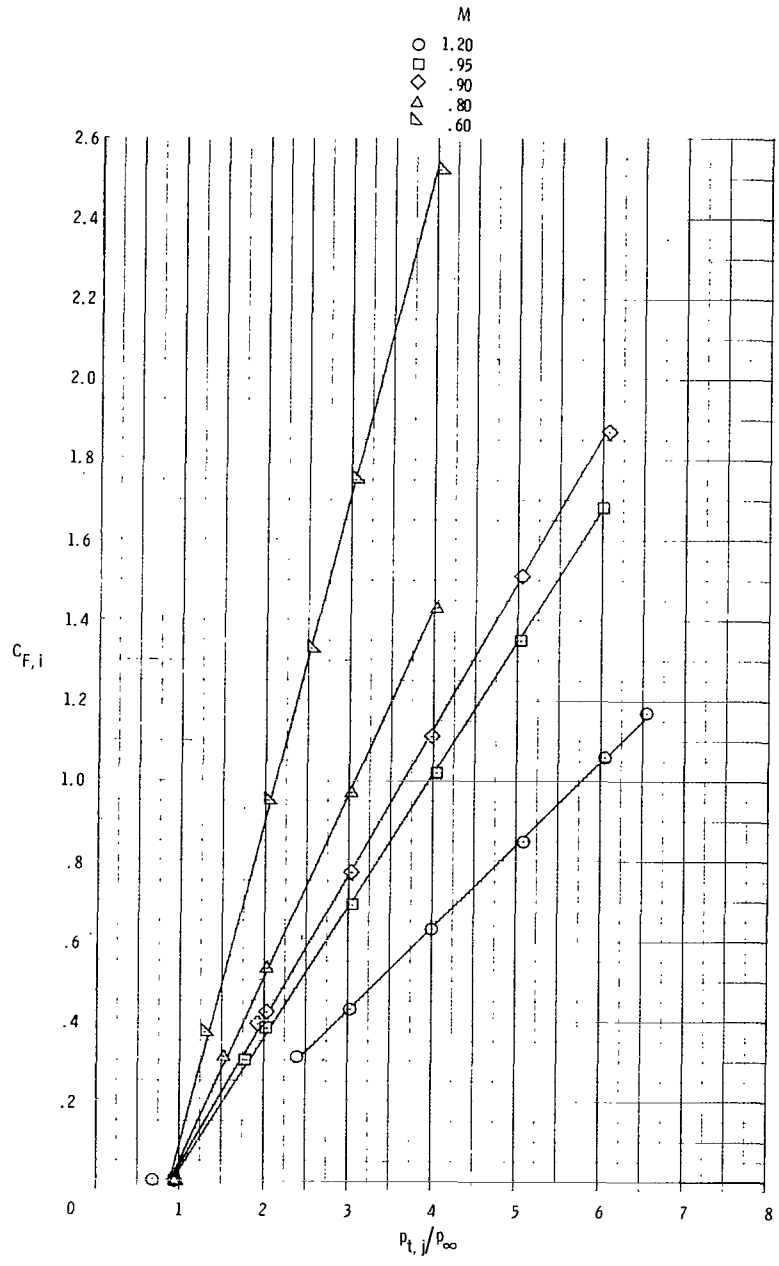

(r) $\beta_c = 18^o$; $A_e/A_t = 1.10$; short wedge; $\beta_w = 13.3^o$.

Figure 38.- Continued.

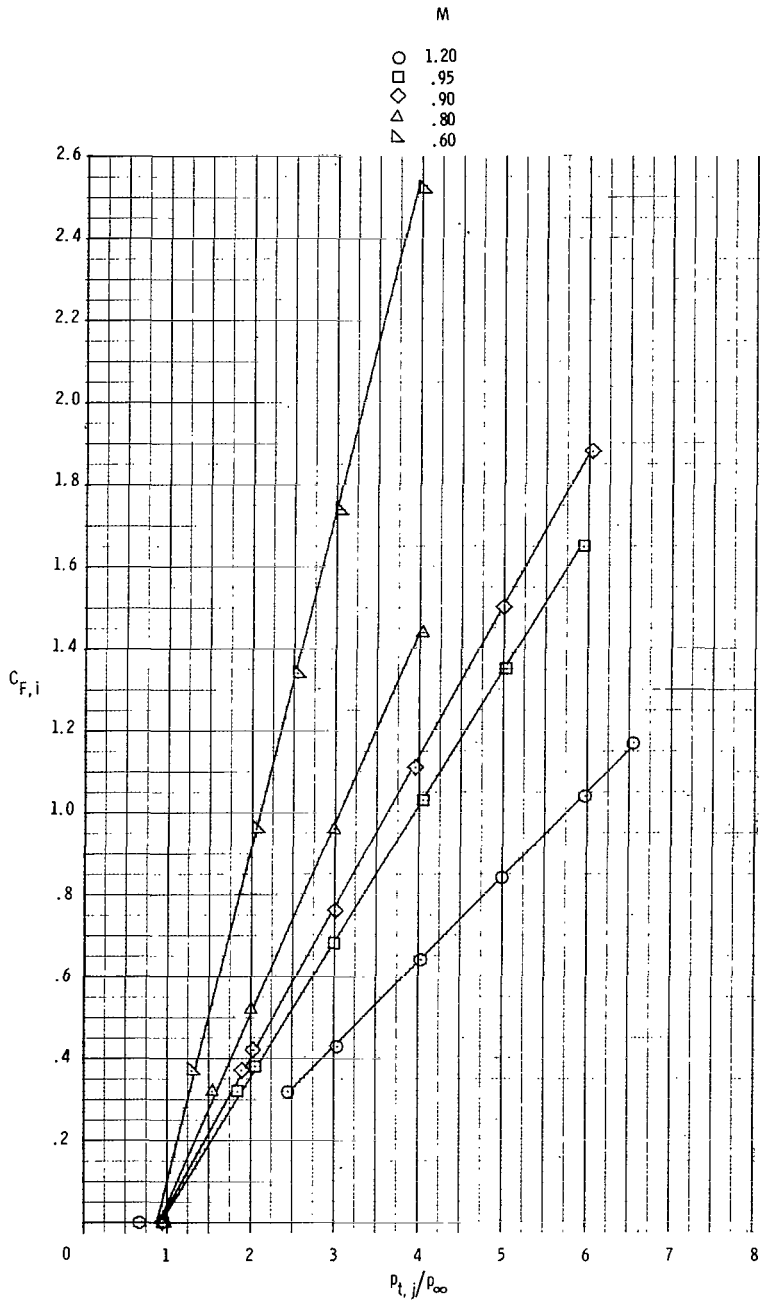

(s) $\beta_c = 18^o$; $A_e/A_t = 1.30$; $\beta_w = 4.5^o/9^o$.

Figure 38.- Concluded.

NATIONAL AERONAUTICS AND SPACE ADMINISTRATION
WASHINGTON, D.C. 20546

OFFICIAL BUSINESS
PENALTY FOR PRIVATE USE $300

SPECIAL FOURTH-CLASS RATE BOOK

POSTAGE AND FEES PAID
NATIONAL AERONAUTICS AND SPACE ADMINISTRATION
451

U.S.MAIL

705 001 C1 U A 760813 S00903DS
DEPT OF THE AIR FORCE
AF WEAPONS LABORATORY
ATTN: TECHNICAL LIBRARY (SUL)
KIRTLAND AFB NM 87117

If Undeliverable (Section 158 Postal Manual) Do Not Return

"The aeronautical and space activities of the United States shall be conducted so as to contribute . . . to the expansion of human knowledge of phenomena in the atmosphere and space. The Administration shall provide for the widest practicable and appropriate dissemination of information concerning its activities and the results thereof."

—NATIONAL AERONAUTICS AND SPACE ACT OF 1958

NASA SCIENTIFIC AND TECHNICAL PUBLICATIONS

TECHNICAL REPORTS: Scientific and technical information considered important, complete, and a lasting contribution to existing knowledge.

TECHNICAL NOTES: Information less broad in scope but nevertheless of importance as a contribution to existing knowledge.

TECHNICAL MEMORANDUMS: Information receiving limited distribution because of preliminary data, security classification, or other reasons. Also includes conference proceedings with either limited or unlimited distribution.

CONTRACTOR REPORTS: Scientific and technical information generated under a NASA contract or grant and considered an important contribution to existing knowledge.

TECHNICAL TRANSLATIONS: Information published in a foreign language considered to merit NASA distribution in English.

SPECIAL PUBLICATIONS: Information derived from or of value to NASA activities. Publications include final reports of major projects, monographs, data compilations, handbooks, sourcebooks, and special bibliographies.

TECHNOLOGY UTILIZATION PUBLICATIONS: Information on technology used by NASA that may be of particular interest in commercial and other non-aerospace applications. Publications include Tech Briefs, Technology Utilization Reports and Technology Surveys.

Details on the availability of these publications may be obtained from:

SCIENTIFIC AND TECHNICAL INFORMATION OFFICE

NATIONAL AERONAUTICS AND SPACE ADMINISTRATION

Washington, D.C. 20546